DOKUZ EYLÜL UNIVERSITY
GRADUATE SCHOOL OF NATURAL AND APPLIED SCIENCES

INVESTIGATION OF HEAT TRANSFER AND FLOW CHARACTERISTICS OF HOUSEHOLD APPLIANCES

by
Funda KURU

September, 2023
İZMİR

INVESTIGATION OF HEAT TRANSFER AND FLOW CHARACTERISTICS OF HOUSEHOLD APPLIANCES

A Thesis Submitted to the
Graduate School of Natural and Applied Sciences of Dokuz Eylül University
In Partial Fulfillment of the Requirements for the Degree of Doctor of Philosophy in Department of Mechanical Engineering, Energy Program

by
Funda KURU

September, 2023

İZMİR

PhD THESIS EXAMINATION RESULT FORM

We have read the thesis entitled **"INVESTIGATION OF HEAT TRANSFER AND FLOW CHARACTERISTICS OF HOUSEHOLD APPLIANCES"** completed by **FUNDA KURU** under supervision of **PROF. DR. DİLEK KUMLUTAŞ** and we certify that in our opinion it is fully adequate, in scope and in quality, as a thesis for the degree of Doctor of Philosophy.

Prof.Dr. Dilek KUMLUTAŞ

Supervisor

Doç Dr. Mustafa Turhan ÇOBAN	Prof. Dr. Yalçın ÇEBİ
Thesis Committee Member	Thesis Committee Member
Prof. Dr. Mustafa GÜNEŞ.	Assoc. Prof. Dr. Utku ŞENTÜRK
Examining Committee Member	Examining Committee Member

Prof. Dr. Okan FISTIKOĞLU

Director

Graduate School of Natural and Applied Sciences

ACKNOWLEDGEMENTS

First, I thank my supervisor, Prof. Dr. Dilek KUMLUTAŞ, for her incomparable knowledge, moral support, valuable advice, and guidance throughout this thesis study. Her wisdom, dedication, and unwavering commitment to my success have enlightened my academic journey and significantly impacted my life.

Also, thanks and regards to my dear jury supervisors; Prof. Dr. İsmail Hakkı TAVMAN, Prof. Dr. Yalçın ÇEBİ, and Assoc. Prof. Mustafa Turhan ÇOBAN. I also wish to thank my dear fellows and Ph.D. companions from the Department of Mechanical Engineering Energy Program for their patience. I want to thank my colleagues Dr. Özgün ÖZER and Assoc. Prof. Oğuz Emrah TURGUT for their scientific and valuable support.

This study is initially and partially supported by the Republic of Turkey Ministry of Industry and Trade with the 00998STZ2011-2 encoded SANTEZ project and VESTEL White Goods Company. I want to express my gratitude about being in this company and project.

Finally, I want to express my heartfelt gratitude to my family for their endless encouragement, patience, trust, and invaluable support in every aspect of my life. Sincere thanks to my dear brother Görkem KURU for his unwavering motivation. Specially thanks to my beloved parents, my mother, İlhan KURU and my father, Mesut KURU. I am confident that the skills and knowledge I have gained from my family will continue to shape my life. This thesis is dedicated to them with my endless love and respect.

Note to myself and to those researchers who read this thesis; No matter how slowly the thesis progresses and how much time it takes, I have consistently advanced and expanded my knowledge in every step through this Ph.D. study journey. It has empowered me to grow academically and personally.

Funda KURU

INVESTIGATION OF HEAT TRANSFER AND FLOW CHARACTERISTICS OF HOUSEHOLD APPLIANCES

ABSTRACT

This thesis study reveals the numerical and experimental results of household-type washer & dryer machine system components which consist of a centrifugal fan, a heater, and a condensation unit inside. Distinctly from the current literature studies, system elements were evaluated as a part of the entire drying system. This study aims to investigate the drying process frequently encountered in many domestic and industrial systems using the merits of Computational Fluid Dynamics (CFD) method. Theoretical analyses were carried out for the numerical model ability of the dehumidification process of humid air conditioned by forced convection in a water-cooled direct contact condensation unit.

Within the scope of this thesis study, all system components involved in the dehumidification process of a washer & dryer machine were modelled numerically. The results of the CFD analysis were validated experimentally by the compiled data obtained from Stereo Particle Image Velocimetry (SPIV) method, conventional measurement methods, and qualitative visualization method. After experimental verification, the variational influences of different operational drying system parameters, such as fan flow rate, heater channel design, condensation unit efficiency, and laundry conditions in the design of the washer-dryer machine, were numerically examined.

The numerical and experimental results showed that CFD-based analysis could be recognized as a practical solution procedure.

Keywords: Condensation, condenser, computational fluids dynamics, washer-dryer, particle image velocimetry.

BEYAZ EŞYALARDA ISI TRANSFERI VE AKIŞ KARAKTERİSTİKLERİNİN İNCELENMESİ

ÖZ

Bu tez çalışması, santrifüj fan, ısıtıcı ve yoğuşma ünitesinden oluşan ev tipi bir kurutma özellikli çamaşır makinesi sistem bileşenlerinin sayısal ve deneysel sonuçlarını ortaya koymaktadır. Mevcut literatür çalışmalarından farklı olarak, sistem elemanları tüm kurutma sisteminin bir parçası olarak değerlendirilmiştir. Bu çalışmanın amacı, birçok ev tipi ve endüstriyel sistemde sıkça karşımıza çıkan nem alma veya kurutma sürecini Hesaplamalı Akışkanlar Dinamiği (HAD) yöntemi ile incelemektir. Su soğutmalı, doğrudan temaslı bir yoğuşma ünitesinde zorlanmış taşınım ile şartlandırılmış nemli havanın nem alma döngüsünün sayısal olarak modellenebilirliği için analiz yapılmıştır.

Bu tez çalışması kapsamında, yıkayıcı- kurutucu makinenin nem alma işlemine katılan tüm sistem bileşenleri sayısal olarak modellenmiştir. HAD analizinin sonuçları Stereo Parçacık Görüntülemeli Hız Ölçüm (SPGHÖ) metodu, geleneksel ölçüm metotları ve niteliksel görselleştirme deney yönteminden elde edilen verilerle doğrulanmıştır. Deneysel doğrulamadan sonra, fan akışı, ısıtıcı kanalı, yoğuşma birimi ve çamaşır koşulları gibi farklı kurutma sistemi parametrelerinin, çamaşır kurutma makinesinin tasarımındaki etkileri sayısal olarak incelenmiştir.

Sayısal ve deneysel sonuçlar, HAD bazlı analizin etkili bir çözüm prosedürü olarak tanınabileceğini göstermiştir.

Anahtar sözcükler: Yoğuşma, kondenser, hesaplamalı akışkanlar dinamiği, yıkayıcı-kurutucu, parçacık görüntülemeli hız ölçümü

CONTENTS

Page

PhD THESIS EXAMINATION RESULTS FORM ii
ACKNOWLEDGEMENTS iii
ABSTRACT iv
ÖZ…… v
CONTENTS vi
LIST OF FIGURES ix
LIST OF TABLES xvi
LIST OF SYMBOLS xvii
ABBREVIATIONS xix

CHAPTER ONE - INTRODUCTION 1

1.1 Literature 2
1.2 Literature Survey Summary ..... .16
1.3 Aim and Motivation ..... .18

CHAPTER TWO - WASHER&DRYER MACHINE DRYING PRINCIPLE.. 19

2.1 Condenser Type Washer & Dryer System 19
2.2 The Condensation Process 21
2.3 Numerical and Experimental Study Strategy for the Entire Drying System ... 25

CHAPTER THREE - HUMIDITY MEASUREMENTS INSIDE THE DRYER SYSTEM 27

3.1 Mathematical Modelling of Specific Humidity 27
3.2 Experimental Evaluation of the Condenser Performance 28
3.2.1 Test 1: Spray water is continuously ON 34
3.2.2 Test 2: Spray Water is Continuously Off 36
3.2.3 Test 3: Spray Water Valve Activation is Alternately On & Off 38

3.2.4 Test 4: Spray Water and One Heater are Simultaneously Off 40
3.2.5 Test 5: Spray Water and Heaters are Simultaneously Off 42
3.3 Air Flow Rate Measurements 45

CHAPTER FOUR-DEVELOPING THE NUMERICAL MODEL 56

4.1 Numerical Model of the Drying Unit 56
4.2 Numerical Modelling of the Fan Driven Flow 64
4.3 Stereo Particle Image Velocimetry Experimental Validation Method 69
4.4 Numerical and Experimental Analysis on the Heating Unit 72

CHAPTER FIVE- DESIGN AND PERFORMANCE DEVELOPMENT STUDIES 77

5.1 Dryer Unit Design Optimization 77

CHAPTER SIX- DROPLET MODEL 87

6.1 Direct Contact Heat Transfer Model of a Droplet 87
6.2. JAVA Code Solver 88
6.3 Water Droplet Simulation 91
6.4 Discrete Phase Modeling 93
6.4.1 Simplified Model for DPM 96
6.4.2 Actual Model for DPM 99

CHAPTER SEVEN- LAUNDRY DRYING 107

7.1 Mathematical Model to Simulate the Dehumidification Process 107

CHAPTER EIGHT- RESULTS AND DISCUSSIONS 122

8.1 Results and Discussions 122

CHAPTER NINE- CONCLUSIONS 129

REFERENCES..... 131

LIST OF FIGURES

Page

Figure 1.1 CFD results with cross section plots of a) air velocity; b) temperature c) vapour mass fraction in a wind tunnel model and d) experimental settings schematics 5
Figure 1.2 Variation of condensation efficiency in the flow direction for a hollow-cone spray 8
Figure 1.3 Schematics of a conventional air-vented dryer test set-up 10
Figure 1.4 Moisture content difference of a 2D textile model 11
Figure 1.5 Schematic description of coupled heat and mass transfer inside the domestic dryer 12
Figure 1.6 The centrifugal fan geometry and the velocity contours 13
Figure 2.1 Washer & Dryer system 19
Figure 2.2 a) Washer & Dryer machine construction b) dryer system assembly 20
Figure 2.3 General graphical representation of the a) washer & dryer machine and b) dryer unit 20
Figure 2.4 Psychrometric chart representing the cooling with dehumidification process 22
Figure 2.5 3D model of the condenser part and spray nozzle 23
Figure 2.6. Moist air and sprayed water T-s diagram 23
Figure 2.7 An induced-draft counterflow cooling tower 24
Figure 2.8 Schematic diagram of Washer-Dryer system 26
Figure 3.1 Condesner channel inlet and outlet zones 29
Figure 3.2 Placement of the humidity probes for simultaneous humidity measurement inside the condenser at inlet and outlet zones 29
Figure 3.3 ALMEMO FNAD 46 handy held psychrometer type humidity probe and technical specification 30
Figure 3.4 Test setup for washer & dryer machine 31
Figure 3.5 Absolute humidity measurements at condenser inlet and outlet during the one hour drying program 32
Figure 3.6 a) Relative humidity and b) temperature measurements for Test-1 35
Figure 3.7 Absolute humidity measurements for Test-1 36

Figure 3.8 a) Relative humidity and b) temperature measurements for Test-2 37
Figure 3.9 Absolute humidity measurements for Test-2..... 38
Figure 3.10 a) Relative humidity and b) temperature measurements for Test-3 39
Figure 3.11 Absolute humidity measurements for Test-3..... 40
Figure 3.12 a) Relative humidity and b) temperature measurements for Test-4 41
Figure 3.13 Absolute humidity measurements for Test-4..... 41
Figure 3.14 a) Relative humidity and b) temperature measurements for Test-5 43
Figure 3.15 Absolute humidity measurements for Test-5..... 43
Figure 3.16 Comparison of the absolute humidity for five different test conditions. 44
Figure 3.17 Comparison of the absolute humidity of new derived condition with Test 1 & Test 4..... 45
Figure 3.17 Comparison of the absolute humidity of new derived condition with Test 1 & Test 4..... 46
Figure 3.18 Volume of washing group due to the 3D geometry..... 46
Figure 3.19 Volume of drying group due to the 3D geometry 46
Figure 3.20 The volume of laundry measurement 40
Figure 3.21 Almemo FV A935- TH5 type thermo-anemometer probe and technical specifications..... 47
Figure 3.22 Velocity probe measurement conditions at the condenser inlet 48
Figure 3.23 Velocity probe measurement inside the machine 48
Figure 3.24 Traverse on round duct area 49
Figure 3.25 Velocity measurement points at the condenser inlet 49
Figure 3.26 a) Velocity distribution at the condenser channel according to the CFD analysis b) 3D model of the condenser channel inlet, c) detail view of the velocity distribution at inlet 51
Figure 3.27 Schematic of the test bench, outlet chamber setup – multiple nozzles in chamber..... 52
Figure 3.28 Standard nozzles with varying inner diameters 53
Figure 3.29 Test chamber view..... 54
Figure 3.30 Test chamber with test fan testing setup..... 54
Figure 3.31 Comparison of test results for validation..... 55
Figure 4.1. Drying system model apart from the machine..... 56

Figure 4.2 Spray nozzle a) fluid volume model and b) actual part 57
Figure 4.3 Numerical grid models of the entire dryer components 58
Figure 4.4 CFD model and boundary conditions definitions of the condenser model as a part of dryer 59
Figure 4.5. Temperature volume render for the dryer 59
Figure 4.6. Spray water particles tracking 60
Figure 4.7 Fluid volume model of the condenser and nozzle 61
Figure 4.8 Numerical model of the condenser fluid volume 62
Figure 4.9 Two phase volume of fluid model of the condenser spray a) real model, b) CFD model 63
Figure 4.10 a) Experimental set-up for the sight window of condenser spray channel, b) water spray with fan work and c) water spray without fan work 64
Figure 4.11 Washer & Dryer machine assembly and drying system 65
Figure 4.12 Centrifugal fan's a) solid model, b) blade geometry 66
Figure 4.13 Centrifugal fan's a) simulation model, b) fan housing air volume Model and c) numerical model for CFD analysis 66
Figure 4.14 Centrifugal fan with external ambient air volume a) geometry, b) numerical model 67
Figure 4.15. Centrifugal fan speed distribution a) midplane b) outlet 68
Figure 4.16. The distribution of stream lines within ambient a) air and b) the outlet of the fan 68
Figure 4.17 SPIV a) test setup and b) test view 70
Figure 4.18 Test planes positions 71
Figure 4.19 Outlet velocity comparison with the methods of a) CFD and b) SPIV .. 71
Figure 4.20 Volumetric three-dimensional speed data obtained from the mouth of the fan and ambient air a) CFD and b) SPIV (inner surface, the outer surface of 7 m/s, 3 m/s) 71
Figure 4.21 Termocouple measuring points on the heater surface 72
Figure 4.22 Volumetric three-dimensional speed data with a) heater channel without resistance unit, b) CFD and c) SPIV results 73

Figure 4.23 Volumetric three-dimensional speed data with a) heater unit with heaters and without lamellas design, b) CFD and c) SPIV results..... 73
Figure 4.24 Volumetric three-dimensional speed data with, a) heater unit with heaters and lamellas design b) CFD and c) SPIV results..... 74
Figure 4.25 750-Watt heater tube's surface temperature distributions according to the CFD results 74
Figure 4.26 The temperature distributions on the outer surface of the heater in the case of two 750-Watt resistances work for a) anodized aluminum surface (Ɛ = 0.2) b) polished aluminum surface (Ɛ = 0.05) 75
Figure 4.27 a) Temperature and b) velocity distributions across the dryer system ... 76
Figure 5.1 Design parameters of the heater unit 77
Figure 5.2 Heating channel outlet section velocity distributions at a) 4 mm, b) 8 mm, c) 12 mm, d) 16 mm narrowed width 78
Figure 5.3 Influences of channel width lengths over the average outlet velocity..... 79
Figure 5.4 Drying system air volume models a) existing design b) proposed design 80
Figure 5.5 Optimized new heater channel, a) air volume model and b) numerical grid model..... 81
Figure 5.6 Convergency graphic of the numerical analysis..... 81
Figure 5.7 Velocity streamlines along the heater channel for existing design..... 82
Figure 5.8 Velocity streamlines along the heater channel for novel design 82
Figure 5.9 Heater placements inside the a) new and b) current design heater channels 83
Figure 5.10 Energy analysis results of new heater design 84
Figure 5.11 Heater channel position and assembly of novel designed heater prototype 85
Figure 5.12 Heater channel outlet SPIV measurement plane positions at a)z=0 mm, b) z=40 mm, c) z=80 mm 85
Figure 5.13 a) Heater outlet and equivalent speed volumes for b) current, c) novel design 86
Figure 6.1 Variation of heat transfer coefficient rates along the channel 89
Figure 6.2 Increases in the droplet masses across the channel length 90
Figure 6.3 Variations in the droplet velocity rates along the channel..... 90

Figure 6.4 Droplet diameter variations in the channel 91
Figure 6.5 Droplet temperature rise along the channel 91
Figure 6.6 Actual condenser model and JAVA -based simulation model 92
Figure 6.7 Spray channel and spray nozzle model for CFD simulation and temperature distribution of the droplet along the channel 93
Figure 6.8 Temperature distribution of the droplet along the line 93
Figure 6.9 The evaporation of a liquid droplet as a function of time..... 94
Figure 6.10 A cone injection for 3-D models only where particle streams are injected in a conical pattern 95
Figure 6.11 Solution residuals 96
Figure 6.12 Spray channel model and actual condenser model for CFD simulation. 97
Figure 6.13 Droplet and air temperature distributions after spray injection for the simplified model 98
Figure 6.14 DPM summary report 98
Figure 6.15 Spray nozzle and condenser channel model for CFD simulation..... 99
Figure 6.16 a) Droplet temperature and b) air temperature distributions after spray injection for real model 101
Figure 6.17 Particle track with the change of particle diameter 101
Figure 6.18 a) Experimental set-up for the sight window of condenser spray channel, b) water spray with fan work and c) water spray without fan work 102
Figure 6.19 Particle tracking with a) visualized sprayed model and b) CFD method..... 103
Figure 6.20 DPM summary report for the actual working condition..... 104
Figure 6.21 Particle track of particle diameter variance for actual condition..... 105
Figure 6.22 Particle tracks of particle diameter variance for 3 different conditions a)1st Condition, b) 2nd Condition, c) 3rd Condition which are given in Table 6.4..... 106
Figure 6.23 Particle track of particle diameter variance for a) actual condition and b) efficient 3rd condition 106
Figure 7.1 Schematic of cotton sample inside tunnel dryer 107

Figure 7.2 The fabric drying process curve illustrates the three different stages of drying 109
Figure 7.3 Convective textile drying process boundary volume illustration. 111
Figure 7.4 Drum and laundry volume model for CFD simulation 112
Figure 7.5 Numerical grid model of drum and laundry volume 112
Figure 7.6 Temperature distribution for the laundry 113
Figure 7.7 Velocity streamlines for the inside volume of the washer-dryer system 114
Figure 7.8 Schematic representation of laundry model 114
Figure 7.9 a) Water Mass Fraction of the laundry and b) flow distribution inside the drum 115
Figure 7.10 Moisture source definitions a) surface type, b) spherical one body, c) multiple source points 116
Figure 7.11 Multiple injection source points definition 116
Figure 7.12 a) Multiple injection source b) water mass fraction of the wet laundry source and c) flow distribution inside the rotating drum 117
Figure 7.13 a) CFD and b) SPIV results of the velocity distribution and c) velocity map at the heater outlet 118
Figure 7.14 Defining the outlet velocity distribution as a boundary condition for the drum-inlet 119
Figure 7.15 SPIV data assisted velocity distribution simulation a) at inlet and b) inside the drum 119
Figure 7.16 a) H_2O mass fraction and b) water liquid particle diameter distribution 120
Figure 7.17 DPM summary report 120
Figure 7.18 Comparison of the velocity distributions of a) experimental SPIV input and b) constant velocity input 121
Figure 8.1 a) Relative humidity, b) temperature variation and c) absolute humidity charts 122
Figure 8.2 Cumulative water measurements 123
Figure 8.3 Temperature distributions for a) drum inlet and b) drum outlet 124
Figure 8.4 Water liquid particle diameter tracking lines by time 125

Figure 8.5 Particle diameter changes from t:0 to t:3 seconds 125
Figure 8.6 Reduction in the particle diameter with respect to elapsed time 126

LIST OF TABLES

Page

Table 2.1 Components of the drying unit 20
Table 2.2 Mathematical model representing the energy and mass balance equations for the cooling tower 25
Table 2.3 Numerical model and validation methods table 26
Table 3.1 Governing equations for process air 28
Table 3.2 Handy held psychrometer type humidity probe technical specifications 30
Table 3.3 Varying experimental conditions for the comparative study 33
Table 3.4 Technical specifications of thermo-anemometer probe 47
Table 3.5 Measurement points and velocity data for loaded machine 50
Table 3.6 Comparison of theoretical and CFD calculations of mass flow rates 50
Table 4.1 Comparison of resistance temperature results between CFD and experimental measurement 74
Table 5.1 Heater channel outlet section area 78
Table 5.2 Heaters surfaces area 84
Table 6.1 CFD model inputs 92
Table 6.2 Specification for channel model 96
Table 6.3 Experimental conditions of droplet 100
Table 6.4 DPM summary report for the actual working condition 102
Table 6.5 Droplet parameters for 3 different conditions 104
Table 6.6 Summary of the operational conditions 105
Table 7.1 Material definition for cotton 113
Table 8.1 DPM summary 127
Table 8.2 Mass transfer summary 127
Table 8.3 Energy transfer summary 127

LIST OF SYMBOLS

T	: Temperature
T_{dp}	: Dew point temperature (K)
h_{air}	: Process air enthalpy (J)
ω_{air}	: Absolute humidity of the process air (kg/kg)
ν_{air}	: Specific volume of the process air (m^3/kg)
P_{air}	: Partial pressure of the air (Pa)
R_{air}	: Universal gas constant for the process air (J/kgK)
T_{air}	: Temperature of the process air (K)
$C_{p,air}$	: Specific heat of the process air at constant pressure (J/kgK)
s	: Entropy (J/K)
$\dot{m}$	: Mass flow rate (kg/s)
m_v	: Total vapor mass in the air (kg)
m_a	: Total mass of dry air (kg)
P_a	: Partial pressure of dry air (Pa)
P_v	: Partial pressure of water vapor (Pa)
P_{atm}	: Atmospheric pressure (Pa)
$\dot{E}$	: Energy potential of the process fluid (J)
ω	: Absolute humidity (kg/kg)
RH	: Relative humidity
P	: Pressure, (Pa)
V	: Volume (m^3)
R	: Universal gas constant (J/kgK)
h	: Enthalpy (J)
C_p	: Specific heat at constant pressure (J/molK)
ν	: Specific volume (m^3/kg)
φ	: Relative humidity
$\Delta\omega$	: Variation in absolute humidity rates
RH_{in}	: Relative humidity of the process air at the inlet
RH_{out}	: Relative humidity of the process air at the outlet
T_{oot}	: Outlet temperature (K)
T_{in}	: Inlet temperature (K)
D	: Diameter (m), Droplet diameter (m)

$V_{air,n}$: Process air inlet velocity (m/s)

$A_{air,in}$: Cross-sectional area perpendicular to the inlet process air (m^2)

Ψ_n : n^{th} root of a transcendental equation

N_{FO} : Fourier number

U : Droplet velocity (m/s)

T_v : Vaporization temperature (K)

T_b : Boiling temperature (K)

$\upsilon_{air,in}$: Volumetric flow rate of the inlet process air (m^3/h)

ρ_{air} : Density of process air (kg/m^3)

ρ,Q : Density (kg/m^3)

ε : Emissivity

w : Width (m)

z : z-axis

h_s : Heat transfer coefficient (W/m^2K)

Re : Reynolds number

Pe : Peclet number

T_{sat} : Saturation temperature (K)

T_i : Initial temperature (K)

C_D : Drag coefficient

g : Gravitational constant (m/s^2)

k : Thermal conductivity (W/mK)

α : Thermal diffusivity (m^2/s)

D_i : Initial droplet diameter (m)

D_0 : Pre-exponential factor of Arrhenius-type equation (m^2/s)

D_{eff} : Effective diffusivity coefficient (m^2/s)

E_a : Activation energy (J/mol)

MR : Moisture ratio

L : Flat thickness (m)

X : Moisture content (kg H_2O / kg dry solid)

X_0 : Initial moisture content (kg H_2O / kg dry solid)

X_e : Equilibrium moisture content (kg H_2O / kg dry solid)

t : Elapsed time (sec)

ABBREVIATIONS

ANSI	: American National Standards Institute
AMCA	: Air Movement and Control Association
ASHRAE	:American Society of Heating, Refrigerant and Air Conditioning Engineers.
CAD	: Computer Assisted Design
CFD	: Computational Fluid Dynamics
CFDHT	: Computational Fluid Dynamics and Heat Transfer
DPM	: Discrete Phase Model
MR	: Moisture Ratio
ND:YAG	: Neodymium-Doped Yttrium Aluminium Garnet
NTC	: Negative Temperature Coefficient
PIV	: Particle Image Velocimetry
RPM	: Revolution Per Minute
SANTEZ	: Sanayi Tezleri
SPIV	: Stereo Particle Image Velocimetry
TC	: Thermocouple
3D	: Three Dimensional
2D	: Two Dimensional

CHAPTER ONE
INTRODUCTION

Designing for energy efficiency has become increasingly important in engineering applications in recent years. Governments and international organizations have acknowledged the significance of reducing energy consumption due to the depletion of energy resources and concerns about climate change. Specific regulations and standards have been implemented to regulate energy demand in the production and sales of household appliances. Many households are subject to strict regulations and standards. Governments and international organizations set energy efficiency requirements that appliances must meet to be sold in the market. These requirements often dictate the maximum energy consumption or specify specific efficiency ratings that appliances must achieve. Manufacturers of household appliances are now placing greater emphasis on the design and production processes to ensure compliance with energy efficiency standards. The company focuses on research and developing technologies that consume less energy and enhance the effectiveness of its products.

Laundry is essential to daily life as it ensures hygiene and comfort. However, drying clothes after washing is often time-consuming and energy intensive. To address this challenge, home appliance manufacturers have been working on the development of washer-dryer machines. These machines aim to minimize the required space, energy, and water consumption for drying clothes. The demand for high-performance and efficient washer-dryer products has been increasing steadily. Consequently, the design of an effective drying system has become of paramount importance in the industry.

This thesis study aims to enhance the thermal and aerodynamic design of the drying system in household-type washer & dryer machines. We aim to enhance the drying system's overall performance, ensuring it meets consumer demands and expectations more efficiently. To improve the performance of the dryer system; the airflow pattern created by the fan's operation inside the washer dryer machines, the condensation process inside the direct contact condensation unit, the heater unit design, and the dehumidification of a fabric inside the drum was investigated experimentally and

theoretically. The drying process and system components consisting of a centrifugal fan, heater, and condensation unit are numerically simulated by using the merits of the Computational Fluid Dynamics (CFD) method. Distinctly from the current literature studies, each constituent component is evaluated separately within the whole body of the drying system. The representative numerical model is established on the coupled heat and mass transfer process taking place inside a washer & dryer machine. The results of the CFD analysis are validated against the compiled data obtained from Particle Image Velocimetry (PIV) experimental method. It is seen that the numerical outcomes of the proposed mathematical model well-agree with the experimental data and comprehended that CFD-based analysis could be an effective solution for investigating the variational influences of different operational drying system parameters such as fan flow, heater channel design, condensation efficiency and laundry model in the design of the washer & dryer machine.

1.1 Literature

Removing water from a material such as vegetables, laundry, and chemicals is one of the most commonly used processes in the industry and household appliances. This dehumidifying process is also called drying, and the working principle of the drying system relies on the condensation process. Condensation is the most common phase change method used in the drying systems such as industrial drying, cooling towers, and household appliances. In this thesis, the dryer elements, and the dehumidification process of a household-type washer & dryer machine system are studied.

This study aims to conduct a numerical investigation of the phase change phenomena occurring in the condensing unit of a washer and dryer machine. This specific area of research has gained significance due to the growing utilization of washer and dryer machines in household appliances. The study aims to develop a mathematical procedure to accurately model and simulate the phase change processes within the condensing unit. The numerical investigation will utilize computational methods and simulations to analyse condensation, including the heat and mass transfer

phenomena. By employing numerical techniques, the study aims to gain a deeper understanding of the phase change behaviour and optimize the design and performance of the condensing unit.

The obtained numerical results will be compared against experimental data to ensure the mathematical procedure's accuracy. This comparison will verify the numerical model's reliability and predictive capabilities, ensuring that it accurately represents the real-world behaviour of the condensing unit in the washer and dryer machine. Overall, the study seeks to enhance our understanding of phase change phenomena in the condensing unit of washer and dryer machines through a numerical investigation and establish the accuracy of the developed mathematical procedure by validating it against experimental data.

In common usage, washer-dryer machines typically employ three types of condensation systems. One of these systems is an air-cooled condenser dryer with a heat exchanger unit. In this configuration, the dryer's humid and warm process air passes through a crossflow type condenser unit, where it is cooled down, and the moisture is condensed. In this heat exchanger, the surrounding air acts as the cooling medium. As the warm process air flows through the condenser unit, it releases its heat to the surrounding air, causing the heat to be transferred from the dryer to the environment. Consequently, this heat transfer process increases the temperature of the room where the washer-dryer machine is located.

The less common type of washer-dryer system is the heat pump cycle. Unlike air-cooled condensation dryers that utilize ambient air as a coolant, heat pump washer dryers employ a heat pump system. The system is composed of multiple components., including a compressor to pressurize the cooling fluid, a heat exchanger for the evaporation and condensation processes, and auxiliary pipelines to direct the refrigerant. In this system, the hot and humid air from the tumble is driven to the heat exchanger. The cold side, known as the evaporator, condenses the water vapor, which is drained away. The hot side, known as the condenser, reheats the air for reuse. By operating in this manner, the heat pump system retains heat within the dryer rather

than air being transferred to the surroundings. This allows for improved energy efficiency and conservation of heat within the system.

The third most applied (utilized) type of washer-dryer condensing system, also considered a configuration for the thesis study, is a water-cooled condenser. This system we are interested in in this study is based on a direct contact water cooling dehumidification process. While hot and humid air passes through this condensing channel, relatively cold water is injected directly into the process air. The coupled heat and mass transfer mechanism in the dehumidification process follows the principles of thermodynamics. The essentials of this mechanism and the working principles of the washer & dryer system will be stated in detail in Chapter Two.

First and foremost, extensive research is carried out for understanding condensation and phase change processes through experimental and numerical studies. Direct-contact condensation, utilized in various engineering applications like steam injectors and direct contact water heaters, has been mainly explored. To analyse the influence of nozzle size and shape on heat transfer, which plays a significant role in direct contact steam condensation, a hydrodynamic model was developed by Gulawani, Shah, RamaPrasad & Shukla (2006). Montazari, Blocken & Hensen (2015) examined the evaporative cooling mechanism in the water spray system and conducted an experimental validation to ensure the applicability of the numerical results of the developed CFD simulations. The study discussed the water spray investigation involving a complex two-phase flow. This analysis considers various factors such as the velocity and temperature patterns, relative humidity, characteristics of droplets, and interactions between the continuous phase and droplets and between droplets themselves. The dynamics and relationships within the system were presented in the mentioned study (Figure 1.1).

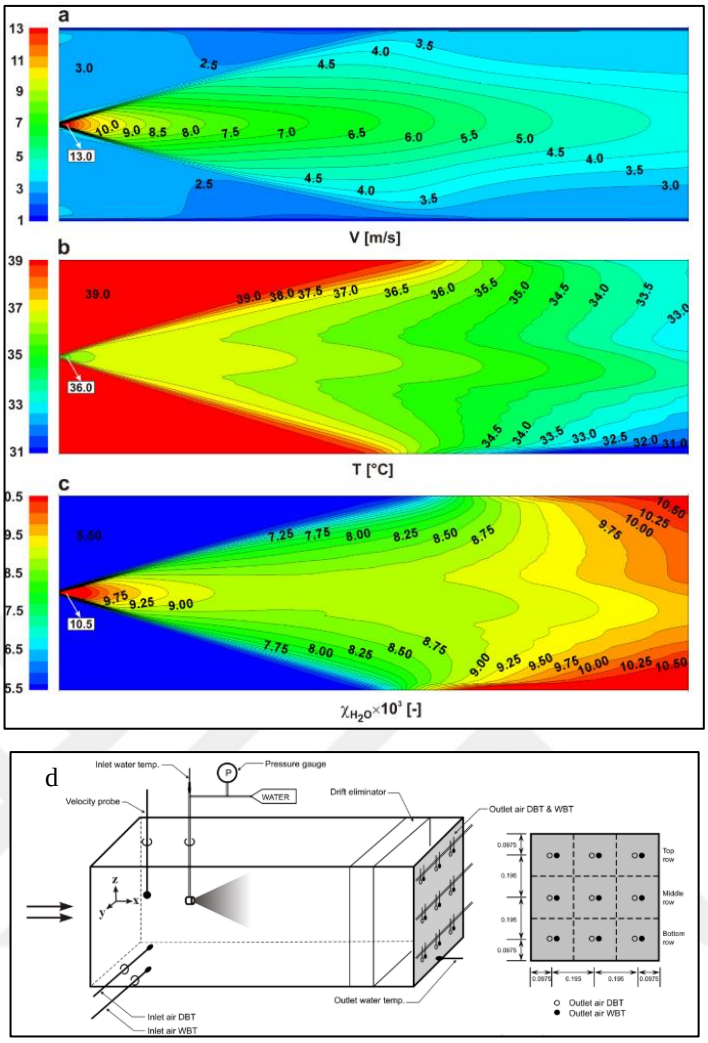


Figure 1.1 CFD results with cross section plots of a) air velocity; b) temperature c) vapour mass fraction in a wind tunnel model and d) experimental settings schematics (Montazeri. Blocken, & Hensen, 2015)

The study represents the culmination of many years of research conducted by Fletcher et al. (2006), specifically focusing on investigating the basic flow behaviour in dryers. The research aimed to understand the complex dynamics involved in dryer operation, particularly regarding the flow patterns within the dryer. The researchers developed a mathematical model using a commercial Computational Fluid Dynamics (CFD) code as part of their work.

In the study conducted by Apanasevich, Lucas, Beyer, and Szalinski (2015), a CFD-based strategy was presented for modelling two-phase flows involving heat and

mass transfer across a moving steam-water interface caused by direct contact condensation. The approach utilized the two-fluid phase-average model to simulate the flow behaviour and interactions between the steam and water phases. One significant aspect of the study was the thorough assessment of the mathematical modelling of two key parameters: the drag and waterside heat transfer coefficients. The drag coefficient represents the resistance to motion experienced by the phases, while the waterside heat transfer coefficient characterizes the heat transfer rate between the steam and water phases. By meticulously examining and refining the mathematical models for these coefficients, the study aimed to improve the accuracy and reliability of the CFD simulations for stratified two-phase flows with direct contact condensation.

Li, Wang, and Lu (2015) conducted simulations of the direct-contact condensation (DCC) process involving subsonic steam injection into a subcooled water pool. The study employed the Volume of Fluid (VOF) multiphase flow model and the Large Eddy Simulation (LES) turbulent flow model within the commercial Fluent software. These models allowed for accurately representing the complex interaction between the steam and water phases during the condensation process. Similarly, Zbicinski (1995) focused on developing and empirically verifying momentum, heat, and mass transfer models tailored explicitly for spray drying processes. The study aimed to enhance comprehension of the intricate relationship between droplets and the surrounding air and how heat and mass are transferred during drying.

Madejski, Kuś, Michalak, Karch & Subramanian (2022) conducted an extensive literature review focusing on experimental and numerical investigations conducted thus far on direct contact condensers. Their study aimed to explore the current scientific research and address the persistent challenges associated with direct contact condensation. The authors specifically analyzed and compared various numerical models developed to simulate the heat and mass transfer mechanisms involved in the condensation of fluids. Moreover, they highlighted significant experimental studies conducted on different types of direct contact condensers, which have had a notable impact on the field.

Researchers have shown significant interest in the direct contact condensation of steam on subcooled water droplets because of its multiple industrial applications. Gumruk and Aktas (2015) conducted a study to investigate the effects of different factors on heat transfer between air and subcooled water droplets in direct contact condensation. The study focused on exploring the variations in thermophysical conditions of the air, water spray flow rate, and spray configuration and how these factors influence heat transfer. Experimental results revealed that increasing the amount of liquid droplets increased the lateral area of water droplets. This increase in surface area enhanced the heat transfer rates between the air and water droplets. However, as more liquid droplets were introduced, the available humidity ratio in the process air decreased. In summary, the study's findings indicate that increasing the number of liquid droplets in direct contact condensation enhances the heat transfer rates by increasing the water droplet lateral area. However, this increase in heat transfer is accompanied by a decrease in the humidity ratio available in the process air.

The study conducted by Takahashi, Nayak, Kitagawa, and Murakoso (2001) focused on investigating the condensation heat transfer of saturated steam in a hollow cone spray of subcooled water. The research involved experimental and theoretical analyses in gaining insights into the heat transfer mechanisms occurring during the direct contact condensation of steam on the subcooled water spray. One notable aspect of the study was the use of smaller thermocouples with fast response times, enabling the researchers to obtain reliable temperature distributions in the spray's sheet and droplet regions. By measuring the temperature rise in the water spray, the researchers could compare it with predictions made by pure heat conduction models. The experimental results revealed that the measured temperature rise in the water spray was significantly higher than predicted by pure heat conduction models, both in the spray sheets and droplets. This finding indicated that the heat transfer mechanism during direct contact condensation of steam on subcooled water spray involved more complex phenomena beyond pure heat conduction (Figure 1.2).

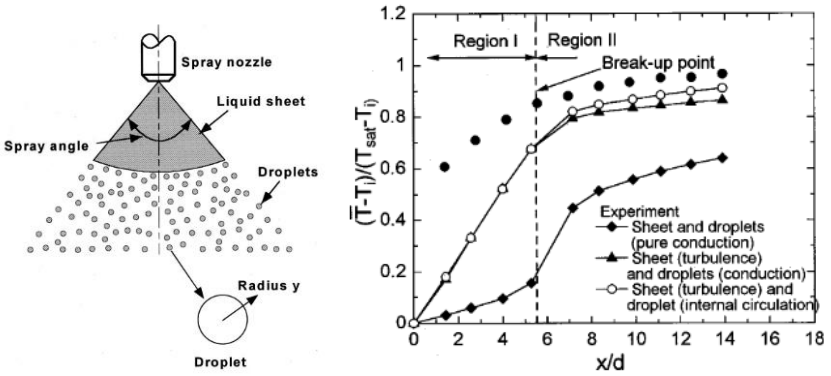


Figure 1.2 Variation of condensation efficiency in the flow direction for a hollow-cone spray (Takahashi, Nayak, Kitagawa & Murakoso, 2001)

A good deal of experimental studies on this issue has also been maintained through the years, supported mainly by a numerical background to verify the obtained experimental data. Lekic & Ford (1980) theoretically and experimentally examined the direct contact condensation of the moist air on the subcooled spray water. The study extensively examined the effects of drop size distribution and the characteristic motion of the drops on heat transfer efficiencies. Besides that, a mathematical model based on the acquired experimental data was proposed to obtain transferred heat between mediums. Lee & Tankin (1984) studied the behaviour of a subcooled water spray in a water-steam environment. Their research focused on understanding the characteristics of the spray, explicitly examining the length of the sheet region and the pressure drop in the liquid sheet. They discovered that these factors played a significant role in the contraction of the spray angle in the presence of non-condensable gases, contrary to the prevailing belief that the contraction was primarily due to the imposed drag on droplets. To better understand and predict the behaviour of the subcooled water spray, Lee and Tankin developed an empirical-mathematical model. This model aimed to estimate the breakup length of the sheet region, which was found to be influenced by dimensionless Weber and Jakob numbers. They could predict the breakup length by incorporating these dimensionless numbers into their model. Numerical results from the propounded mathematical model mostly agree with the experimental outcomes. Celata, Cumo & Farello (1989) performed experimental research focused on the direct contact condensation of saturated steam on subcooled liquid jets. During

their study, they identified deficiencies in existing literature correlations, particularly the inability to predict both the liquid jet's local conditions and the total heat transfer amount. These limitations prompted them to develop a new correlation to overcome these inherent drawbacks of the existing mathematical models. Comparison between the proposed model, former correlations, and experimental data showed that results are within acceptable limits. However, the experimental study only covers the laminar flow regime, and therefore the applicability of the developed mathematical model over the entire flow regime needs to be revised. Chavez & Mayinger (2019) and Chavez, Mayinger & Gebhard 2020) measured the development of subcooled spray droplets in a saturated vapor through the utilization of pulsed laser holography. Exact measurements strongly connected the saturated vapor pressure and spray geometry.

The drying- kinetics of laundry is also distinctly considered for the thesis study. The research conducted by Akal, Kahveci, Akyol, and Cihan in 2017 focused on investigating the drying kinetics of laundry, specifically cotton yarn bobbins. The study aimed to determine the optimal drying conditions in terms of drying time and energy consumption. The researchers conducted experiments to examine the effects of various drying parameters, including drying air temperature, pressure, and volumetric flow rates. They found that the minimum energy consumption occurred when using low drying air temperatures and pressures and moderate to high drying air volumetric flow rates. A semi-empirical model simulates the drying behaviour of cotton yarn bobbins. This model provided insights into the overall drying process and helped predict the drying time and energy consumption based on the selected drying conditions.

In another study, Johann, Siva, Lima & Pereira (2014) developed a mathematical model based on finite difference approximation to represent the convective drying process of textile materials. Simulation results were compared with experimental data which were obtained from the literature. They claimed that their proposed model has a %95 confidence interval. According to Johann et al. (2014), the main difference between their model is that they mathematically simulate the convective drying process of textile material without neglecting this transfer mechanism.

While only a few publications specifically focus on the washer and dryer machine drying system, significant literature is available on the theoretical and experimental analysis of the drying process within a tumble dryer. In one such study, Yadav & Moon (2008) proposed an empirical relation to predicting the overall performance of the dryer across different loads and ambient conditions. They conducted experiments using a typical tumble dryer model, employing a specific experimental setup as depicted in Figure 1.3. These tests aimed to assess the performance characteristics of the machine according to various standards while considering different operating conditions.

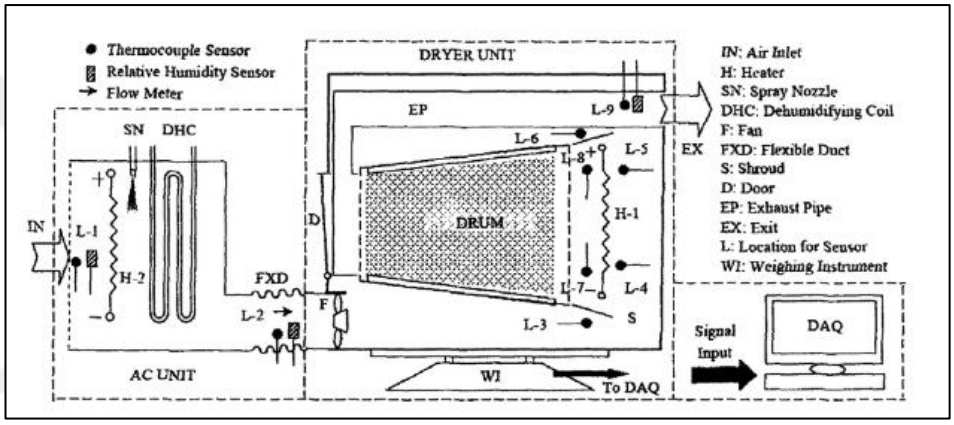


Figure 1.3 Schematics of a conventional air-vented dryer test set-up (Yadav & Moon, 2008)

COMSOL Multiphysics environment was utilized as an alternative design tool for modelling the stationary drying process inside a tumble dryer by Zeineldin (2008), and a 2D computer-aided design model of laundry was generated. This study modelled the good tendency for the moisture content change in agreement with the considered ideal drying profile (Figure 1.4).

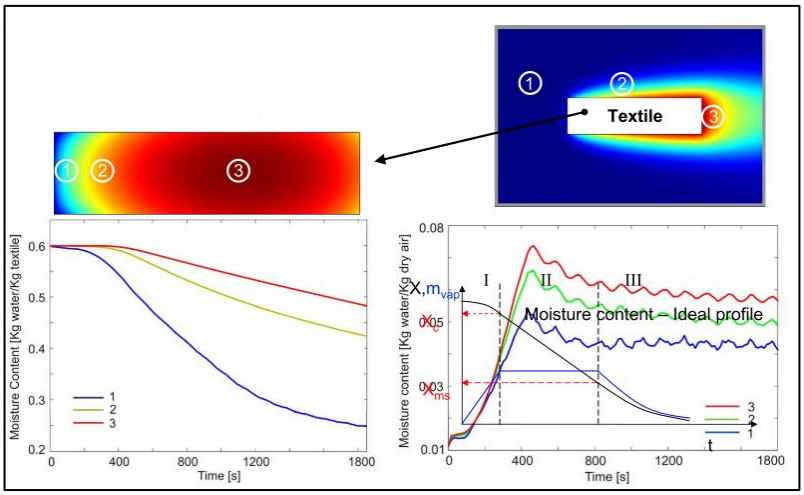


Figure 1.4 Moisture content difference of a 2D textile model (Zeineldin, 2008)

The main objective of research on textile drying is to develop techniques that reduce drying time and boost energy efficiency. By enhancing the smoothness of cotton fabric and minimizing energy consumption, businesses may preserve their worldwide competitiveness by improving the design and operation of current drying programs. In 2017, Wei, Hua, and Ding proposed a model to enhance the ability to predict fabric temperature and moisture content while drying under different typical settings. This aims to achieve better results during the drying process. As shown in Figure 1.5, these conditions in a household dryer comprise heater power, rotation speed, and air velocity. According to the study, the most significant variables influencing the rate at which clothes dry are heater power, air velocity, and rotation speed. The suggested modelling approach is a helpful tool for examining the effects of essential parameters on fabric drying efficiency since it considers the simultaneous movement of heat, mass, and momentum. This all-encompassing strategy enables researchers to optimize drying conditions, resulting in increased energy efficiency and improved fabric look. It also provides for a greater understanding of the drying process.

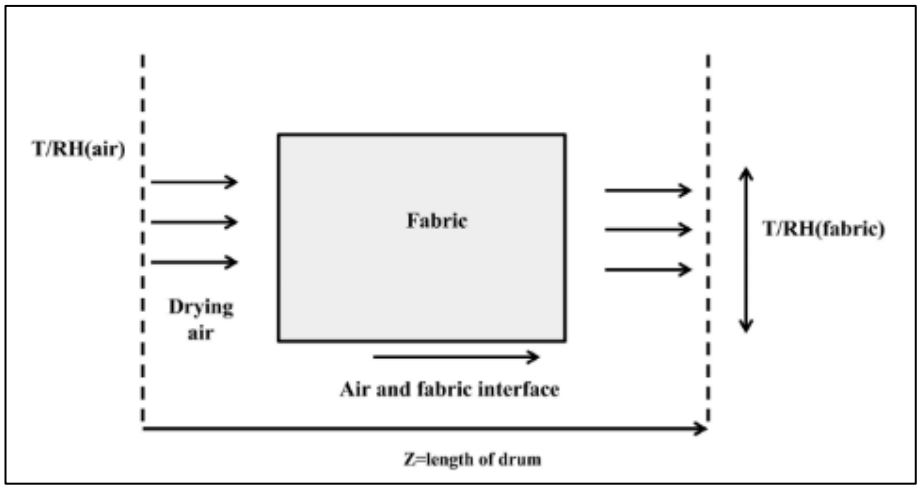


Figure 1.5 Schematic description of coupled heat and mass transfer inside the domestic dryer (Wei & Ding, 2017)

In the context of a washer & dryer machine, the centrifugal fans play a crucial role in the drying performance. They are used for directing the humid air to the condenser and then through the heater channel before ultimately blowing the drying air into the drum. Although there is a lack of specific articles discussing the centrifugal fans within washer-dryer machines, experimental and numerical studies are available that examine these fans as standalone components.

Radial fans take place in industrial applications in a very large spectrum ranging from air-conditioning to conventional clothes drying. The household-type washer-dryer machines have forward curved radial fans for circulating the process air through the heater and condenser unit to dry the clothes.

Due to the inherent complexity of the induced flow in centrifugal fans and their corresponding broad range of applications, they have been considered hot-spot research subjects by many literature studies. Forward curved winged, irregular flow centrifugal fans and their associated acoustic behaviour have been investigated numerically and experimentally by Younsi, Bakir, Kouidri & Rey. (2007). They determined that the irregular wing dimensions, fan blade number, and radial distance between fan circumference and fan housing significantly affect noise level and fan performance. As a result of this mentioned research study (Figure 1.6), a well-

established correlation was observed between the pressure fluctuations in the wall and the sound signals in the remote area.

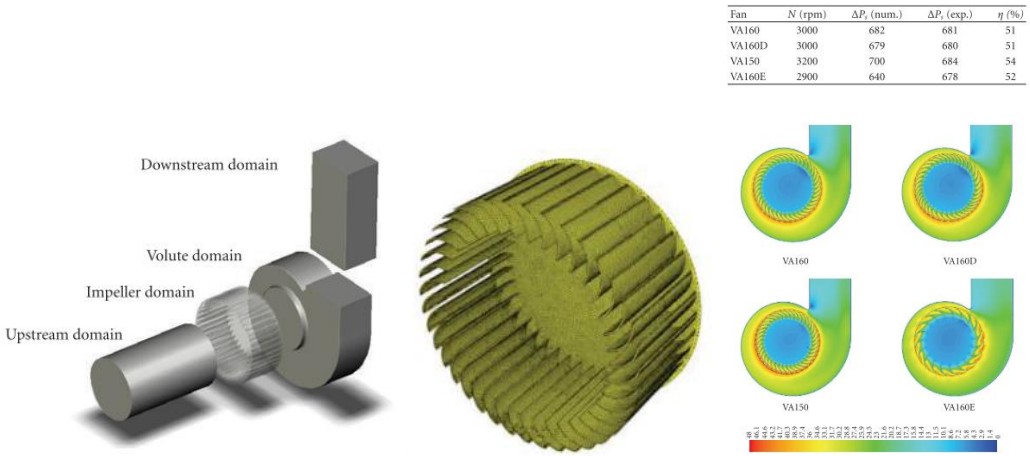


Figure 1.6 The centrifugal fan geometry and the velocity contours (Younsi, Bakır, Kouidri & Rey, 2007)

In a study conducted by Velarde-Suarez, Ballesteros-Tajadura, Hurtado-Cruz, and Santolaria-Morros (2006), they investigated the aerodynamic noise sources of a tilted winged centrifugal fan through experimental means. The researchers measured acoustic pressure at the outlet of the fan while varying the flow rates and pressure drops. Additionally, they also took measurements from specific points on the fan housing surfaces. The findings of the study revealed that the most significant source of sound originated from the interaction between the fluctuating air and the guiding tongue of the fan housing. This interaction occurred as the air was leaving the wings of the fan.

In another relevant study presented by Datong, Yijun, Xiaoliang, and Minjian (2009), their objective was to reduce noise levels in centrifugal fans. They compared the performance and sound characteristics of forward horizontal wing centrifugal fans and examined the similarities and differences with forward-tilted centrifugal fans described in the existing literature. The researchers designed various fan slot combinations with different geometries to evaluate the impact of the fan housing slope, fan blade opening, and intake and their effects on acoustic performance. Through their experiments, they found that both noise levels and performance could be improved. According to the study's findings, it was shown that by optimizing factors such as the

fan housing slope, fan blade opening, and intake, it was possible to achieve a reduction in noise levels while enhancing the performance of centrifugal fans.

Wernet (2000) studied the flow characteristics of a centrifugal fan through the Particle Imaging Velocity Measurement (PIV) method in the flow areas of fans in continuous and time-dependent conditions. Using this proposed method, the flow between the turbo engine blades in which the complex flow occurred is compared to the visualized Computational Fluid Dynamics (CFD) studies, and the turbulence intensity of the flow is determined.

The study by Siwek, Górski, and Fortuna in 2014 focused on investigating centrifugal fans' flow characteristics through numerical and experimental methods. The researchers evaluated the performance of the fan device by employing the finite volume method. The study aimed to document the real, physically correct impact of the internal flow structure on the operation conditions and performance of the centrifugal fan. Using numerical simulations and experimental measurements, the researchers were able to analyse the internal flow patterns and understand their influence on the fan's overall performance. The findings of the study likely provided valuable insights into the behaviour of centrifugal fans, enabling a better understanding of their internal flow dynamics.

PIV was discovered in the early 1980s as an efficient visualization technique for studying fluid flow fields. This non-intrusive method provides whole-field and quantitative measurements. The effectiveness of PIV in flow field studies led to its continued development and improvement over the next decade. Czernek et al. (2021) numerically investigated sedimentation tanks' two different modelling designs to remove fine particles from the rainwater. Numerical studies were conducted employing CFD modelling results and PIV measurements for varying operational flow rates. They concluded that the prevailing flow patterns vary across the tube length. They deduced that the PIV method is a promising non-destructive technique to verify the accuracy of the numerical results obtained from CFD simulations.

Gabi, Dornstetter, and Klemm (2003) conducted one of the initial studies using a PIV-based solution procedure to investigate a Cross Flow Fan (CFF) flow. This study demonstrated the applicability of PIV in analysing the flow characteristics of CFF. Additionally, the research indicated that PIV could serve as a reliable tool for proving the CFD data. The findings of this study highlighted the value of PIV in understanding and analysing flow behaviour in CFF systems. Furthermore, it demonstrated the potential of PIV as a means to validate numerical simulation results, helping to ensure the accuracy of computational models in predicting flow characteristics in similar systems.

Kumlutaş, Karadeniz, and Kuru (2013) and Karadeniz, Kumlutaş, and Özer (2013) focused on investigating the behaviour of cross-flow fans within a split air conditioner. These studies employed a combination of CFD and Stereo Particle Image Velocimetry (SPIV) methods. In the CFD study, the researchers used SPIV as a validation tool to evaluate the precision of the CFD results. They could assess the reliability of the computational model in predicting the flow characteristics of the cross-flow fans by comparing the experimental SPIV measurements with the numerical results from CFD simulations. The experimental part of the research involved using the SPIV method to investigate the entire outflow area of the split air conditioner. This investigation was conducted layer by layer to obtain a three-dimensional (3D) average flow profile. By analysing the SPIV data, the researchers could comprehend the fan's complex flow patterns. The CFD and SPIV methods provided an approach to studying the behaviour of cross-flow fans in a split type air conditioner indoor unit. The validation of CFD results using SPIV measurements and the 3D flow visualization from SPIV contributed to a better understanding of the fan's performance and helped improve the design of the system.

1.2 Literature Survey Summary

My Master Thesis study entitled "Numerical Study of Heat Transfer Performance on the Air Side of Evaporator for Split Air Conditioning Systems" focused on investigating the heat transfer performance of the air side of the evaporator in a three-dimensional model of a split air-conditioner indoor unit. The study employed Computational Fluid Dynamics and Heat Transfer (CFDHT) analyses to determine the air-side heat transfer performance of the heat exchanger. In order to create an accurate simulation, several factors were taken into account during the modelling process. These factors included the geometry of the cross-flow type fan, the air volume between the two fin sections, and the characteristics of the ambient air. By considering these aspects, it is aimed to achieve the most realistic simulation possible. To validate the numerical simulation results, a comparison was made with conventional measurement techniques and Particle Image Velocimetry (PIV) method measurements. These measurements were conducted at the outlet of the air-conditioner indoor unit. The objective of this comparison was to assess the agreement between the numerical and experimental results. The findings of the study indicated that the numerical results obtained from the CFDHT analyses aligned well with the measurements obtained from the conventional and PIV methods. The results exhibited a coherent pattern within the acceptable range of error limits. This agreement between the numerical and experimental results suggests that the numerical simulation accurately represented the heat transfer performance on the air side of the evaporator in the split air-conditioner indoor unit.

Overall, that Master Thesis study demonstrated the successful application of numerical simulation techniques to analyse the heat transfer performance of the air side of an evaporator in a split air conditioning system. The consistency between the numerical and experimental findings provides confidence in the accuracy of the simulation and its ability to capture the real-world behaviour of the system. In light of that compiled knowledge and according to the literature research's estimation, the usage and reliability of CFD analysis were concluded for household appliances' heat transfer and flow performance determination.

Flow characteristics in the water-cooled condenser of a washer dryer machine were experimentally and theoretically investigated. The limited focus of literature studies on solving both heat transfer and fluid flow analysis of household appliances together with CFD methods was identified.

In this thesis study, flow characteristics and the governing heat transfer mechanism that occurred in the considered household appliances will be investigated by means of CFD codes, considering phase change phenomena. In case of the incapability of the computational fluid dynamics codes for simulating the common conditions, additional auxiliary codes will be developed by using the features of user-defined CFD codes or utilizing the merits of other available options for simulations.

As mentioned in the literature in strongly, CFD methods are very successful in understanding the nature of the complex characteristics of flow systems. It can be comprehended from the exhaustive literature survey that research studies regarding the current topics dealt with in this thesis mostly carried out two-dimensional and partial analyses of system components. The deficiency of comprehensive studies in the existing literature addresses the simultaneous analysis of heat transfer, fluid flow, and dehumidification processes using CFD. While individual aspects of these processes have been extensively investigated, there is a noticeable gap in research that considers all three phenomena together. According to literature research, for washer-dryer machine drying performance evaluation, the necessity of three-dimensional CFD analysis of the drying unit, which involves a centrifugal fan, heater channel, and direct contact condensation unit, was concluded. To address this gap, researchers must develop integrated models and simulation approaches that effectively account for the interactions between heat transfer, fluid flow, and dehumidification processes. This may entail advancements in numerical methods, turbulence models, and the representation of phase change and moisture transport. Experimental validation studies would also be essential to verify the accuracy and reliability of the developed models.

Namely, unlike other past studies, this thesis study deals with the concurrent evaluation and discussion of three-dimensional heat transfer, forced convection fluid flow, and spray-type condensation analyses, including phase-change phenomena, to determine the optimum washer-dryer machine system design and drying performance.

1.3 Aim and Motivation

The vertical architecture and rapid increase of urban density limited the living space of houses at metropoles worldwide. Architects, designers, and engineers are trying to develop new technologies to provide basic needs and comfort in such small volumes. Urban life became an important issue that it finds a place in the sustainable development goals of the European Commission (Goal 11: Make cities and human settlements inclusive, safe, resilient, and sustainable).

One of the substantial basic needs in daily life is laundry. It is crucial for hygiene and life comfort. It is also one of the most volume-consuming processes in the house. Especially the drying process needs a large area. If it is done inside a room, it takes a long time because of the need for more airflow and increases the room's humidity. Additionally, it has an anti-aesthetic effect which generally depresses people if it takes place in the living quarter. Last but not least, this process has high energy and water consumption.

White Good companies have been developing washer-drier machines to overcome these issues, and they try to handle this process with minimum volume, energy, and water consumption. In this responsibility awareness, this research work was initially and partially supported by the Republic of Turkey Ministry of Industry and Trade and partly supported by the Vestel White Goods Company with the 00998.STZ.2011-2 encoded SANTEZ project. We gratefully acknowledge this support for the start of this study. All entire original and up-to-date work has been carried out within the scope of the Ph.D. thesis study.

CHAPTER TWO
WASHER & DRYER MACHINE DRYING PRINCIPLE

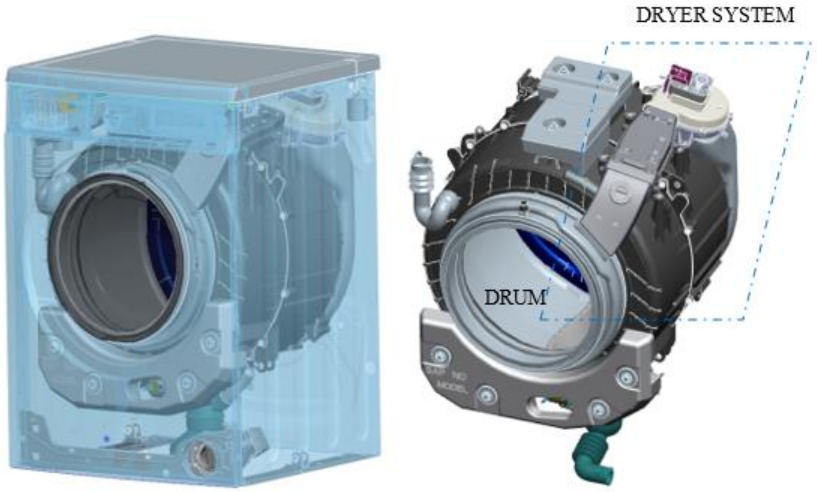
2.1 Condenser Type Washer & Dryer System

One of the common applications of drying technology is removing the inherent moisture from porous fabrics such as clothes. This study focuses on enhancing the design and performance of a commercial washer-dryer machine drying system shown in Figure 2.1. Drying technology plays a crucial role in this application, and the aim is to meet customer demands and expectations by improving the efficiency and effectiveness of the system.



Figure 2.1 Washer & Dryer system (commercial model)

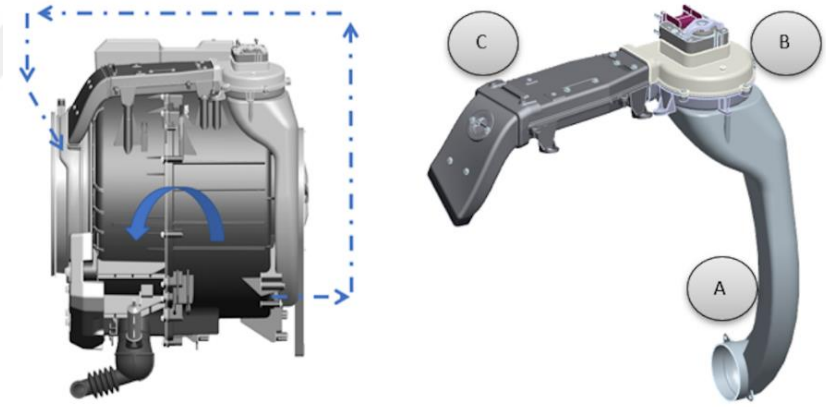
The system at hand has a closed-loop drying principle, as shown in Figure 2.2 and Figure 2.3, accompanied by a water-cooling condenser.



a. b.

Figure 2.2 a) Washer & Dryer machine construction b) dryer system assembly

Components of the drying systems are briefly expressed in Table 2.1 and Figure 2.3.



a. b.

Figure 2.3. General graphical representation of the a) washer & dryer machine and b) dryer unit

Table 2.1 Components of the drying unit

Location in Figure 2.3	Associated section in the system
A	Condenser
B	Fan
C	Heater Unit

The dehumidification process takes place in the condenser channel, as shown in Figure 2.3-b. During the drying process, the fan absorbs the air from the drum and passes through the condenser. The air moisture is taken by the cooling water.

In order to supply the required heat and increase the air volume, the dehumidified air is heated by means of a resistance-type heater. The heated process air is blown inside the drum where clothes are kept. Finally, the extracted moisture is thrown away from the system by the drain.

2.2 The Condensation Process

Condensation is one of the most common phase change phenomena frequently occurring in drying systems. Drying, which aims to eliminate moisture from a material, is a commonly employed process in various daily life applications and is known to consume a significant amount of energy. Among different drying technologies, drying porous fabrics like clothes hold great significance. Therefore, it is crucial to highlight a combined heat and mass transfer mechanism that governs the drying and phase change processes occurring in the condenser section of the entire system.

Under normal conditions, the air contains varying levels of water vapor, and its capacity to hold water is influenced by temperature. Heated air has a higher water-holding capacity against cold air. When the air reaches its maximum capacity to hold water vapor at a specific temperature, it becomes saturated. If the air temperature decreases further, reaching the saturation point, it is called the dew point. When the temperature reaches a specific point, known as the critical temperature, the air becomes saturated and cannot hold any more water vapor. If the temperature decreases beyond this point, the excess water vapor will begin to condense into liquid water. The quantity of water vapor that condenses is equivalent to the surplus vapor beyond the air's 100% Relative Humidity (RH) at its new temperature. Consequently, when warm air encounters colder air or a cold surface, the warm air is cooled, causing its temperature to decrease to a level where it can no longer retain all the water vapor it contains.

Therefore, some of the water vapor condenses and forms liquid water through a process known as condensation.

During a simple cooling process, as air is cooled, its specific humidity remains constant. Since the cooler air's moisture-holding capacity is reduced, its relative humidity increases. Dehumidification involves reducing the relative humidity of the air while maintaining a constant dry bulb temperature. This process is drawn on a psychrometric chart in Figure 2.4. The cooling process is typically shown as a diagonal line from the initial condition to the final condition, while the dehumidification process is depicted as a vertical line. The chart allows visualization and analysis of the changes in temperature, humidity, and other properties of air during these processes. The cooling and dehumidifying process is also plotted on the psychrometric chart in Figure 2.4.

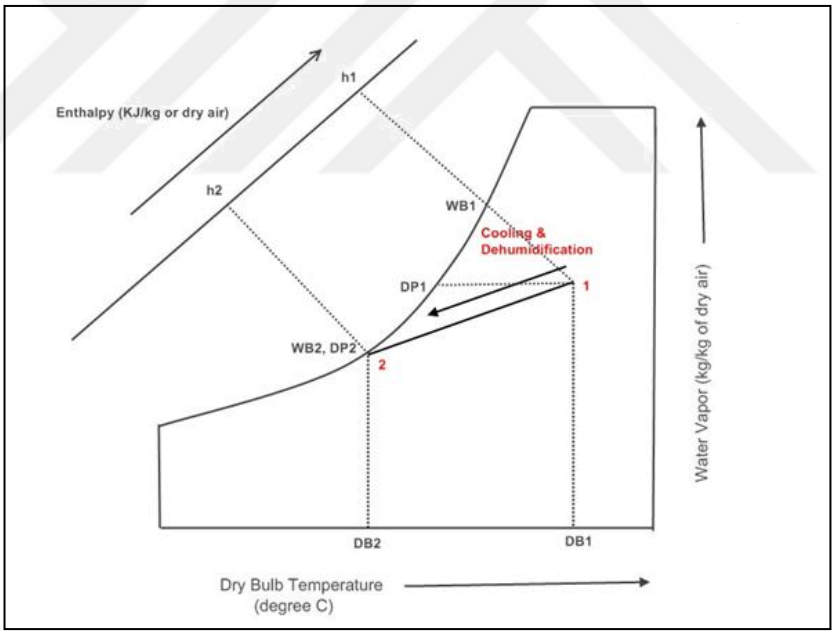


Figure 2.4 Psychrometric chart representing the cooling with dehumidification process

Water vapor at the dew point becomes a multi-phase fluid where condensation begins, and moist air interacts with the water spray, schematically shown in Figure 2.5, which increases the total mass of the water droplet that occurred through the condensation process.

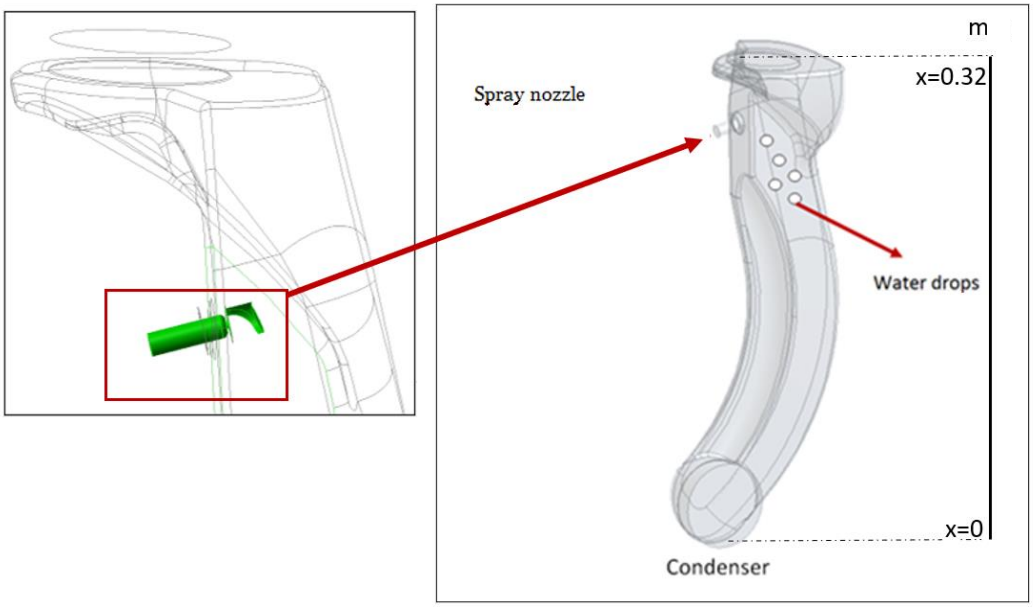


Figure 2.5 3D model of the condenser part and spray nozzle

Considering the influence of the water spray having an initial speed and temperature, the moist air will be cooled down until the incipience of the dew point, whose schematic representation is shown in Figure 2.6 through the line directed from point 1 to point 2.

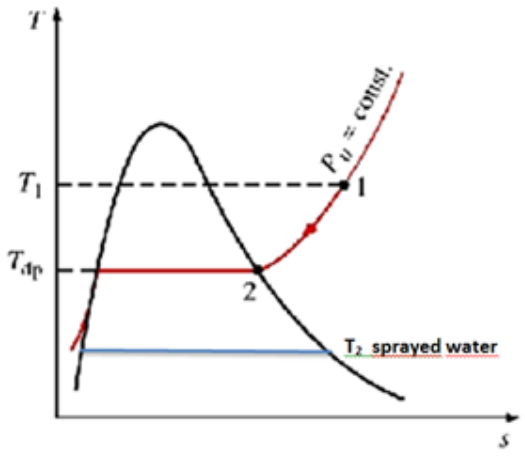


Figure 2.6. Moist air and sprayed water T-s diagram (Çengel, Boles, *Thermodynamics*, 3th edition)

A wet cooling tower operates as a semi-enclosed system that utilizes the principles of direct contact condensation. It serves as a practical example of this process. The tower works by introducing warm water from a condenser at the top and spraying it into an airstream within the tower. The spraying motion enables direct contact between water and air, facilitating efficient heat transfer. Some of the water droplets evaporate while falling, leading to the cooling of the remaining water. This process of direct contact condensation transfers the heat from the warm water to the surrounding air. As a result of this combined heat-mass transfer mechanism, the air becomes hotter and more humid. The cooled water is collected at the bottom of the tower and recirculated back to the condenser, where it absorbs additional waste heat. Therefore, wet cooling towers demonstrate the principles of direct contact condensation and effectively function as evaporative coolers. The energy and mass balance equations are given in Table 2.2.

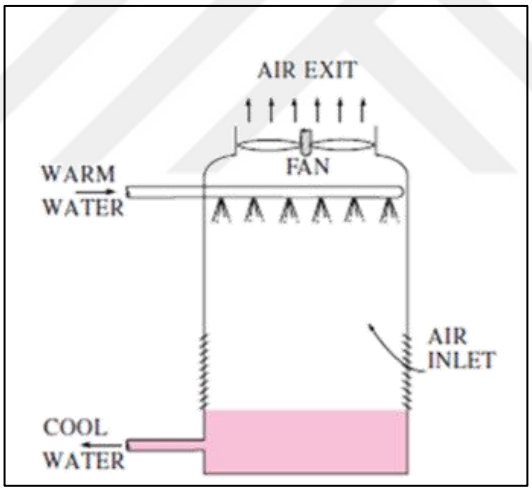


Figure 2.7 An induced-draft counterflow cooling tower (Çengel, Boles, *Thermodynamics: An Engineering Approach*, 5th edition)

Table 2.2. Mathematical model representing the energy and mass balance equations for the cooling tower:

Mass Balance of Air
$\sum \dot{m}_{a,in} = \sum \dot{m}_{a,out} = \dot{m}_a$
Mass Balance of Water
$\sum \dot{m}_{w,in} = \sum \dot{m}_{w,out}$ $\dot{m}_{w,in} + \dot{m}_{a,in}.\ \omega_{a,in} = \dot{m}_{w,out} + \dot{m}_{a,out}.\ \omega_{a,out}$
Total Energy Balance
$\dot{E}_{out} - \dot{E}_{in} = 0$ $\sum \dot{m}_{out} h_{out} - \sum \dot{m}_{in} h_{in} = 0$ $\dot{m}_a \cdot h_{a,out} + \dot{m}_w \cdot h_{w,out} - \dot{m}_a \cdot h_{air,in} - \dot{m}_w \cdot h_{w,in} = 0$ $\dot{m}_a = \frac{\dot{m}_w (h_{w,in} - h_{w,out})}{[(h_{a,out} - h_{a,in}) - (\omega_{a,out} - \omega_{a,in}) . h_{w,out}]}$

2.3 Numerical and Experimental Study Strategy for the Entire Drying System

The complete system works under the principles of a closed-loop drying equipped with a water-cooling condenser. The dehumidification occurs in the condenser channel. During dehumidification, the air is absorbed from the drum through the fan and sucked into the condenser. A schematic diagram of the Washer-Dryer system is given in Figure 2.8.

A comprehensive analysis of the components within a household-type washer-dryer machine system, including a centrifugal fan, a heater, and a condensation unit, is presented in this study. In contrast to existing literature, this study evaluates these system elements in the dryer unit. The aim is to investigate the drying process

commonly encountered in domestic and industrial systems using the Computational Fluid Dynamics (CFD) method. All system components involved in the dehumidification process of a washer-dryer machine, as listed in Table 2.3, will be numerically modelled. The CFD analysis results will be validated through experimental data obtained from Stereo Particle Image Velocimetry (SPIV), conventional measurement methods, and qualitative visualization techniques. By combining numerical and experimental approaches, this study aims to present a complete understanding of the drying process within a washer-dryer machine system.

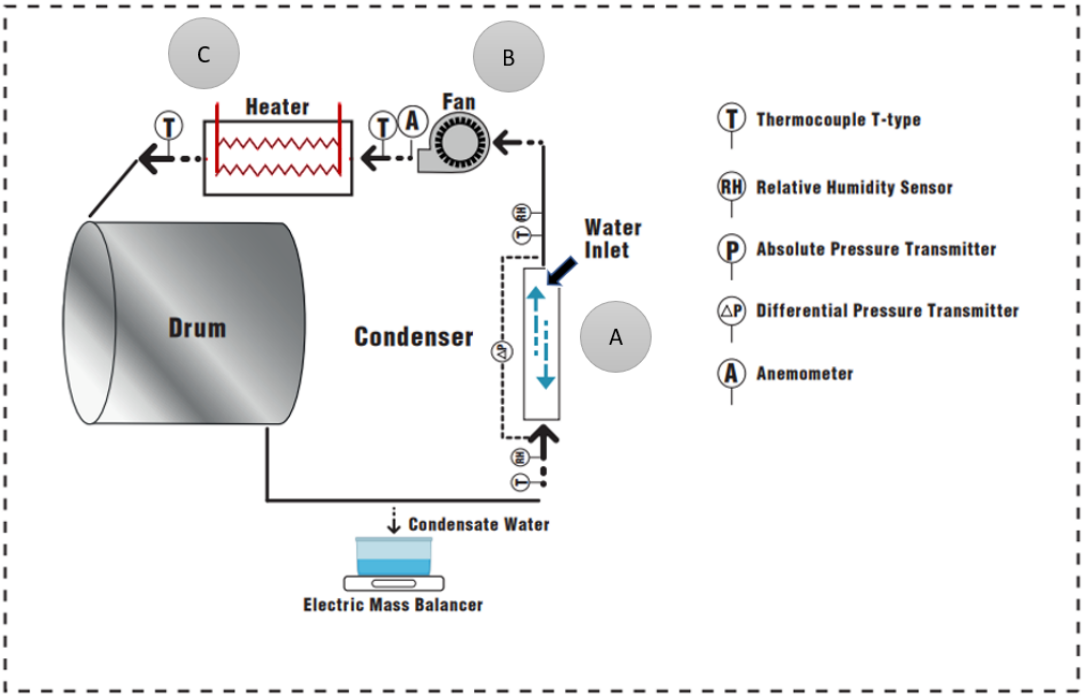


Figure 2.8 Schematic diagram of Washer-Dryer system

Table 2.3 Numerical model and validation methods table

Location in Figure 2.7	Section	Simulation method	Experimental method
A	Condenser	Flow analysis / CFD	Qualitative Visualization
B	Fan	Flow analysis / CFD	SPIV
C	Heater Unit	Thermal & Flow analysis / CFD	SPIV & Thermocouples

CHAPTER THREE
HUMIDITY MEASUREMENTS INSIDE THE SYSTEM

The temperature of the air without considering its moisture content is known as the dry-bulb temperature. It is measured along with the corresponding relative humidity at both the condenser's entry and exit points. This is done to analyse and evaluate the heat and mass transfer effectiveness within the condenser.

Relative humidity and temperature at the condenser entry and exit are measured to determine condensation performance. The weight of the clothes inside the drum, the rate at which moist air moves through a system. and the rotating fan speed are also meticulously measured to investigate the mass transfer in the washer-dryer drum in which forced convection dominates the air circulation.

3.1 Mathematical Modelling of Specific Humidity

In the literature, the specific humidity of air is calculated by the below equation. This is the ratio of water vapor to dry air.

$$\omega = \frac{m_v}{m_a} \tag{3.1}$$

Specific humidity of air can also be alternatively expressed as:

$$\omega = \frac{m_v}{m_a} = \frac{\frac{P_v \cdot V}{R_v \cdot T}}{\frac{P_a \cdot V}{R_a \cdot T}} = \frac{R_a}{R_v} \cdot \frac{P_v}{P_a} = 0.622 \frac{P_v}{P_a} \tag{3.2}$$

Total atmospheric pressure is expressed as the sum of partial pressures of air and water vapor by following equation:

$$P_{atm} = P_a + P_v \tag{3.3}$$

By rearranging equation, specific humidity can be modified in such a way:

$$\omega = 0.622 \frac{P_{atm} - P_a}{P_a} \quad (3.4)$$

Thermal properties of the process air are calculated by the set of equations given in Table 3.1. Based on the operating conditions of the inlet and outlet streams.

Table 3.1 Governing equations for process air

Governing mathematical formulations for the process air
$P_{v,air} = \varphi_{air} \cdot P_{g,air}$ $P_{air} = P_{atm} - P_{v,air}$ $v_{air} = R_{air} \frac{T_{air}}{P_{air}}$ $\omega_{air} = 0.622 \frac{P_{v,air}}{(P_{atm} - P_{v,air})}$ $h_{air} = C_{p,air}(T_{air}) \cdot T_{air} + \omega_{air} \cdot h_{g,air}$
Thermophysical properties of air
$R_{air} = 0.287 \frac{kPa \cdot m^3}{kg.K}$ $C_{p,air} = C_p(T_{air})$

3.2 Experimental Evaluation of the Condenser Performance

In the experimental studies, follow-up tests have been performed to simulate the dehumidification mechanism inside the condenser and convert the governing equations into a feasible mathematical model. The number of tests has been increased to ensure the effectiveness of the developed model. Dehumidifying operation realized by the direct contact condensation occurring inside the condenser unit has been examined by the two distinct humidity probes (Figure 3.2 and Table 3.2), which are placed at the input zone of the condenser and above the water spray nozzle at the outlet zone of the condenser as shown in Figure 3.1.

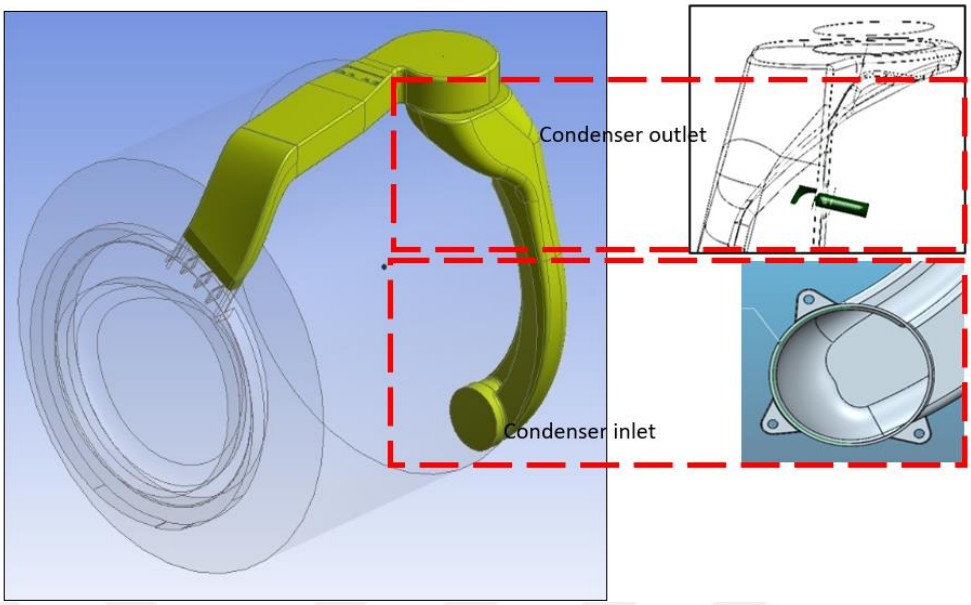


Figure 3.1 Condenser channel inlet and outlet zones

Then, the condenser unit where heat and mass transfer occur is isolated with an isolation material to maintain reliable experimental conditions, as shown in Figure 3.2.

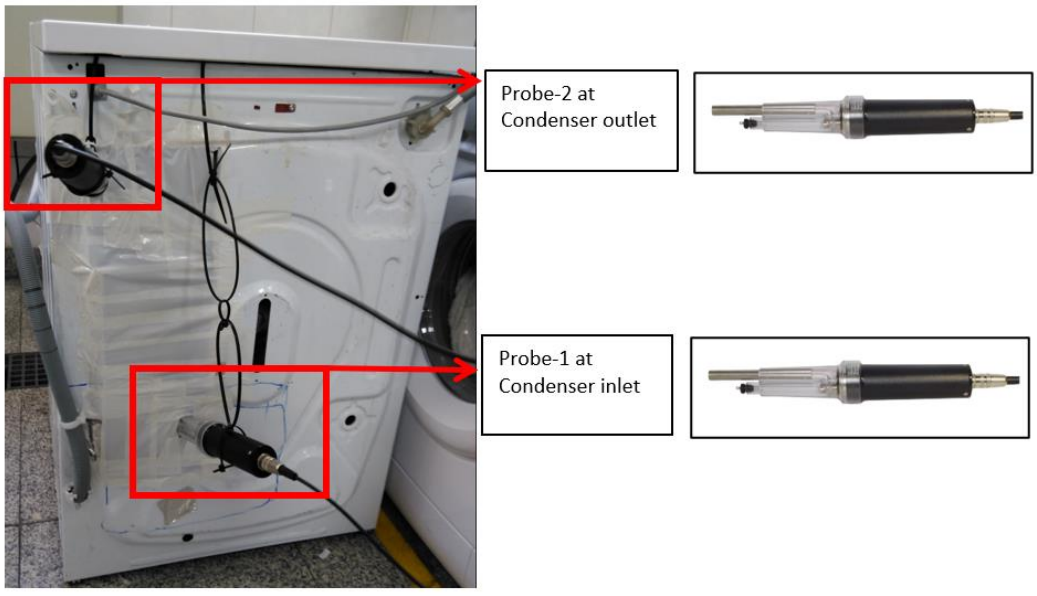


Figure 3.2 Placement of the humidity probes for simultaneous humidity measurement inside the condenser at inlet and outlet zones (Personal archive, 2012)



Figure 3.3 ALMEMO FNAD 46 handy held psychrometer type humidity probe and technical specification

Table 3.2 Handy held psychrometer type humidity probe technical specifications.

Technical Name/Code	**ALMEMO FNAD 46**
Operating temperature	0 to 60 ˚C (no ice)
Humidity measuring range	10 to 100 % RH
Measuring system	psychrometric
Accuracy	± 1 % RH under nominal conditions
Accuracy in measuring range	10... 100 % RH: typ.± 1 % RH. at 25 ˚C ±3K, 1013 mbar
Nominal conditions	at 25 ˚C ±3K, 1013 mbar, 50 % RH
Temperature sensor accuracy	2 x NTC type N ±0.2 K at 0 to 60 ˚C

To obtain the experimental inputs, absolute humidity, temperature, and pressure change tracking tests were performed during a special drying program cycle. Thermo-anemometer probes, humidity probes, test panels, and data loaders were used for these measurements. The amount of the inlet and outlet water was also measured for verification. The test machine was placed onto a weighing device to avoid incorrect measurements as shown in Figure 3.4.



Figure 3.4 Test setup for washer & dryer machine (Personal archive, 2012)

Firstly, absolute humidity data were taken from the condenser inlet and outlet during a one-hour drying program for comparison. To simplify the algorithmic procedure in the drying software, we prepare a trial algorithm that contains only the heater, fan, and valve activation. The air dry bulb temperature, wet bulb temperature, relative Humidity, and total pressure with respect to time were simultaneously obtained with two different humidity probes at the condenser inlet and outlet zones. According to the collected data, absolute Humidity and saturation pressure were calculated.

Absolute Humidity, often known as Humidity, is the volume of water vapor in a specific air sample. The unit of measurement is typically grams of water vapor per kilogram of dry air. The relationship between the moisture content of dry air at a given temperature and the moisture content of moist air at that same temperature is expressed

by relative Humidity. 100% RH indicates the dew point has been reached, while 0% RH denotes dry air with no moisture content.

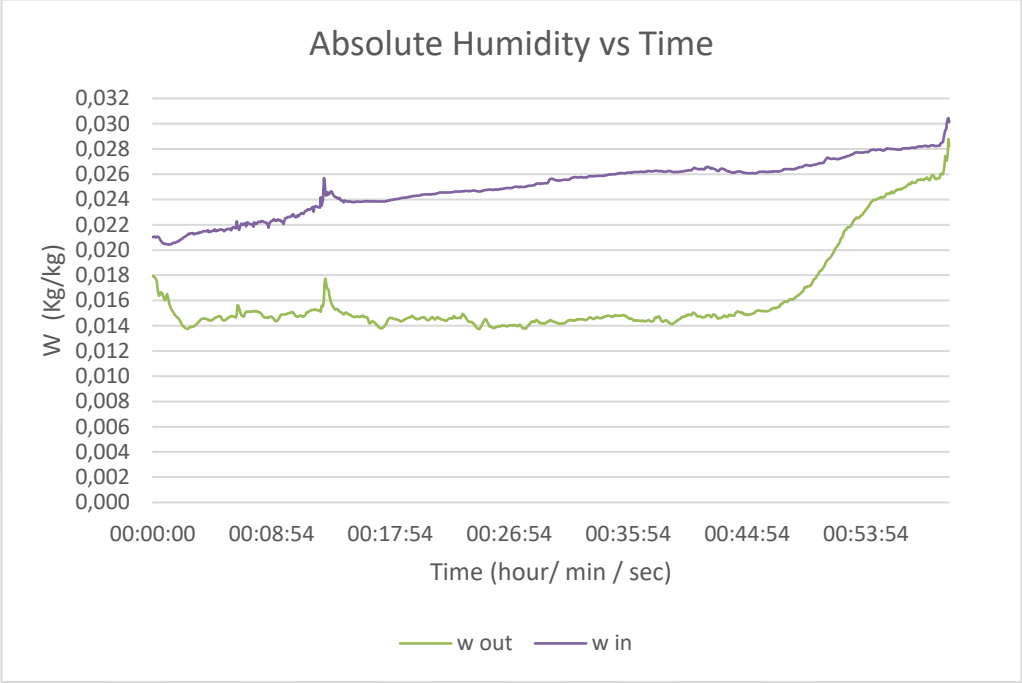


Figure 3.5 Absolute humidity measurements at condenser inlet and outlet during the one hour drying program

Through the retrieved data, as shown in Figure 3.5, time-dependent variation of the relative humidity was evaluated, and it is observed that effective drying can only occur in the last minutes of the drying cycle, which theoretically reaches the 100% relative humidity range on the psychometric chart. Depending on the activation timespan of the spray nozzle, at the exit of the condenser, moist air reaches 100% relative humidity under the influence of the water spray. One can conclude from the observed time-varying inclinations of the experimental data set that a considerable amount of energy and water consumption could be avoided within a profitable time range if an efficient dehumidification regime in which the process air reaches 100 % relative humidity.

The complete system works under the principles of a closed-loop drying equipped with a water-cooling condenser. The dehumidification occurs in the condenser channel, as shown in Figure 3.1. During dehumidification, the air is absorbed from the drum through the fan and sucked into the condenser. The moisture content of the air is

maintained at a level desired by the designer. During the drying cycle, moisture content can vary depending on the capacity of the washer-dryer system, the load size, the load type, and the desired dryness level. For these variations, designers should apply special algorithms (fan flow rate, drum rotation, heater set temperatures, water valve activations, etc.) according to their know-how.

Various experimental tests with different operational conditions have been performed to comprehend the influences of the design parameters of the drying program on the condensation performance as summarized in Table 3.3. Different valve and heaters activations combinations have been varied during the experimental tests. Then, corresponding test results have been compared and evaluated from different points of view.

Table 3.3 Varying experimental conditions for the comparative study

	Test - 1	**Test - 2**	**Test – 3**	**Test - 4**	**Test - 5**
Duration	1 Hour	1 Hour	1 Hour	1 Hour	1 Hour
Spray Water Activation	Continuously ON	Continuously OFF	Valve activation with the software control	Continuously OFF	Continuously OFF
Heater-1 Activation	Continuously ON	Continuously ON	Continuously ON	Continuously ON	Continuously OFF
Heater-2 Activation	Activated with the control of NTC	Activated with the control of NTC	Activated with the control of NTC	Continuously OFF	Continuously OFF
Fan Activation	Continuously ON	Continuously ON	Continuously ON	Continuously ON	Continuously ON

In all tests, relative humidity measurements have been realized just above the spray nozzle. Theoretically, this psychometric process is concerned with removing the available moisture from the process air to a degree as the air temperature falls under the dew point and reaches to %100 relative humidity. These compiled test data account for the essentials of heat and mass transfer mechanism that removes the available amount of moisture from the clothes during the drying circuit. During the one-hour drying cycle, absolute and relative humidity level changes were considered depending on the temperature and water spray activations.

Absolute humidity data taken respectively from the condenser inlet and outlet were comparatively evaluated during the dehumidification process to effectively investigate the amount of energy and water consumption and influencing operating conditions. Furthermore, the outcomes of these test cycles provide meaningful insights to the end-users as to when and how the drying process should be terminated.

3.2.1 Test 1: Spray Water is Continuously On

In the first test condition, the spray water valve and fan were continuously activated during the test. One of the two heaters was continuously active, and the other one was controlled with the NTC. NTC is a negative temperature sensor that measures the air temperature. Employing NTC and software control, heaters activation can be set. In this specified test condition, the water activation effect on the dehumidification process by means of relative humidity, absolute humidity, and temperature measurements were investigated, which are shown in Figure 3.6 and Figure 3.7 during the one-hour trial drying program.

During the initial stages of the experiments, the process air entering the condenser reaches its dew point. However, the relative humidity at the condenser outlet decreases to a minimum value of 55%. This decrease is followed by an increase in relative humidity due to the increased intensity of water spray activation. When the drying process simulation finished, the outlet's relative humidity reached around 93%. On the other hand, the process air at the condenser inlet experiences a rapid increase initially, followed by a stagnation phase caused by the influence of active heaters. The operating air temperature at the condenser exit exhibits a negligible increase throughout the drying experiments, as depicted in Figure 3.6. The absolute humidity gap between the condenser outlet and inlet initially increases for the first forty minutes and then follows a decreasing trend, as shown in Figure 3.7.

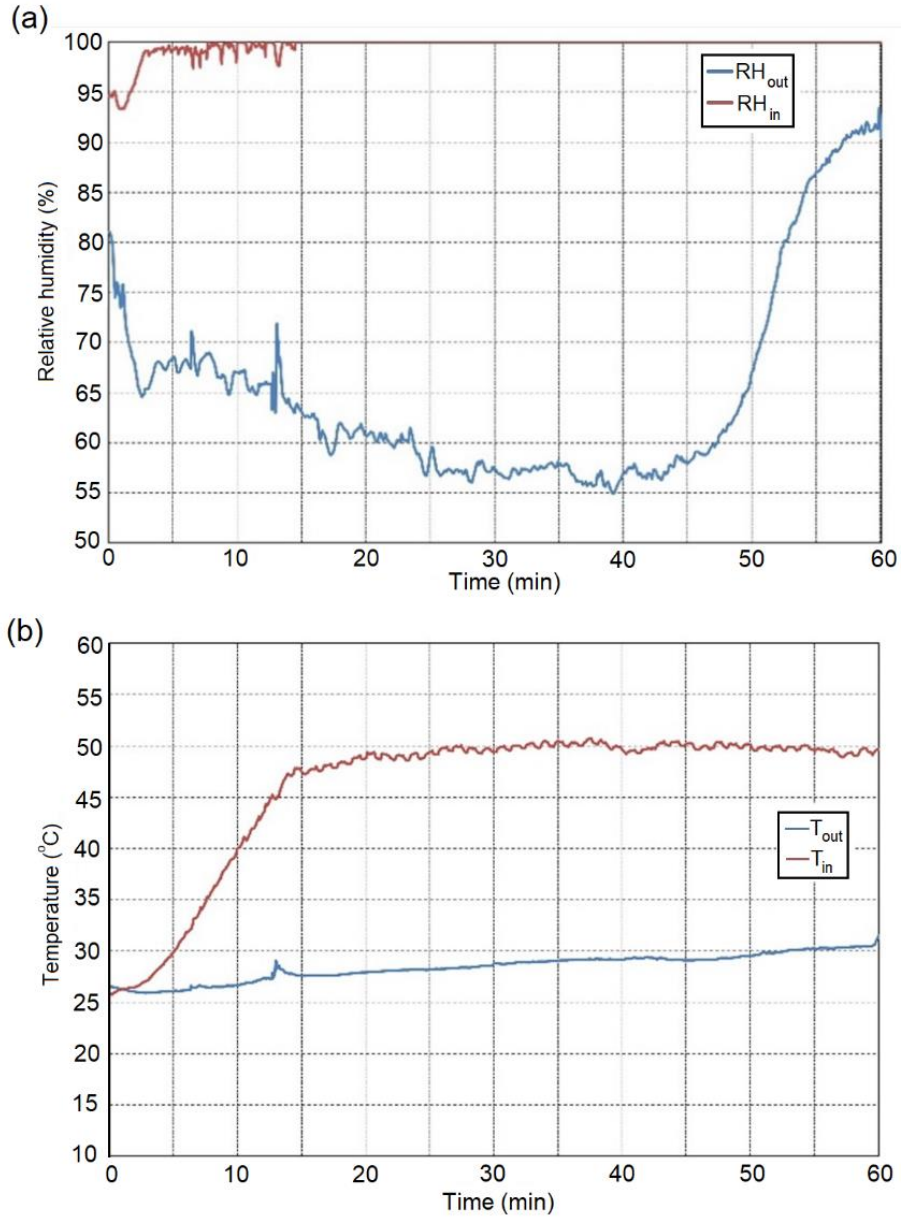


Figure 3.6 a) Relative humidity and b) temperature measurements for Test-1

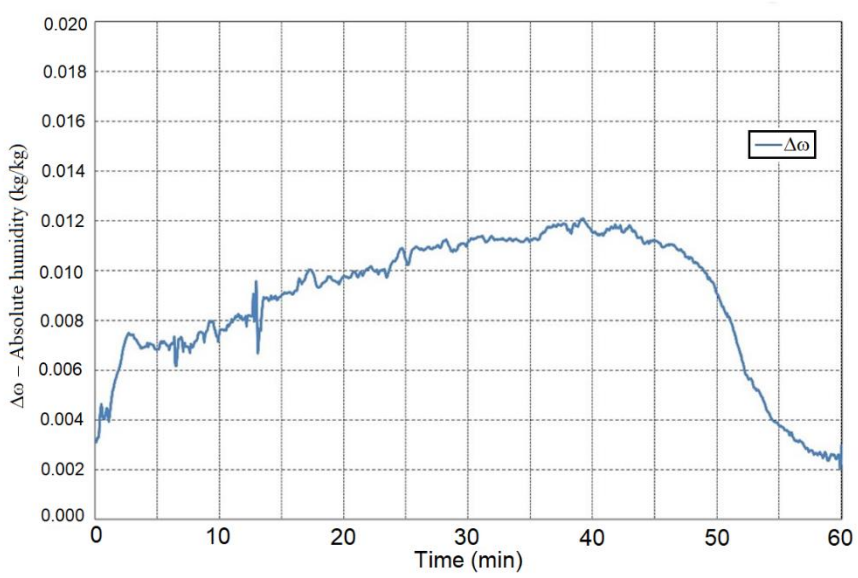


Figure 3.7 Absolute humidity measurements for Test-1

3.2.2 Test 2: Spray Water is Continuously Off

In the second test condition, contrary to the experimental conditions of the first test, spray water was deactivated while fans and heaters were still active. Operational conditions prepared for this experiment data aim to investigate the time-varying inclinations of design variables when spray water is deactivated. The second test condition analysed the impact of not using water during dehumidification. Figure 3.8 and Figure 3.9 illustrate the measurements of relative humidity, absolute humidity, and temperature throughout the one-hour drying program. During the initial two minutes of the drying tests, the process air reaches its dew point. The relative humidity of the process air decreases for the first fifteen minutes, after which the humidity rates start to increase and eventually become saturated after forty-five minutes of drying time.

The variations in these operational parameters significantly influence the changes in absolute humidity rates between the condenser inlet and outlet. There is a noticeable increase in absolute humidity differences between the condenser outlet and inlet, followed by sharp decreases during the drying experiments. These variations highlight the impact of not using water during dehumidification on drying.

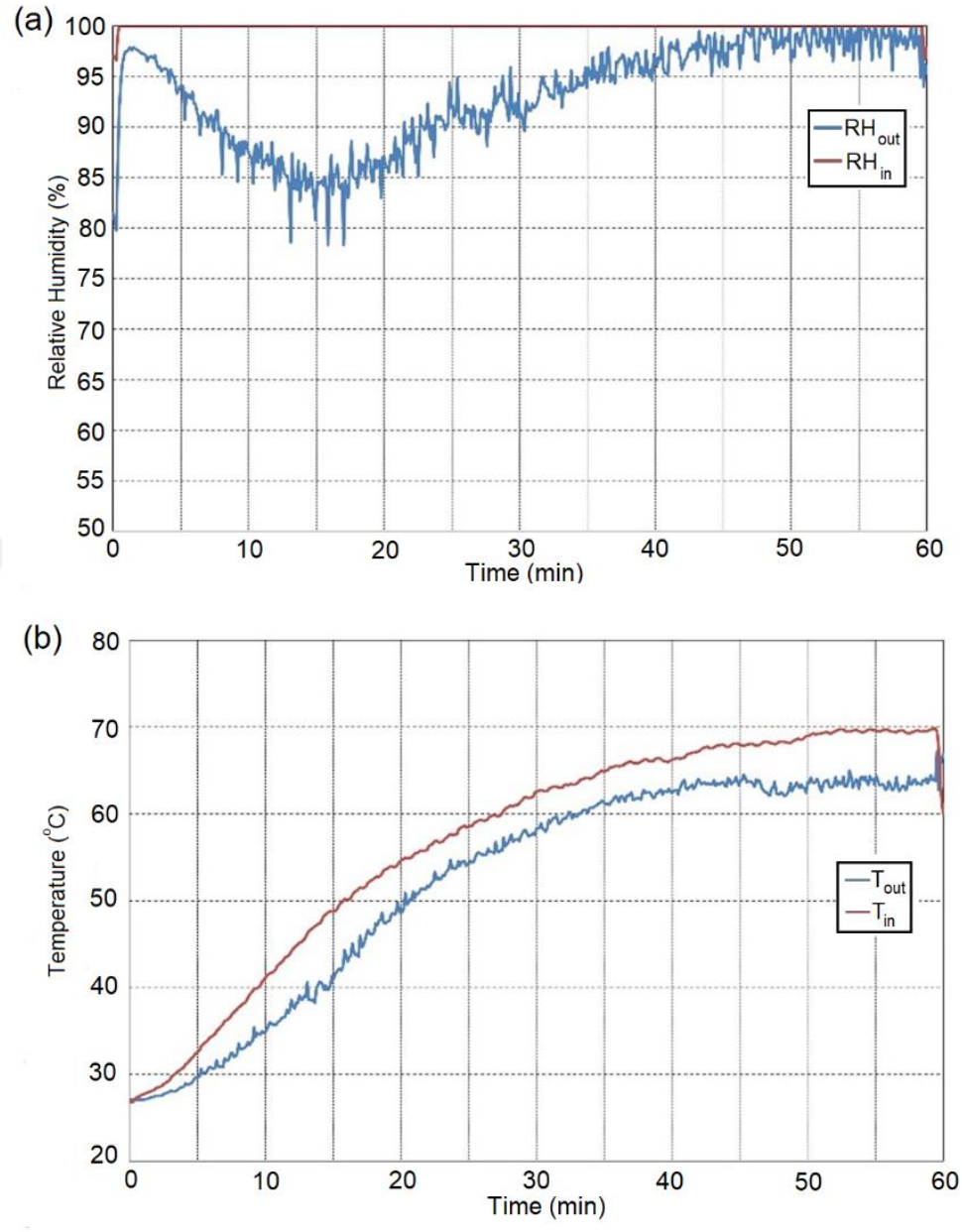


Figure 3.8 a) Relative humidity and b) temperature measurements for Test-2

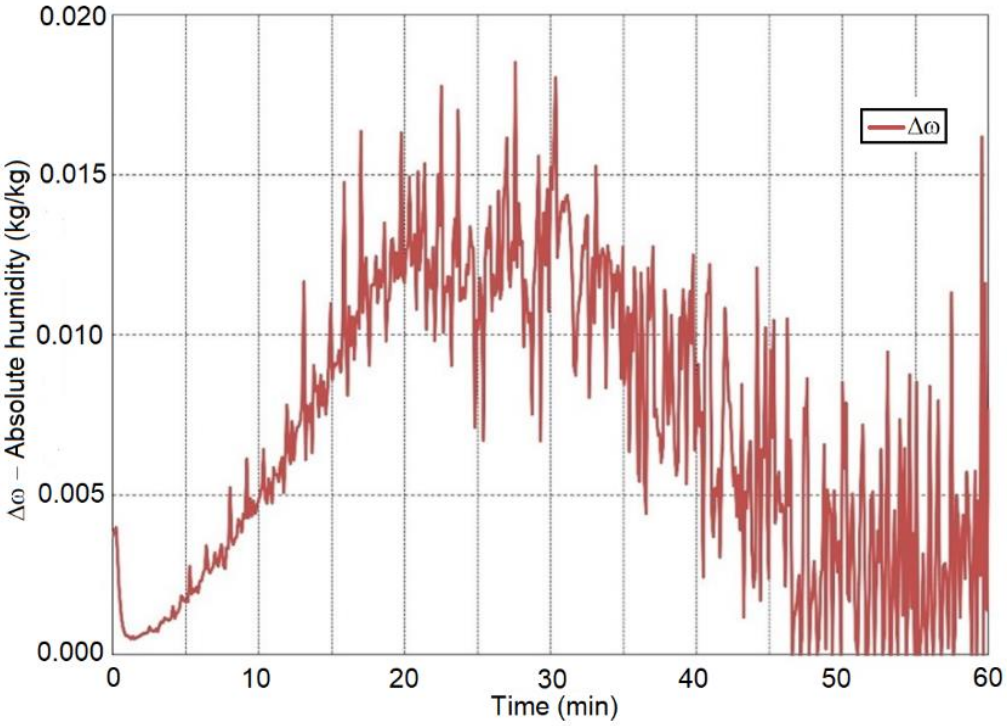


Figure 3.9 Absolute humidity measurements for Test-2

3.2.3 Test 3: Spray Water Valve Activation is Alternately On & Off

In the third test combination, the spray water is initially activated for 15 seconds, followed by a deactivation phase of 65 seconds. This periodic switching between water spray activation and deactivation continues until the end of the experiments under consideration. The other design parameters remain the same as in the first and second experiments.

Figure 3.10 and Figure 3.11 show that similar relative humidity and working temperature measurements are obtained compared to the operational conditions of Test-1 and Test-2. These results indicate that the periodic activation and deactivation of the water spray do not significantly affect the relative humidity and working temperature profiles, which remain consistent with the previous test conditions.

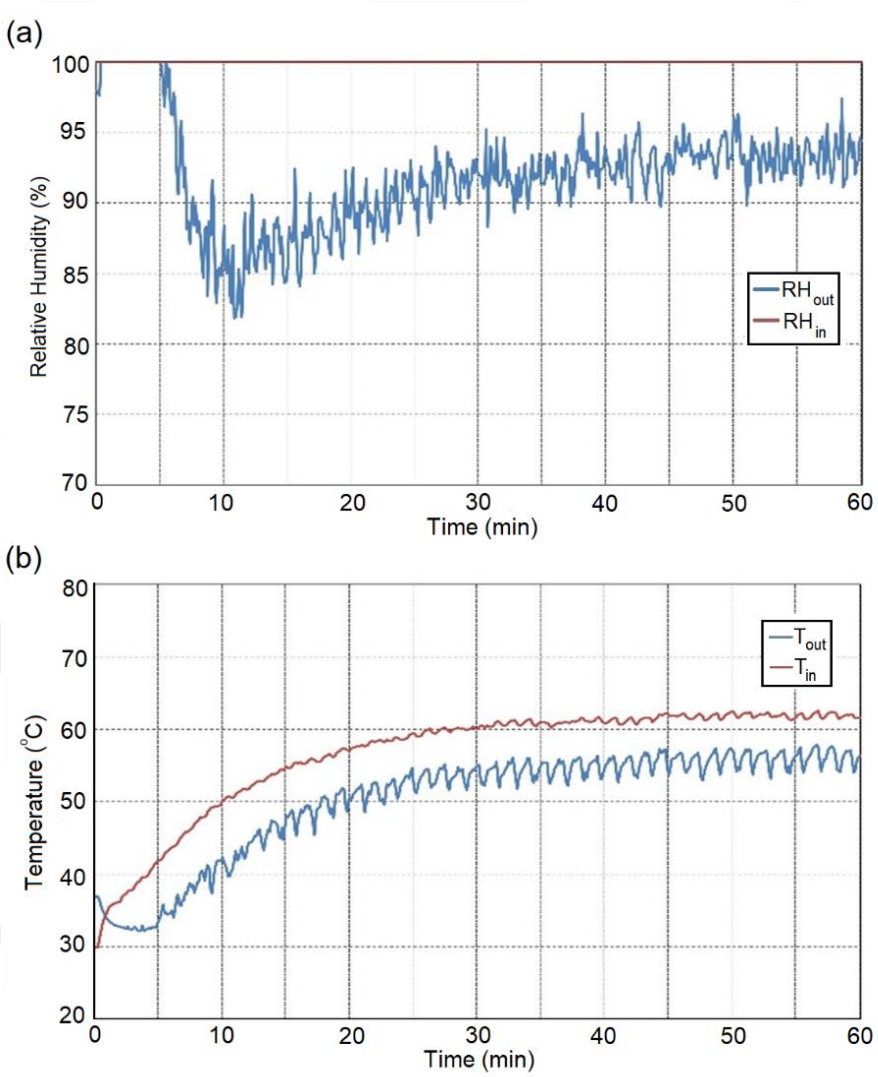


Figure 3.10 a) Relative humidity and b) temperature measurements for Test-3

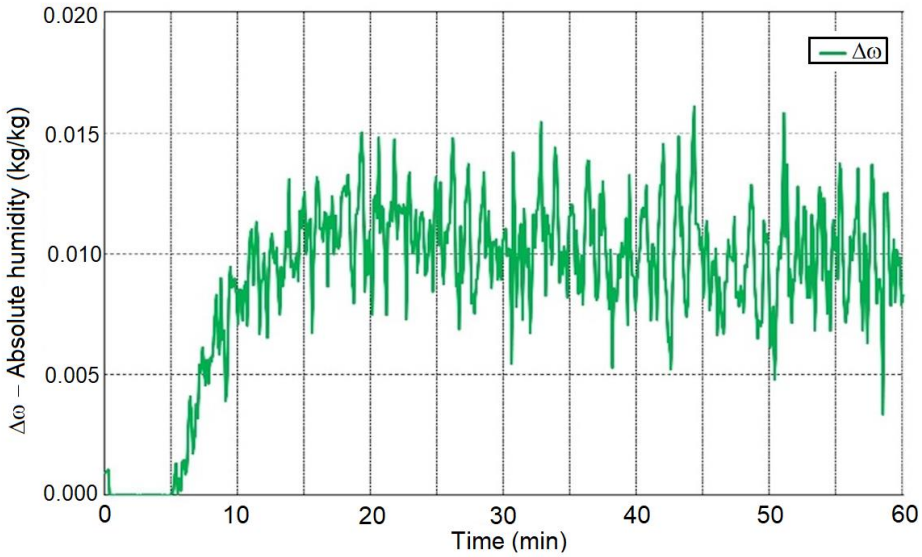


Figure 3.11 Absolute humidity measurements for Test-3

3.2.4 Test 4: Spray Water and One Heater are Simultaneously Off

The experimental results of the first three test conditions highlight the importance of water utilization in the dehumidification process. However, finding the right balance in water consumption is crucial, as using excessively or not using water at all can have significant consequences.

Only one heater is activated in the fourth test condition, while the water spray remains deactivated throughout the experiment. This setup is designed to observe the variations in working temperatures and relative humidity rates. Figures 3.12 and 3.13 depict the measurements of relative humidity, absolute humidity, and temperature. It is observed that the relative humidity rates at the condenser outlet decrease as the elapsed time increases. Meanwhile, the operation temperature of the process air shows an increasing trend at both the inlet and outlet of the condenser. This increase in temperature contributes to a significant change in absolute humidity between the condenser inlet and outlet. These findings highlight the influence of operating conditions on the relative humidity and temperature profiles during the dehumidification process.

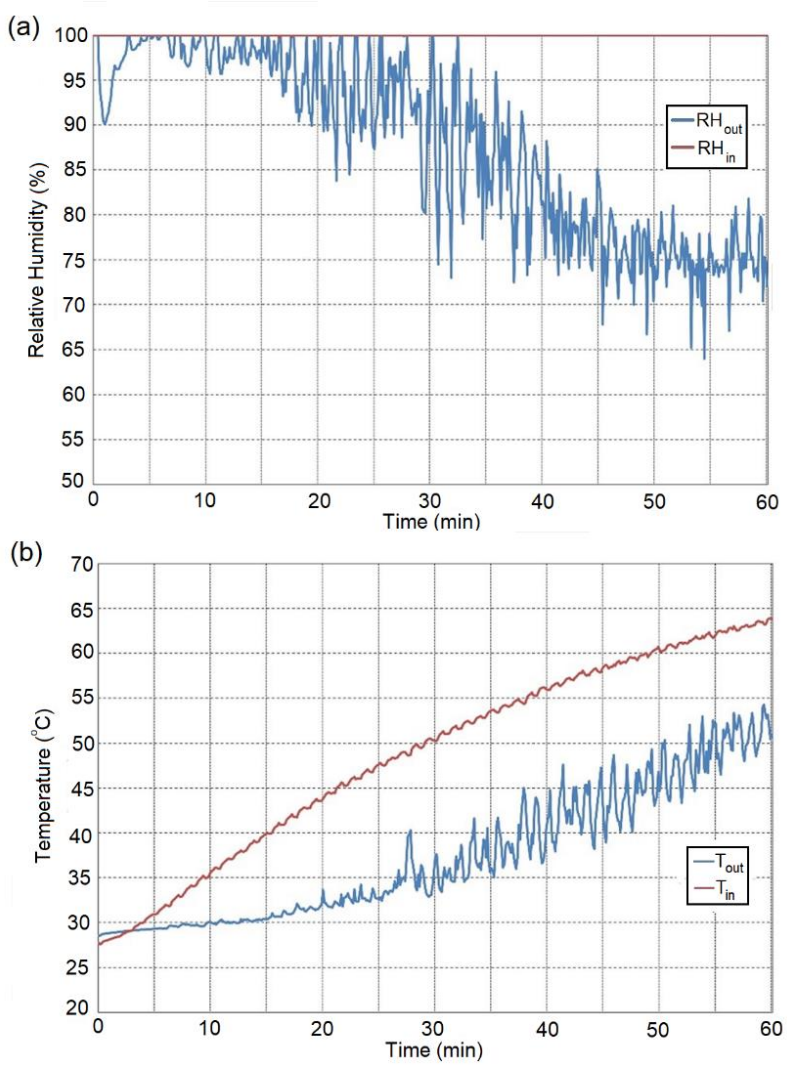


Figure 3.12 a) Relative humidity and b) temperature measurements for Test-4

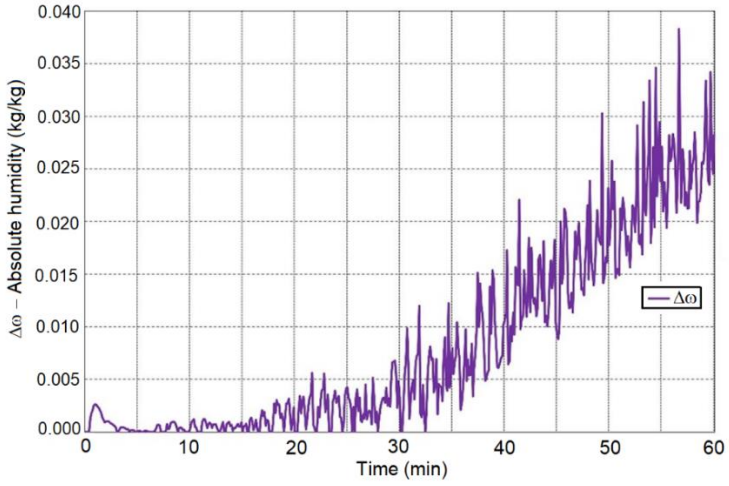


Figure 3.13 Absolute humidity measurements for Test-4

3.2.5 Test 5: Spray Water and Heaters are Simultaneously Off

In the fifth and last test condition, the focus is on observing the effect of fan flow on the total dehumidification performance of the system. Only the fan is activated, while other operational parameters remain deactivated. As given in Figure 3.14, the relative humidity rates at the condenser inlet show a slight increase throughout the experiment's duration. The relative humidity of the outlet process air exhibits an increasing trend and approaches its dew point with unpredictable fluctuations.

During experimental tests, the temperature of the process air decreases initially at the condenser inlet and outlet, followed by stepwise increases. Regarding the absolute humidity, Figure 3.15 shows that the absolute humidity at the condenser outlet is higher than that at the condenser inlet for the first 30 minutes of the experiment duration. These observations shed light on the influence of fan flow on relative humidity, temperature, and absolute humidity profiles during the dehumidification process.

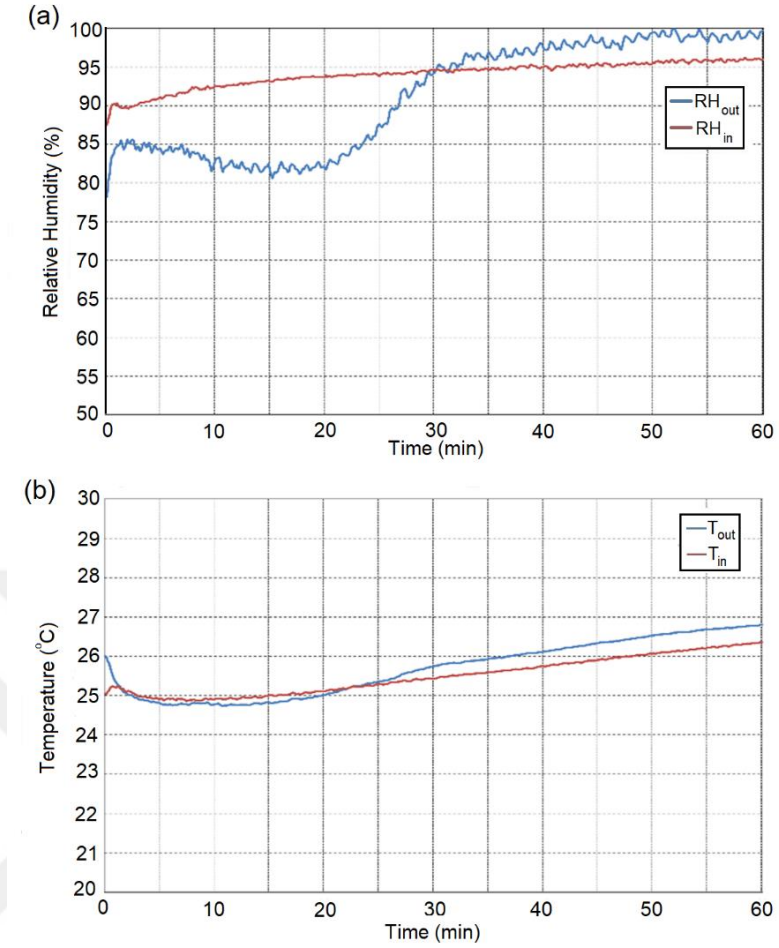


Figure 3.14 a) Relative humidity and b) temperature measurements for Test-5

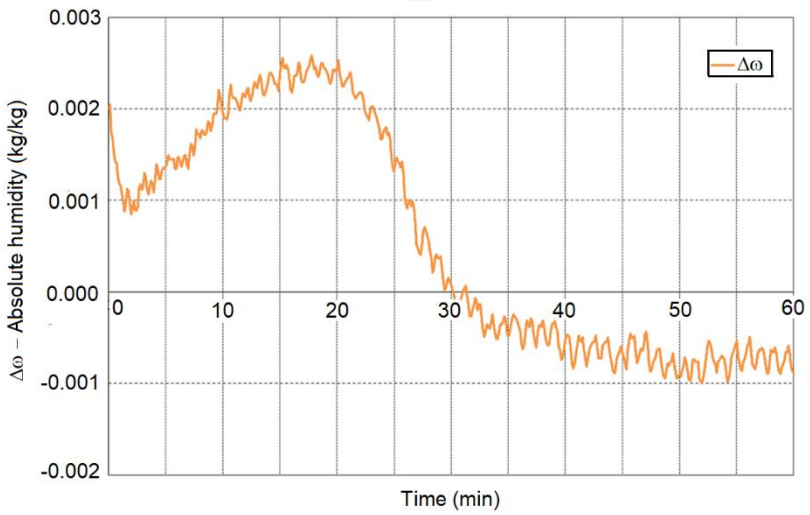


Figure 3.15 Absolute humidity measurements for Test-5

The absolute humidity measurements obtained from the inlet and outlet of the condenser are used to assess the performance of the dehumidification used in the water-cooled condenser. These data provide valuable insights into the drying system's water and energy consumption rates. Additionally, the absolute humidity data can serve as a reliable indicator to determine when the drying process can be concluded. By analysing these measurements, one can assess the efficiency of the dehumidification system and make informed decisions regarding the duration of the drying process.

The experimental results of Test-3 are based on the actual algorithm. However, it is seen that the efficiency of the data could be better and more feasible than that of Test-4 due to the outcomes of the combination tests. As seen from the comparison chart (Figure 3.16), more efficient dehumidification software could be developed if a novel algorithm is built upon the combination of the Test-3 and Test -4 results.

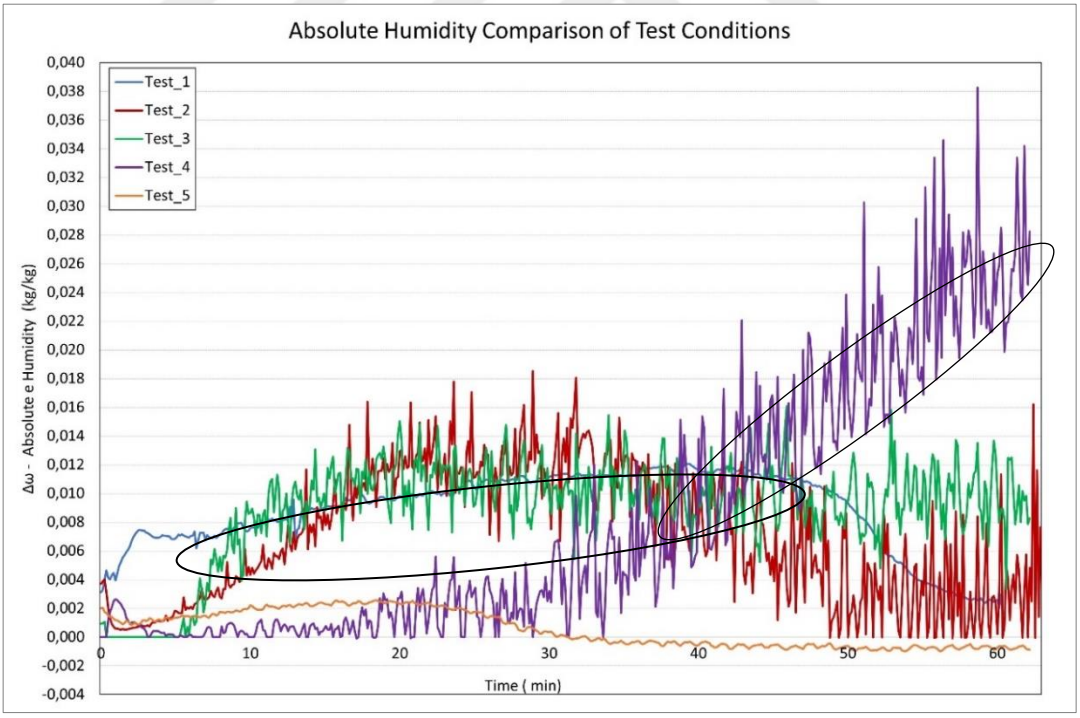


Figure 3.16 Comparison of the absolute humidity for five different test conditions

In the new software, heater, and valve activations are configured like Test-4 conditions 20 minutes before the cooling phase. During these 20 minutes, only one heater is activated, and water spray intake is not allowed. Employing this operational condition entails reduced total energy and water requirements without any loss at dehumidification performance; energy and water requirements were decreased during 20 minutes. The total test duration is also not changed. So, total water consumption was reduced by % 21 compared to the current condition.

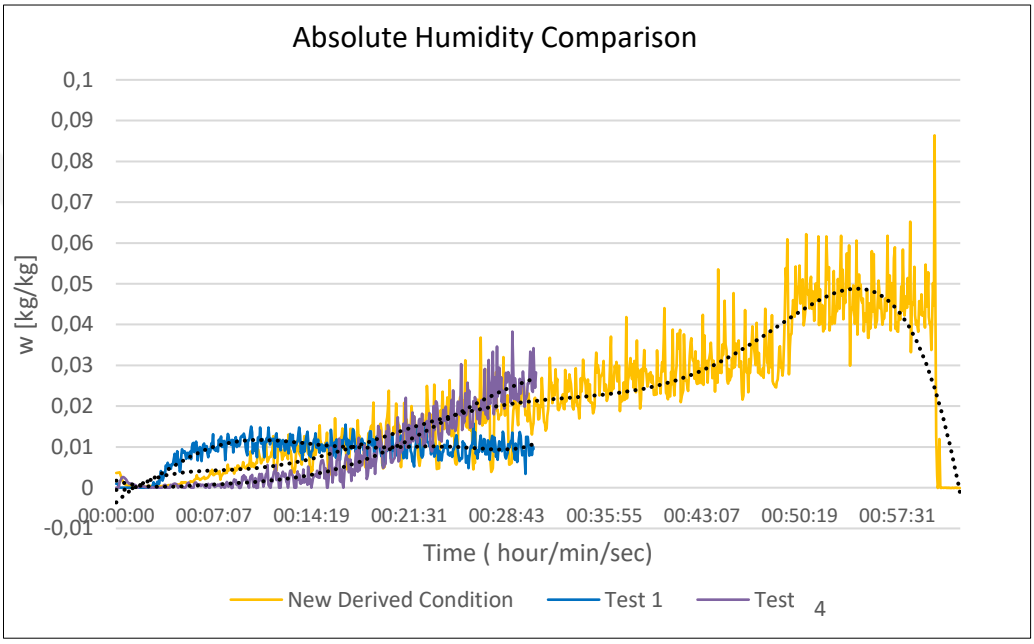


Figure 3.17 Comparison of the absolute humidity of new derived condition with Test 1 & Test 4

3.3 Air Flow Rate Measurements

In order to determine how much humidity hot air can absorb, we calculated the volume of remaining air while clothes were inside the drum. The area average velocity method was utilized to calculate the average mass flow rate of the moist air through the condenser section where the flow regime condition is close to the laminar flow. The total volume of system air is calculated through the CFD simulation. According to 3D simulation, the air volume of the washer group is 0.079 m^3 while the air volume of the dryer group is 0.0032 m^3, as visualized in Figure 3.18 to Figure 3.19.

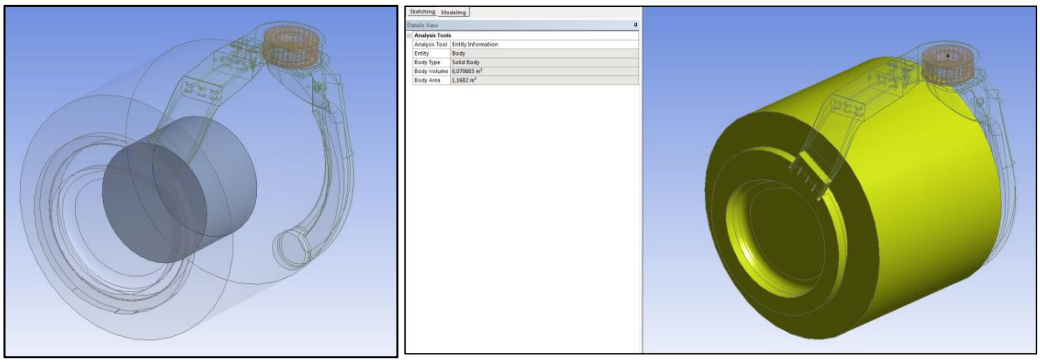


Figure 3.18 Volume of washing group due to the 3D geometry

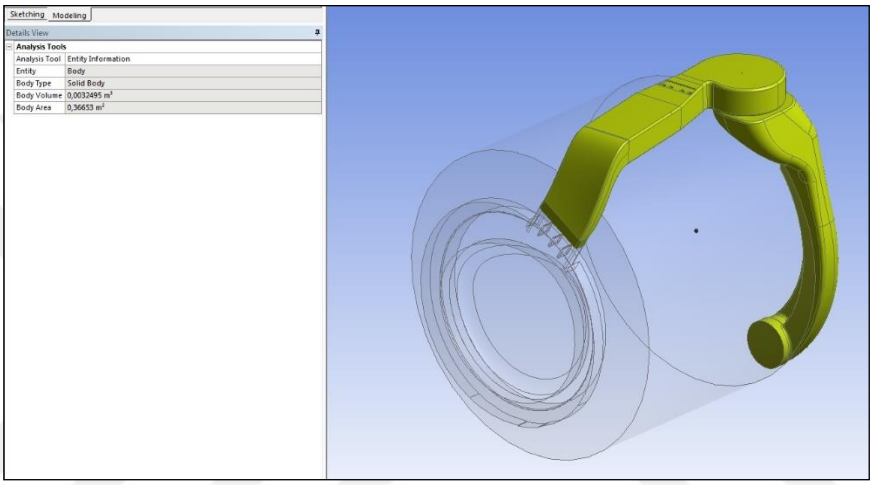


Figure 3.19 Volume of drying group due to the 3D geometry

The volume of the laundry for a 6 kg load is measured as 26.6 lt (0.0266 m^3) by the water volume replacement method as visualised in Figure 3.20.

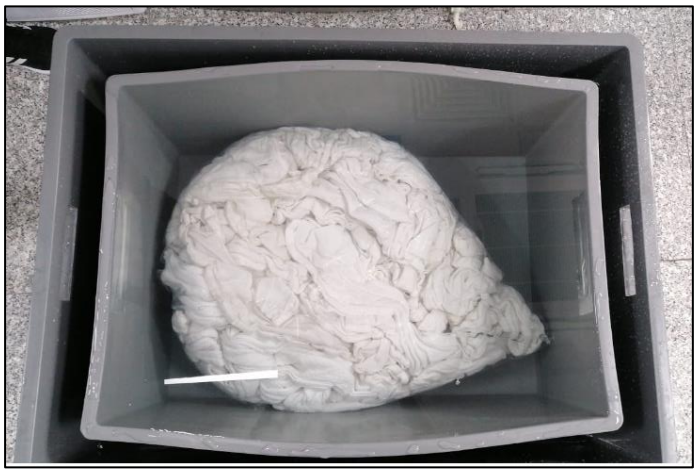


Figure 3.20 The volume of laundry measurement (Personal archive, 2012)

The mass flow rate of the air inside the washer-dryer machine in working conditions should be priorly known for the successful calculation of the moisture removal capacity of the system. For calculating the mass flow, the area average velocity method was used by means of the varying locations of air velocity measurement from 20 points at the condenser inlet zone. The thermo-anemometer probe has been widely used to measure air velocities in narrow channels as given in Figure 3.21.

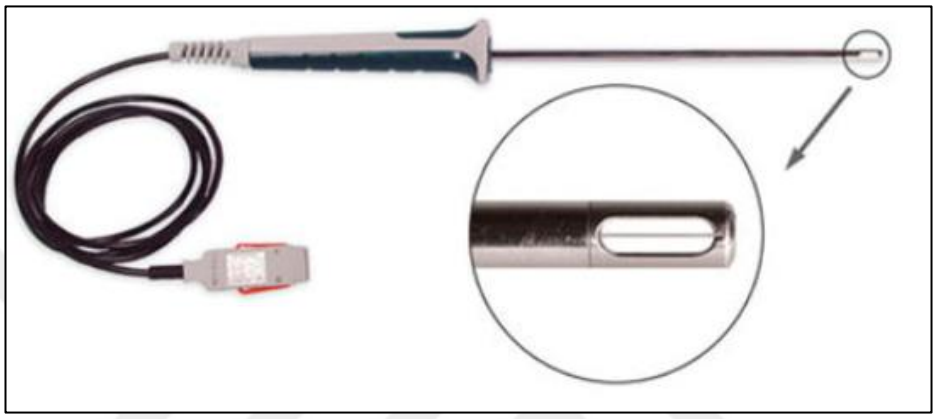


Figure 3.21 Almemo FV A935- TH5 type thermo-anemometer probe and technical specifications

The technical specifications and measurement ranges of the thermo-anemometer probe are given in Table 3.4.

Table 3.4 Technical specifications of thermo-anemometer probe.

Parameters	**Valid ranges**
Flow measuring range	0.2 – 20.0 m/s
Resolution	0.01 m/s
Response time	<1.5 sec.
Measurement accuracy	± (0.2 m/s +2% of meas. val.)
Nominal conditions	22 °C ±2 K - 45 % RH ±10 % RH - 1013 mbar
Temperature compensation	0 to +50 °C
Influence of temperature	±0.3% of measured value /°C at 0.3 to 20 m/s

The velocity of the air is measured for 20 different spatial locations at the condenser inlet. Tests have been made for unloaded conditions and are planned to be repeated due to the upcoming resistances resulting from loaded conditions. Figure 3.22 to Figure 3.25 show the conditions of the velocity probe measurements at the condenser inlet.

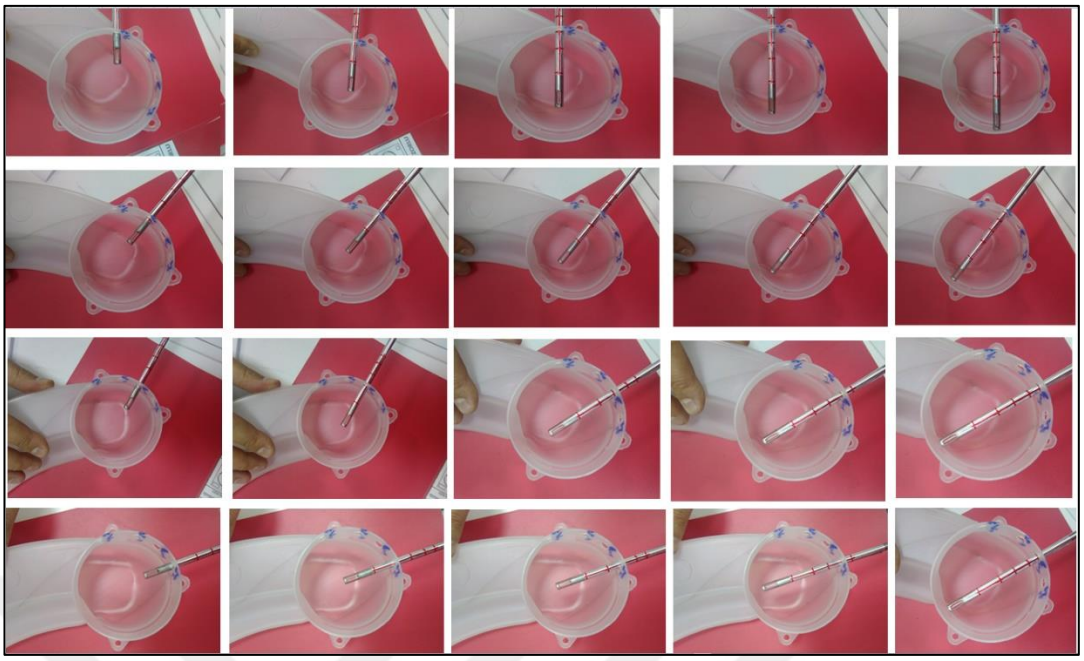


Figure 3.22 Velocity probe measurement conditions at the condenser inlet (Personal archive, 2012)



Figure 3.23 Velocity probe measurement inside the machine (Personal archive, 2012)

In practical situations like this condenser channel application, the speed of the air flowing through the inlet is not consistent throughout the channel's cross-section. Channel wall-induced friction causes deceleration in the forced air flow adjacent to tube walls, which explains the higher stream velocity rates along the center axis of the duct.

To calculate the average velocity in ducts, taking multiple velocity readings at points with equal area is recommended. This can be achieved by conducting traverse

readings, which are taken across the duct cross-section in a formal pattern of sensing points. Figure 3.25 illustrates this process. Figure 3.24 shows related ASHRAE standards for traversing round ducts measurement.

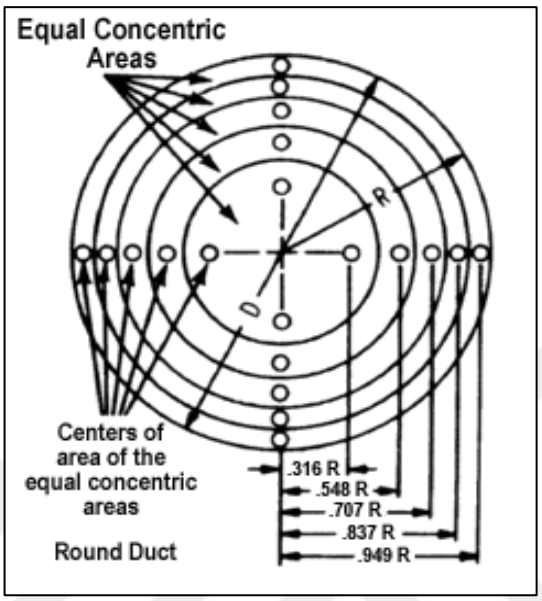


Figure 3.24 Traverse on round duct area (ASHRAE Fundamentals Handbook Section 14, ASHRAE Standard 111, 2005)

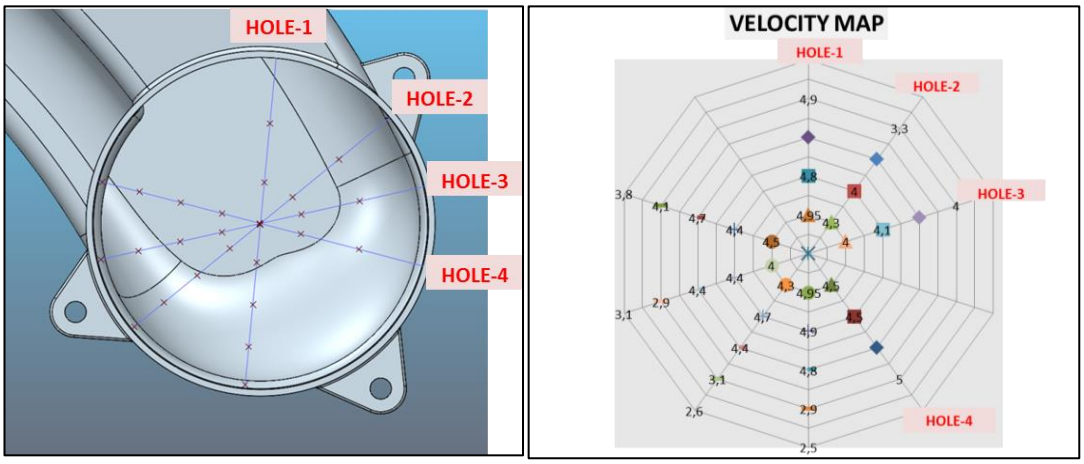


Figure 3.25 Velocity measurement points at the condenser inlet

The average velocity at the condenser inlet area was calculated as 3.37 m/s without a load inside the machine. When the velocity measurements were repeated for 6.0 kg with 50.0% wetted laundry, the average velocity at the condenser inlet area was calculated as 4.4 m/s, as shown in Table 3.5.

Table 3.5 Measurement points and velocity data for loaded machine

For D=78.6 mm	Position 1	Position 2	Position 3	Position 4	Position 5	Position 6	Position 7
Standard * (%) mm	96.8	86.5	67.9	32.1	-	13.5	3.2
Standard-D (%) mm	76.08	67.98	53.36	25.23	-	10.61	2.51
Measurement point **(mm)	77.5	68.5	58.5	48.5	39.5	29.5	15.5
Velocity @							
Hole - 1	2.5	2.9	4.8	4.9	4.95	4.8	4.9
Hole - 2	2.6	3.1	4.4	4.7	4.3	4.0	3.3
Hole - 3	3.1	2.9	4.4	4.4	4.0	4.1	4.0
Hole - 4	3.8	4.1	4.7	4.4	4.5	4.5	5.0
Avg. Velocity (m/s)	3.00	3.25	4.58	4.60	**4.44**	4.35	4.30

***** Traverse reading on round duct area according to the ASHRAE Standard
**Distance between hole inlet and measurement point of the probe (mm)

When comparing the velocity distribution along the condenser as determined by testing data and the CFD findings, it is observed that comparative results between the experimental and theoretical works are in harmony. As shown in Table 3.6, the mass flow average velocity is calculated as 3 m/s with 0.018 kg/s mass flow rate in CFD analysis (Figure 3.26).

Table 3.6 Comparison of theoretical and CFD calculations of mass flow rates

	Theoretical calculation	**CFD Results**	**Units**
$V_{air,in}$	3.37	3	m/s
$A_{air,in}$	0.0048	0.0048	m^2
ρ_{air}	1.225	1.225	kg / m^3
$U_{air,in}$	58.23	51.84	m^3/h
$\dot{m}_{air,in}$	0.020	0.018	kg /s

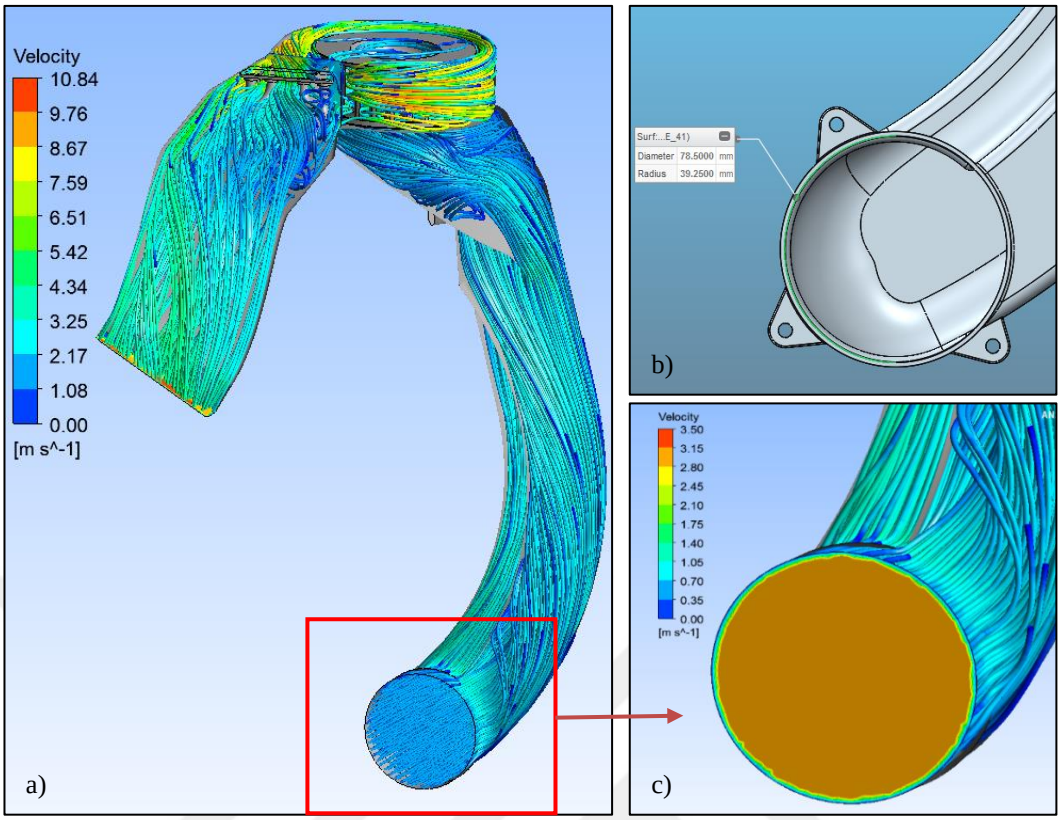


Figure 3.26 a) Velocity distribution at the condenser channel according to the CFD analysis b) 3D model of the condenser channel inlet, c) detail view of the velocity distribution at inlet.

To quantify the volumetric flow of the air, an airflow measurement test chamber was prepared by Vestel according to the ANSI/AMCA 210-16 — ANSI/ASHRAE 51-16 (2016); laboratory methods of testing fans for performance standard was used. This standard provides a set of consistent procedures for conducting laboratory tests on fans or similar air-moving devices. These tests aim to evaluate the device's aerodynamic performance by measuring variables such as airflow rate, air density, rotational speed, and efficiency. The results obtained from these tests are used to determine the device's rating or to provide guarantees regarding its performance.

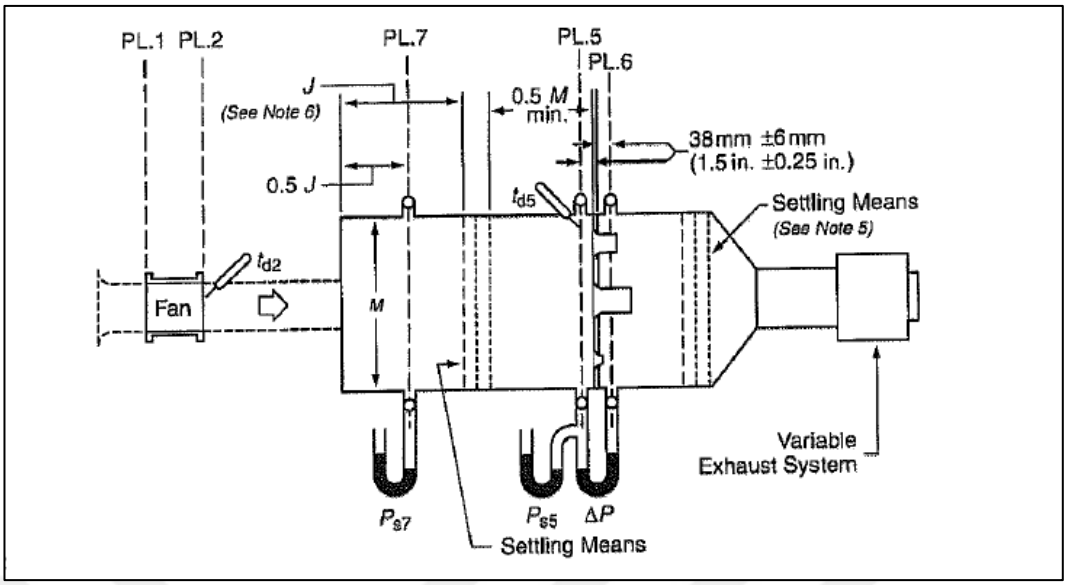


Figure 3.27 Schematic of the test bench, outlet chamber setup – multiple nozzles in chamber. (American Society of Heating, Refrigerant and Air Conditioning Engineers (ASHRAE) Standard 51-16 - ANSI/AMCA Standard 210-16, Laboratory Methods of Testing Fans for Certified Aerodynamic Performance Rating, 2016).

The experimental setup for the nozzle flow test was conducted in accordance with the specifications outlined in ANSI/ASHRAE 51-16 (2016) standards. A schematic of the test chamber can be found in Figure 3.2. To mitigate any disturbances caused by flow turbulence, air straighteners were installed both before and after the nozzles. These air straighteners aimed to minimize any fluctuations in nozzle pressure drop measurements (as shown in Figure 3.28). During the experiment, the motor speed of the test unit was adjusted within the range of 2000 to 2900 rpm to achieve the desired airflow rate. The speed of the chamber blower was also adjusted until the external static pressure reached zero, compensating for losses attributed to the test chamber itself.

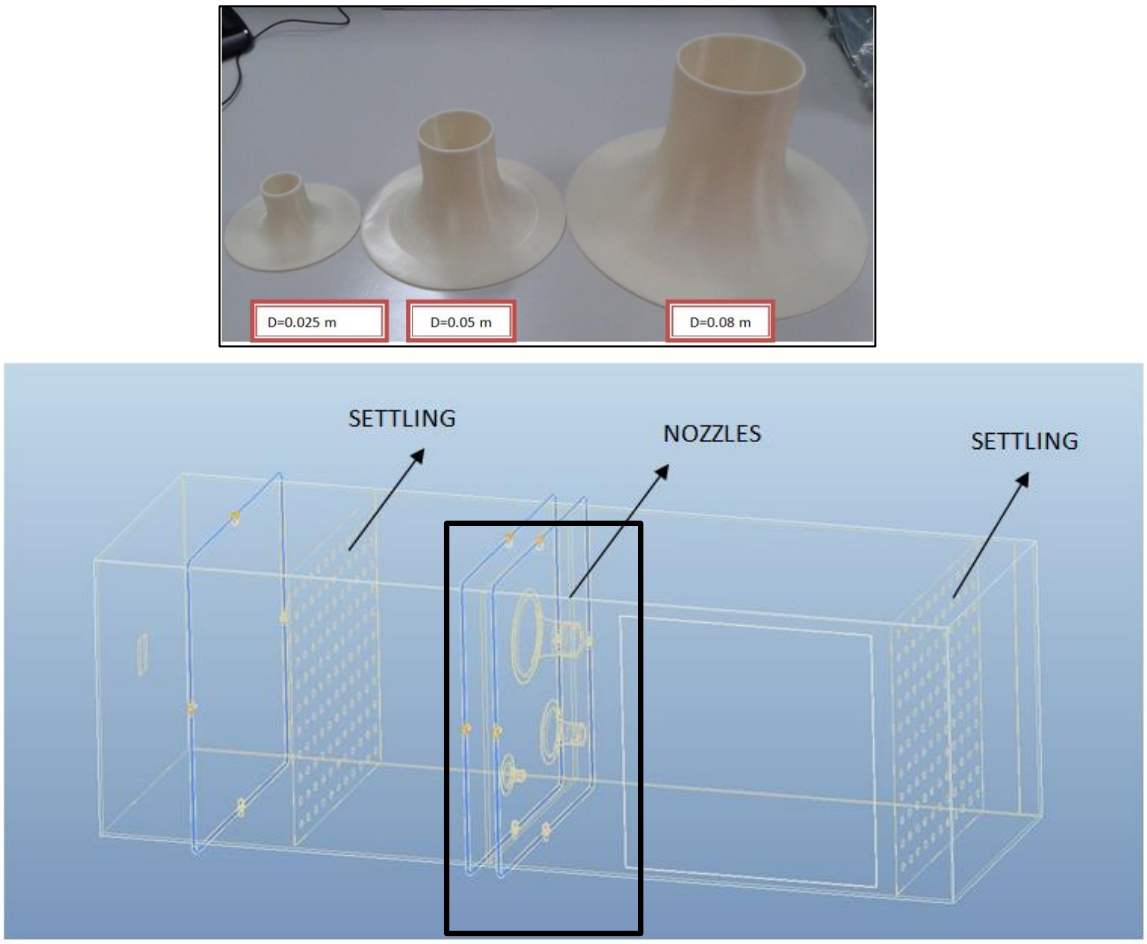


Figure 3.28 Standard nozzles with varying inner diameters

Temperature sensors were employed to measure the air dry and wet bulb temperatures during the experiment. A data logger was utilized to capture these temperature readings. Before taking measurements, the unit was allowed to run for 15 minutes to ensure thermal stabilization (as depicted in Figure 3.29 and Figure 3.30). For each test, three sets of readings were recorded by the data logger, with a one-minute interval between each reading. The average value of these readings was used to calculate the air flow rate. Subsequently, the experimental findings were compared to the simulation results to validate the accuracy and reliability of the simulations.

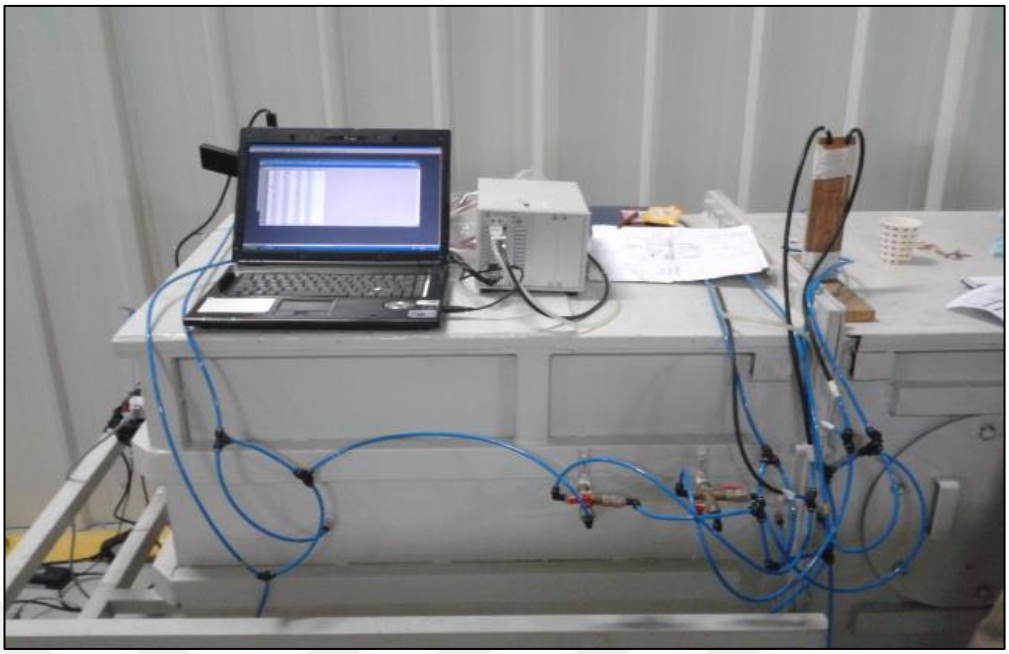


Figure 3.29 Test chamber view (Personal archive, 2013)

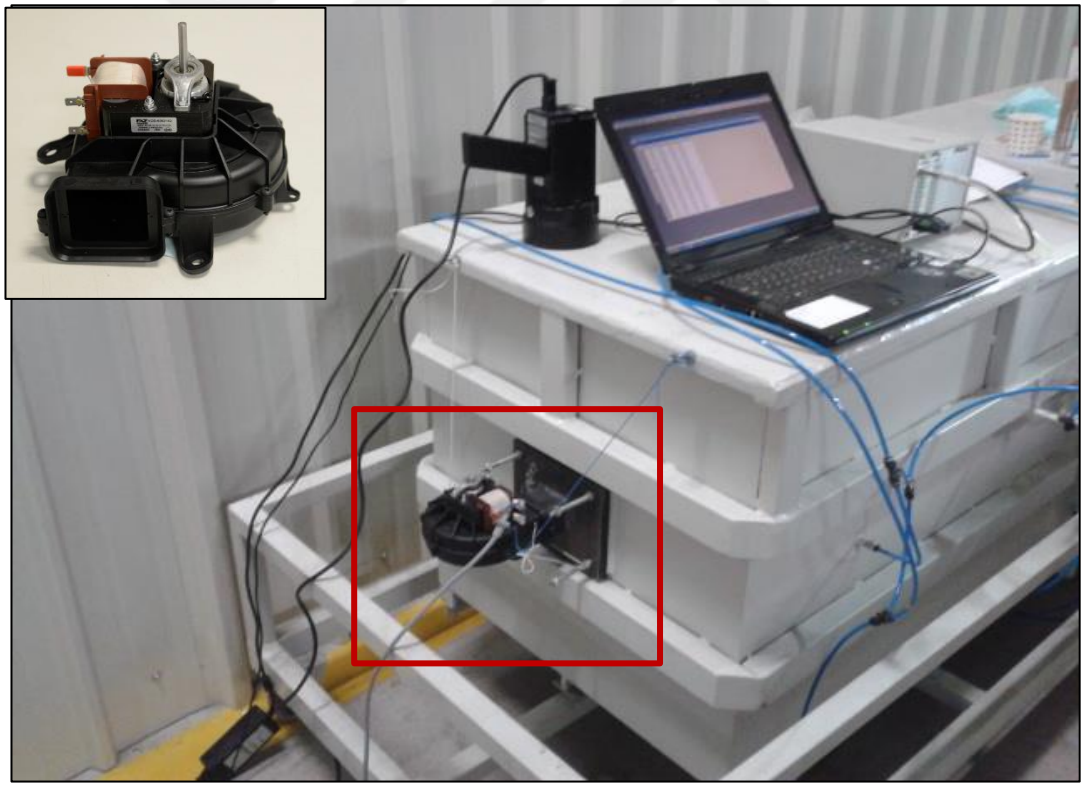


Figure 3.30 Test chamber with fan testing setup (Personal archive, 2013)

The aerodynamic performance and airflow rate of fan-circulated systems were evaluated through test chamber measurements of the blower. The characteristics

curves of the blower and system were generated, and the result of this verification is presented in Figure 3.31. These curves provided insights into the behaviour and performance of the blower under different operating conditions. The corresponding airflow rates indicated by the curves were verified by comparing them with the measurements obtained from the test chamber.

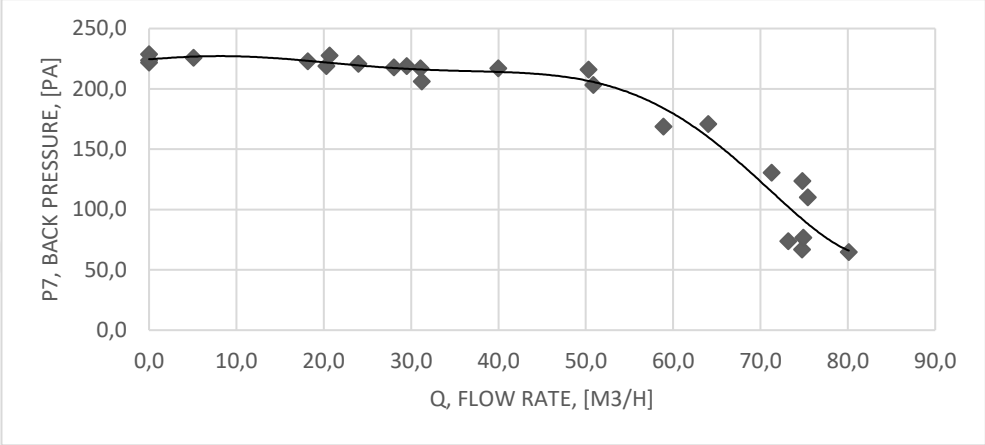


Figure 3.31 Comparison of test results for validation

Air flow rate measurement studies are focused on conducting experiments within a test chamber to assess the aerodynamic performance and airflow rate of fan-circulated systems. Test chamber measurements were carried out specifically on the blower to investigate its performance characteristics. These measurements aimed to determine the airflow rate and validate its accuracy. By comparing the experimental results with the expected performance, the study sought to verify the reliability and effectiveness of the fan-circulated systems in terms of their aerodynamic performance.

CHAPTER FOUR
DEVELOPING THE NUMERICAL MODEL

4.1 Numerical Model of the Drying Unit

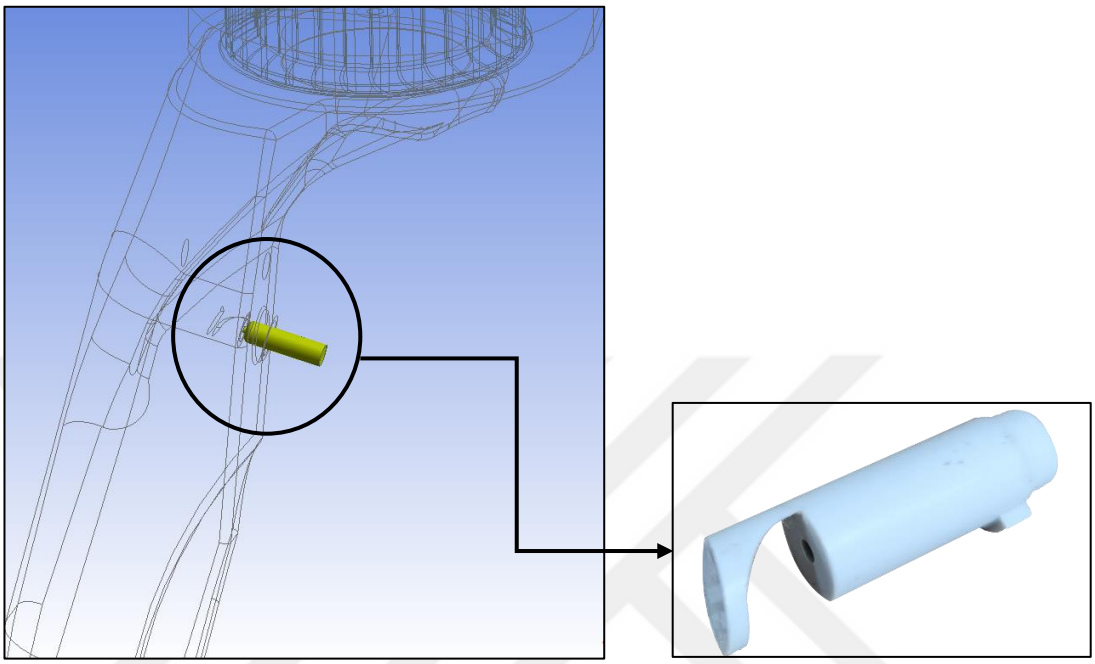
First, single-phase airflow modelling was made for the condenser apart from the system to study the condensation process. For the airflow and condensation performance, a condenser model with whole drying elements (fan, heaters), which is shown in Figure 4.1, was prepared in this term. To develop the condenser performance, its CFD model was investigated first, so its design deficiencies would be revealed and can be solved quickly.



Figure 4.1. Drying system model apart from the machine

A Computer Assisted Design (CAD) program is generated to model the flowing process of air based on the real condenser geometry. A mathematical model constructed upon Computational Fluid Dynamics (CFD) is thoroughly investigated to gain preliminary insights into airflow and condensation performance. Design-specific

deficiencies can be easily eliminated using prior knowledge of the essentials of governing systematic processes. Computer aided fluid volume model of the spray nozzle and its working location inside the condenser system is shown in Figure 4.2 a.b.



a. b.

Figure 4.2 Spray nozzle a) fluid volume model and b) actual part

A numerical grid model was generated by the meshing interface for computational fluid dynamics analysis. Tetrahedral meshes were added to the model to provide an accurate numerical grid, and smaller element sizes were selected for the air near the entrance and outflow to calculate the flow and pressure drop precisely. At the initial phases of the modelling, mesh optimisation and mesh independence studies were conducted. The tetrahedral mesh was used, and various grid sizes were constructed. The effect of element number changes on the simulation results was considered, and this study was repeated for all the following numerical models.

As a mesh optimisation study, Design Parameter tools were used. The input parameter was mesh size, and it was defined as 0.001, 0.002, 0.004, and 0.006 m. As the output parameters, area average velocity through the reference line at the heater outlet, analyse duration, and the number of elements and nodes were defined. 0.004 m

element size was selected after the mesh independence study. The generated numerical grid, as shown in Figure 4.3, involves 3.613.558 elements and 678.640 nodes.

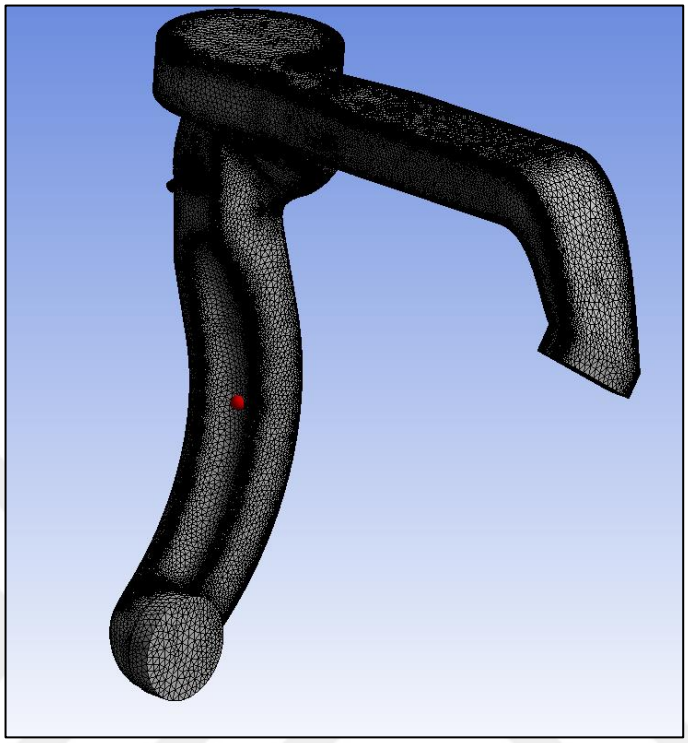


Figure 4.3 Numerical grid models of the entire dryer components

Only the process air in the condenser, accompanied by the entire dryer system, was modelled, and fan geometry was excluded to reduce the computational load on the processing units. The fan-driven flow was not defined to simplify the iterative convergence progress. Instead, mass flow inlet and pressure outlet were defined as initial conditions depicted in Figure 4.4. However, to simulate the heat transfer and moist air phase change by the effect of cooling water injected from a nozzle into the air, the condenser wall, nozzle geometry, water injection, and moist air properties were identified.

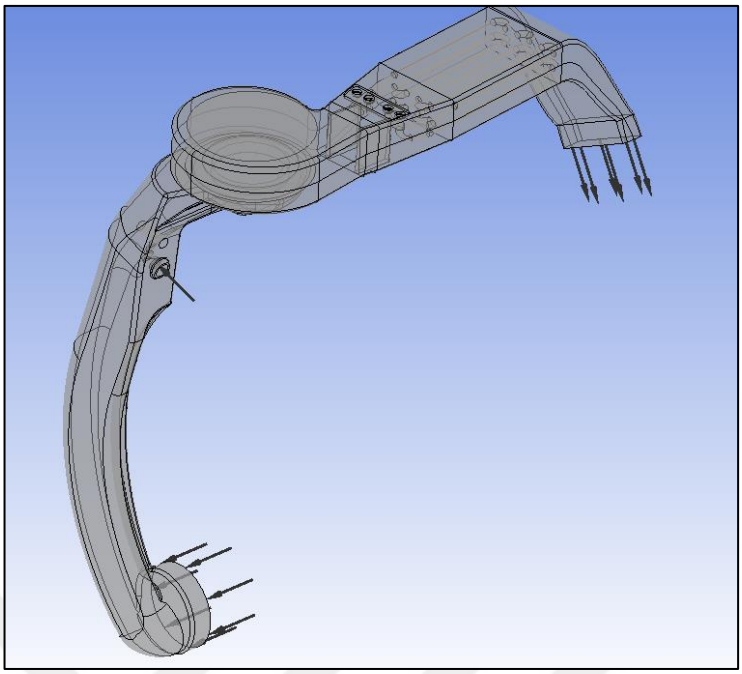


Figure 4.4 CFD model and boundary conditions definitions of the condenser model as a part of dryer

With the definitions of 0.018 kg/s mass flow inlet for the air and 2 m/s for water flow inlet and air-water mixture properties, a preliminary result was carried out as shown below. In Figure 4.5, the air temperature volume rendered in the dryer system with 800 K surface temperature heaters was shown.

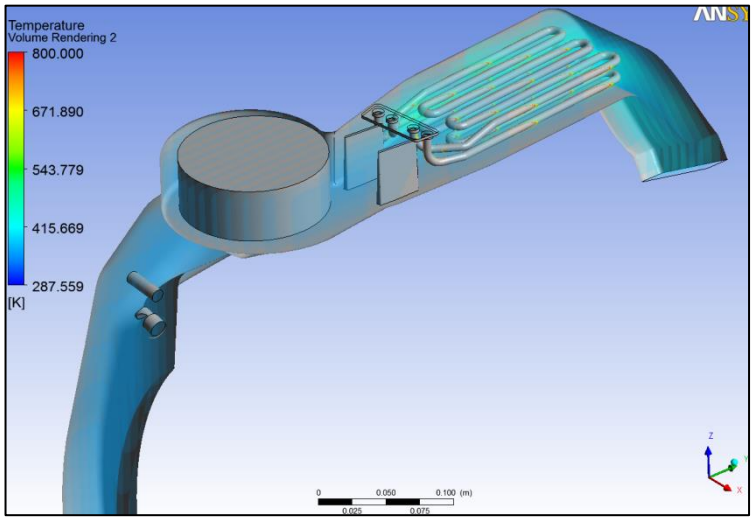


Figure 4.5 Temperature volume render for the dryer

Figure 4.6 shows a CFD-rendered visualization for the sprayed water particle tracking. Air inlet velocity allows water particles to flow through the dryer system rather than drop down to the condenser.

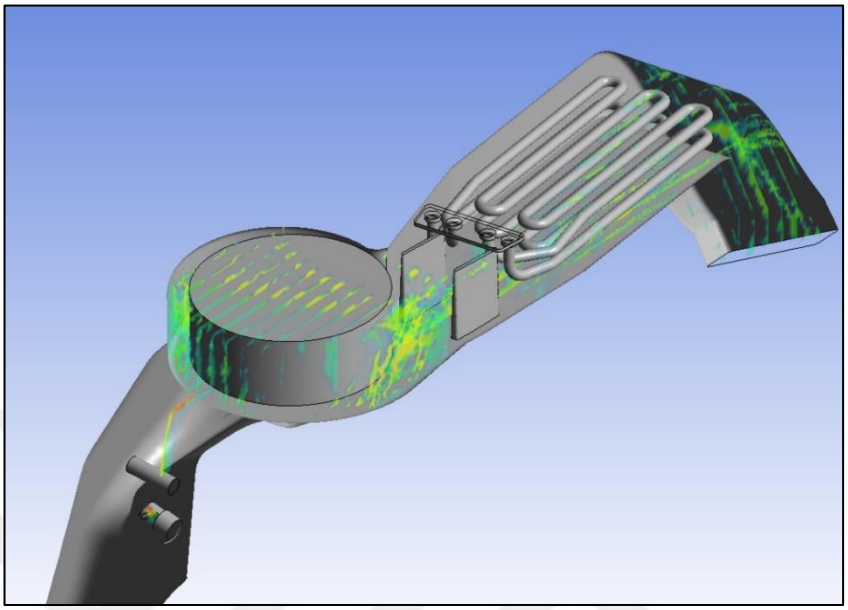


Figure 4.6 Spray water particles tracking

To analyse the coupled heat and mass transfer mechanism effectively, the numerical model was also developed for only the condenser part apart from the system. By means of actual conditions to calculate the amount of the coupled heat and mass transfer and simulate the two-phase model and phase change mechanism taking place in the moist air by the effect of the cooling water, which is sprinkled directly through the nozzle to the process air, condenser wall material, nozzle geometer, water injection conditions, and moist air properties should be clearly identified. Process of air flowing through the passages of the condenser is mathematically modelled by virtue of a CAD program, relying on the exact condenser geometry shown in Figure 4.7.

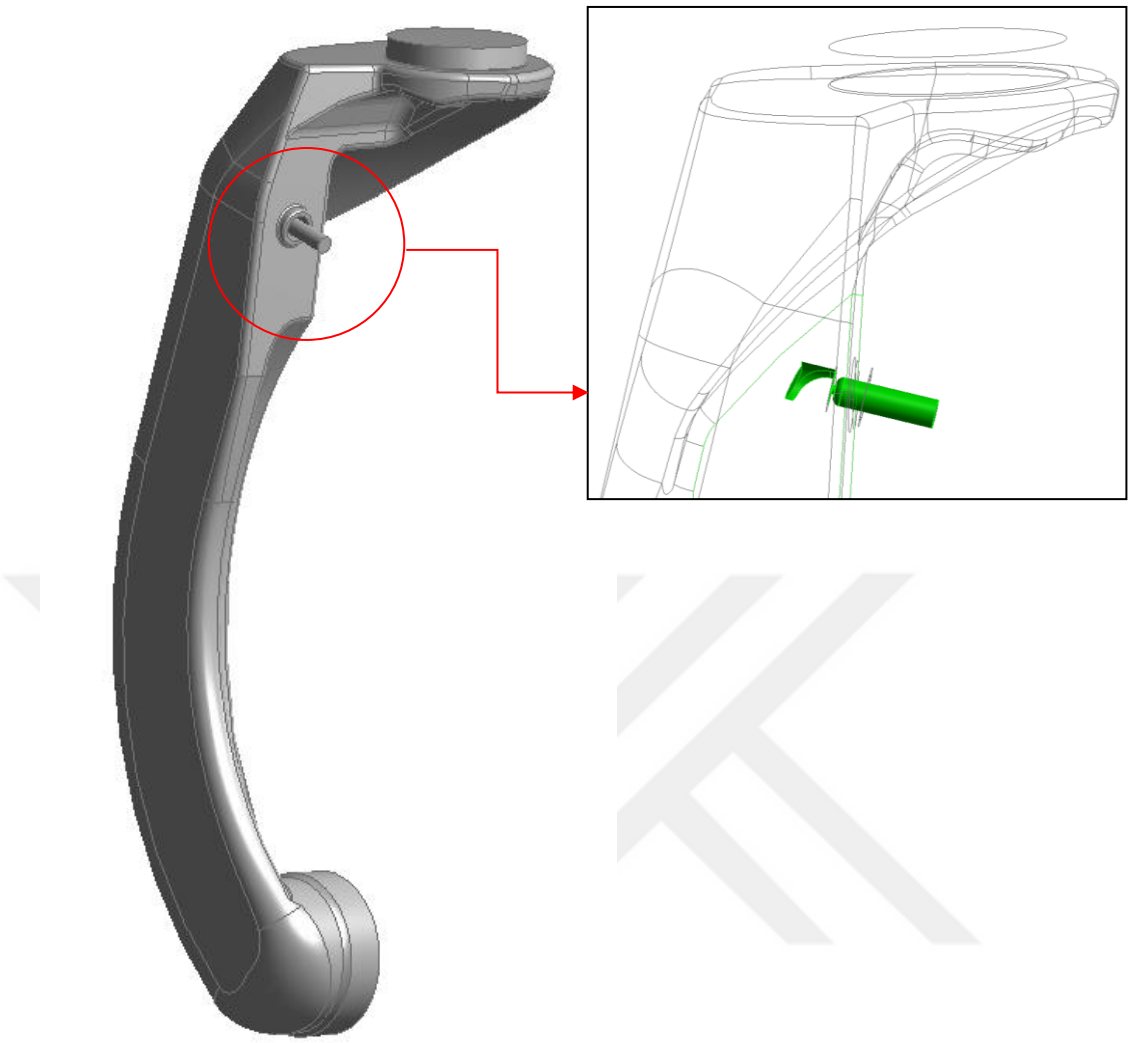


Figure 4.7 Fluid volume model of the condenser and nozzle.

A numerical model was developed by meshing interface for CFD analysis. To define a proper numerical framework, mesh optimization, boundary layer treatment by mesh size, and inflation studies were made at the beginning of the numerical study. Different sizes of grids were generated, and a tetrahedral mesh was applied to developed model. The investigation of the effect of element number changes was taken into consideration. Smaller elements were considered at the inlet and outlet of the condenser zones to determine the flow characteristics and pressure gradient more accurately in the condenser. The numerical grid involves approximately 1.2 million elements, which is explicitly shown in Figure 4.8.

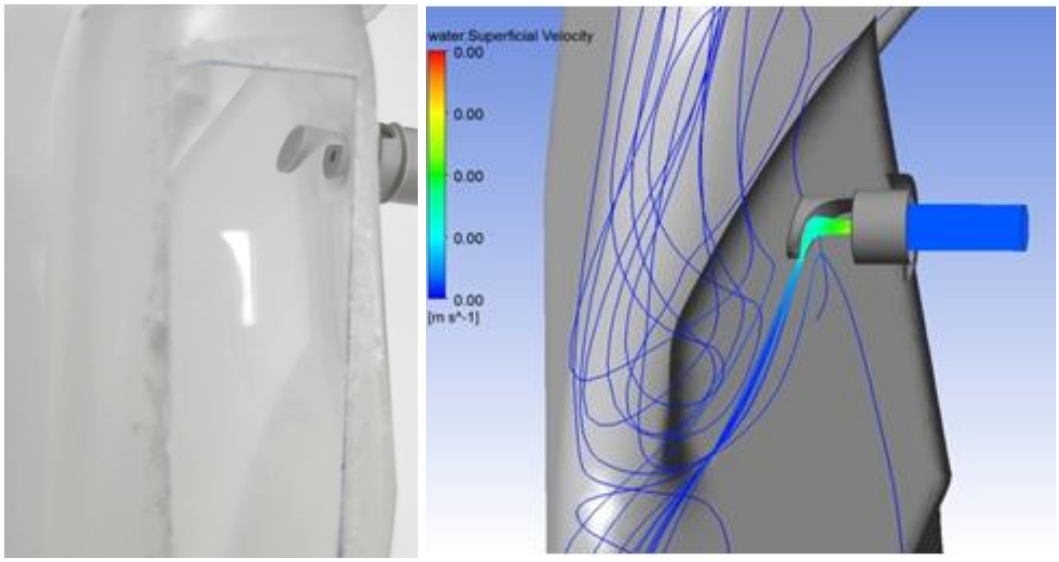


Figure 4.8 Numerical model of the condenser fluid volume

Two-phase air & water flow mixture CFD model was developed to simulate the condenser's heat and mass transfer mechanism apart from the system. Flow analysis was based only on the condenser's process air to reduce the computational load on the central processing units. Initial conditions of the mass flow inlet of the water, the volume fraction of the air & water, and adiabatic walls were defined. 2700 rpm fan work defined the mass flow inlet as initial boundary conditions, while adiabatic conditions were considered for condenser walls.

To understand the phase change modelling process, the condenser water spray nozzle working principle by means of its cooling and phase change effects is being investigated. Pressures inside the condenser are measured by pressure plugs to verify the CFD results with test data. Temperature and humidity measurements inside the condenser during the drying cycle are developing.

The spray nozzle water flow model is represented by CFD analysis and camera, as shown in Figure 4.9. With the help of a sight window on the condenser channel, which we prepared with a transparent PVC part, an experimental view of the water spray with and without fan work is visualized in Figure 4.10. The following section show that fluid flow inside the condenser will be compared in droplet size details. After the verification of CFD and experimental results of two-phase airflow analyses, more complex analyses would be modelled numerically.



a. b.

Figure 4.9 Two phase volume of fluid model of the condenser spray a) real model, b) CFD model



a. b. c.

Figure 4.10 a) Experimental set-up for the sight window of condenser spray channel, b) water spray with fan work and c) water spray without fan work (Personal archive, 2012)

The working principles of the water spray nozzle in the condenser will be effectively investigated regarding its influences on heat and mass transfer capabilities of the process air for a better understanding of the phase change. Moreover, a numerical model for this phase change process will be developed in the upcoming sections.

4.2 Numerical Modelling of the Fan Driven Flow

The centrifugal fans play a significant role in the drying performance of a washer-dryer machine by directing the moist air to the condenser and then through the heater channel before supplying the drying air to the drum. While there is a lack of specific literature research on the centrifugal fans within washer-dryer machines, experimental and numerical studies are available that assess the performance of centrifugal fans assembles outside the system. These studies can provide valuable insights into the design and operation of centrifugal fans, which can be applied to optimize their performance within washer-dryer machines.

Radial fans take place in industrial applications in a very large spectrum ranging from air-conditioning to conventional clothes drying. Washers & dryers with heater

elements to dry clothes and forward-curved radial fans have been used to circulate the system air. The process air is heated inside the heater unit to increase its inherent moisture capacity. The heated air is imposed on a fan-driven force to pass through the high moisture content clothes, resulting in considerable moisture removal from the wetted laundry (Figure 4.11). Radial fans have the capability of supplying the required airflow for drying wet clothes. That is why radial fans are considered functional and beneficial for drying.

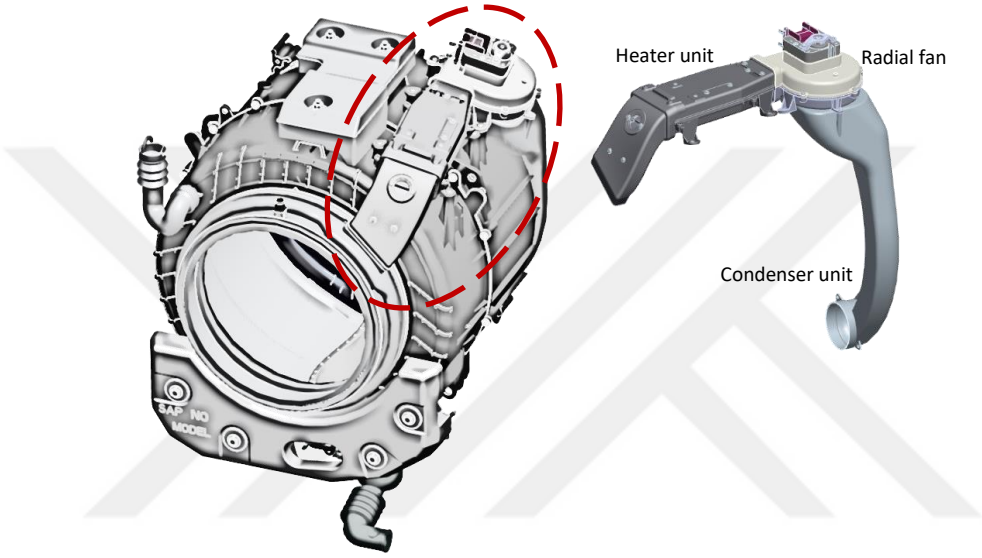
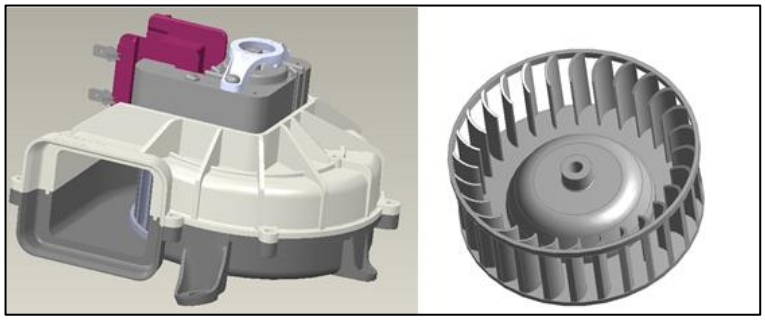


Figure 4.11 Washer & Dryer machine assembly and drying system

Forward-curved radial fans comprise three main parts: the fan housing, the rotary fan wheel, and the electric motor. The process air is sucked from the intake of the fan wheel and passes through the rotating blades with a right angle to the fan outlet and leaves the fan utilizing the centrifugal force. The centrifugal effect entailed by the rotation of the fluid between the blades allows the suction from the diffuser to increase the static pressure and expel the fluid from the fan outlet.

The mathematical modelling of centrifugal fan work is done separately from the drying system to ensure accurate fan-driven flow simulation. The internal and the exit characteristics of the dryer system's centrifugal fan have been inspected employing CFD aspects. The analysis results have been verified by SPIV experimental method.

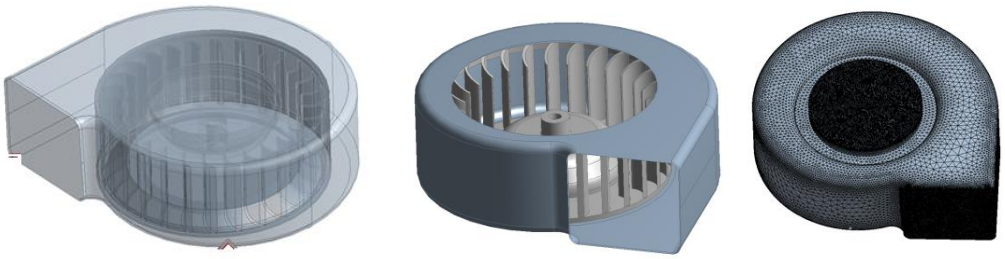
Air volume geometries of the fan housing and its associated forward-curved blades were modelled to accomplish the centrifugal fan's numerical modelling. The mentioned 3D model shown in Figure 4.12 is adapted from the manufacturer.



a. b.

Figure 4.12 Centrifugal fan’s a) solid model, b) blade geometry

Regarding the centrifugal fan working principle, the process air enters a parallel direction to the axis of the fan inlet. It makes a 90° turn and blows out into the ambient from the outlet by the centrifugal effect. To visualize this radial airflow through the fan output by CFD analysis, the ambient air volume having four times the bigger size of the fan impeller diameter has been modelled. Figure 4.13 shows the precise 3D modelling of the ambient air volume and the generated air volume model of the centrifugal fan utilized in numerical analysis.

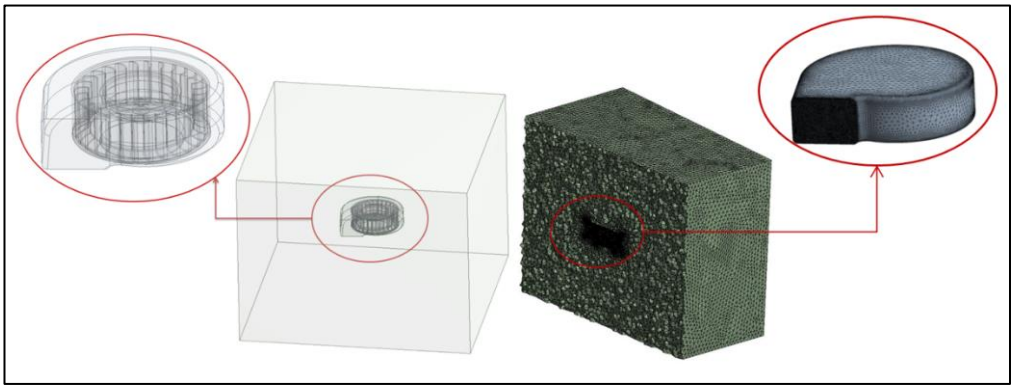


a. b. c.

Figure 4.13 Centrifugal fan’s a) simulation model, b) fan housing air volume model and c) numerical model for CFD analysis

The numerical model considers tetrahedral grid type with a total number of 3.659.175 elements and 3.659.175 nodes. Tetrahedral grid elements, mainly when used at sufficient density, can fit the inclined surfaces well. This element type is consciously considered due to the fan's intrinsic curved and circular surfaces and fan

housing. Figure 4.14 shows the formed grid structure for ambient air and fan housing volume.



a. b.

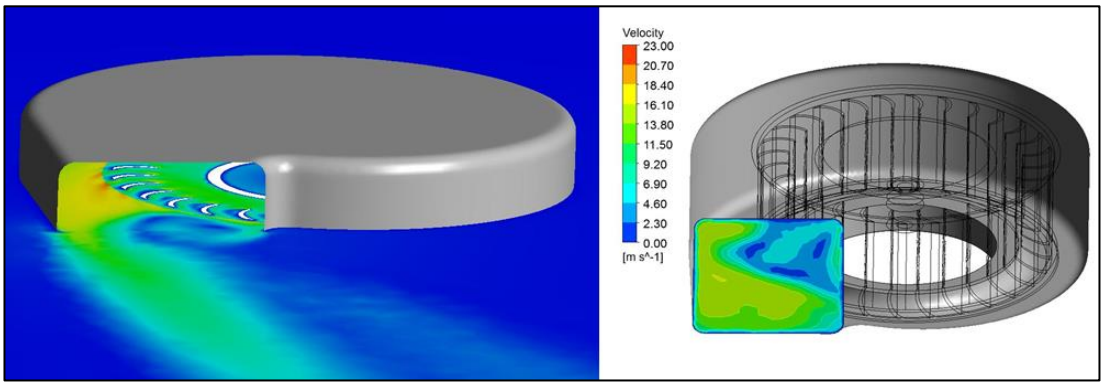
Figure 4.14 Centrifugal fan with external ambient air volume a) geometry, b) numerical model

The centrifugal fan is modelled separately from the system, and the relevant boundary conditions are assigned at the intake and outlet opening conditions. The experimentally acquired fan speed was measured at 1876 rpm and defined as a boundary condition for fan work. Solid domains such as the blower housing and the fan impellers have been defined as adiabatic walls to reduce the computational workload while solving the simulation, in line with the acceptance that the total heat transfer through these regions has a negligible effect on the numerical model despite their imposed influences over the flow conditions.

In the CFD analysis, specific interface models have been established to represent the interaction between the fluid and solid domains accurately. The fan domain is configured as a rotating frame to simulate the centrifugal fan flow. The standard k-ε turbulence model is utilised to capture the turbulent behaviour of the flow. This widely adopted model is chosen for its versatility, stability, numerical robustness, and proven ability to predict flow characteristics accurately.

Velocity distribution contours at the fan outlet have been visualized using CFD analysis in Figure 4.15. As expected, according to the working principle of a

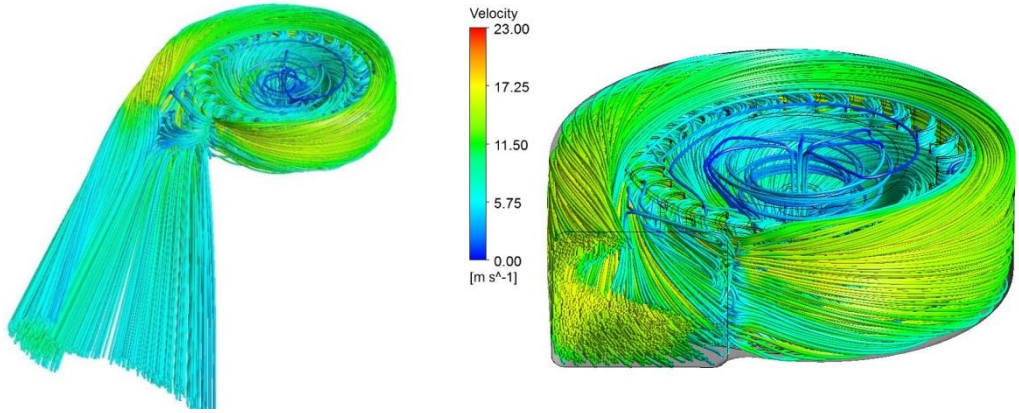
centrifugal fan, airflow reaches relatively higher speeds through the right-side surfaces of the outer walls of the fan housing.



a. b.

Figure 4.15. Centrifugal fan speed distribution a**)** midplane b**)** outlet

Accordingly, in the scope of the numerical studies, the distribution of streamlines of the flow in the fan housing and the outlet zone are respectively given in Figure 4.16. When the flow characteristics of the fan casing design and the geometry of the fan blades are extensively examined, it is observed that the flow separation in the tongue region causes turbulence in the region near the outlet. In addition, the characteristic of the flow leaving the fan housing after flow separation with flow at high velocities in the widening region of the wall of the fan housing wall is easily visualized by the generated air volume region.



a. b.

Figure 4.16. The distribution of streamlines within a) ambient air and b) the outlet of the fan

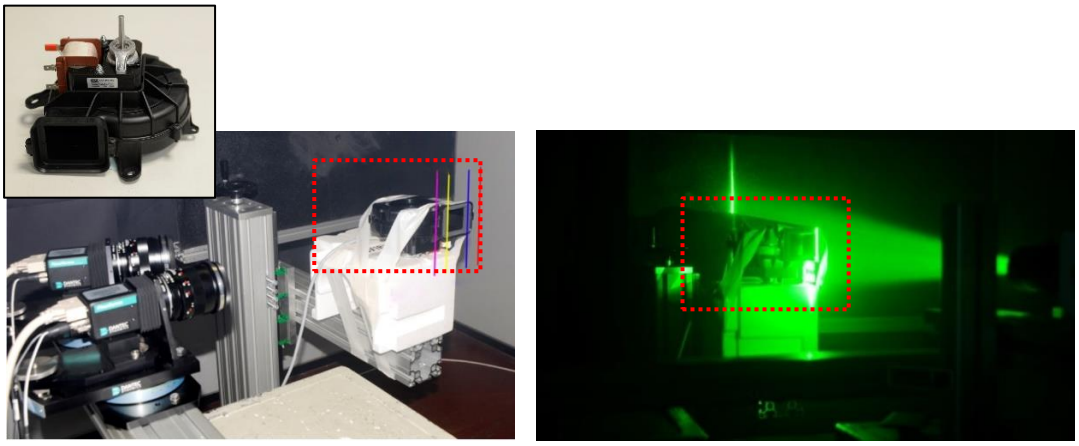
The desired design changes to be made in the fan slot or impeller geometry and the flow behaviour under the interaction with the system to be operated together can also be determined with the CFD modelling method in advance.

4.3 Stereo Particle Image Velocimetry Experimental Validation Method

Numerical experiments provide significant time and cost gains in the design process using several alternative models to identify those worth testing. However, these methods are approximate solution procedures, depending on mathematical modelling and related boundary conditions. Although the numerical study results obtained after the mathematically converged analysis on the order of 10^{-6} error value, the accuracy of the established mathematical model should be in line with the experimental data.

This study uses the Stereo Particle Image Velocimetry Measurement (SPIV) technique as the validation method. This method is one of the effective, state-of-the-art procedures to validate CFD-based numerical studies as a measurement method without interfering with the flow. This technique relies on adding particles that can be moved together with the flow and then displaying them by laser illumination. Compared to images taken at the appropriate frequency, the position difference between the particle, displacement, the ratio of time to displacement, and the particle velocity in the existing region are obtained. This visualization method can be applied to turbo devices such as centrifugal fans, high-speed cameras for imaging, laser for lighting, high-performance workstations for recording and processing data, and a control system to ensure all equipment is operated as peers.

This study uses a double-shot ND: YAG laser with 135 mJ power. The experiments are carried out in the ambient air, which is, in essence, the actual working environment of the fan, and the feeding mist is utilized as a seeding element. Instead of the PIV, which was applied by using only one camera due to the three-dimensional structure of the flow, the SPIV method, using two cameras working at different angles simultaneously, is considered (Figure 4.17).



a. b.

Figure 4.17 SPIV a) test setup and b) test view (Personal and Özgün Özer archive, 2013)

The SPIV data (Figure 4.19-b) extracted from 29 planes (Figure 4.18) at the outlet of the fan was converted to volumetric air geometry by numerical interpolation, thus making it comparable to CFD results (Figure 4.19-a). As a result of the comparative study, the air flow jet's velocity range has been between 12 and 15 m/s in the SPIV and CFD results. The region denoted in red in Figure 4.19-b represents these mentioned velocity distributions. In addition, it is found that the flow profile obtained from the SPIV experiments given in Figure 4.20-b is consistent with the flow profile obtained from the CFD analysis (Figure 4.20-a).

The framework's accuracy has been validated by comparing the outcomes of flow visualisations between CFD analyses and SPIV experiments. As a result, the process air velocity varies between 12 and 15 m/s, both are based on SPIV and CFD results.

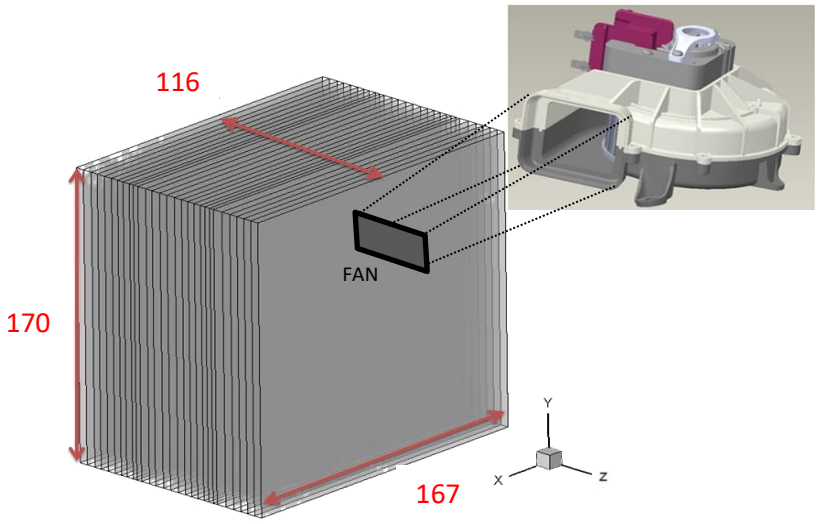
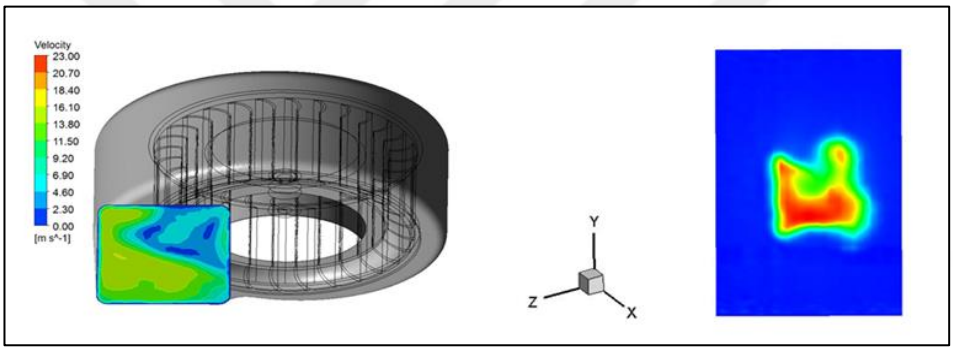
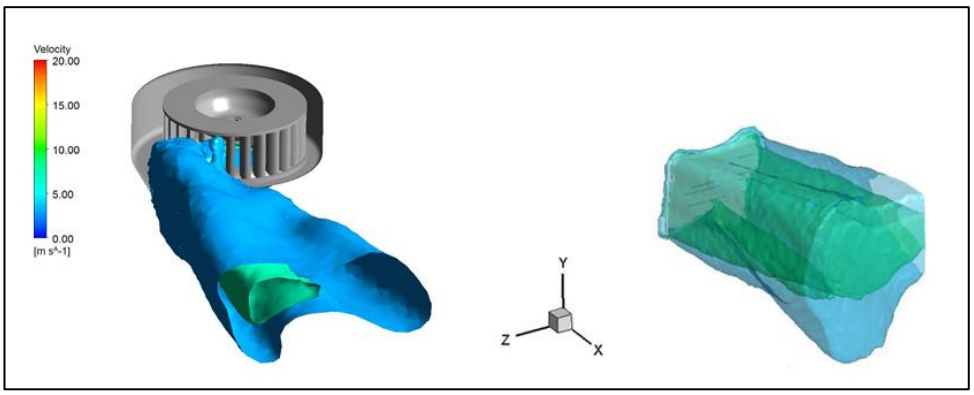


Figure 4.18 Test planes positions



a. b.

Figure 4.19 Outlet velocity comparison with the methods of a**)** CFD and b**)** SPIV



a. b.

Figure 4.20 Volumetric three-dimensional speed data obtained from the mouth of the fan and ambient air a**)** CFD and b**)** SPIV (inner surface, the outer surface of 7 m/s , 3 m/s)

4.4 Numerical and Experimental Analysis on the Heating Unit

For the heating process, which takes place primarily in the white goods sector and many applications, the resistances and their housing units' designs directly affect the heating performance. Having prior knowledge of the fluid flow and heat transfer mechanisms inside the resistance unit can offer significant advantages in observing the impact of design parameters on performance and ultimately achieving the most efficient design.

Corresponding results of the experimental and theoretical CFD analysis are compared to comprehend the influential parameters on heat-producing resistances of the drying system. Temperature measurements for the resistance heaters are made through the K-type thermocouples at illustrated locations in Figure 4.21.

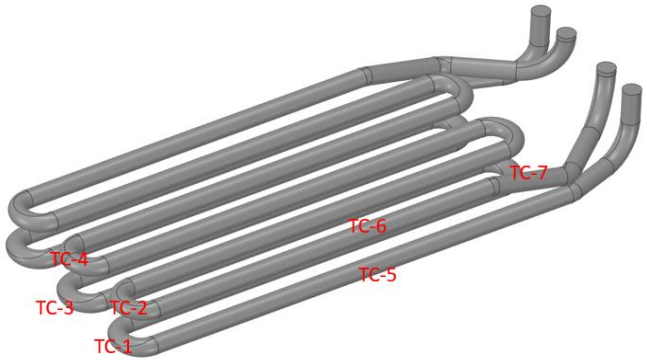
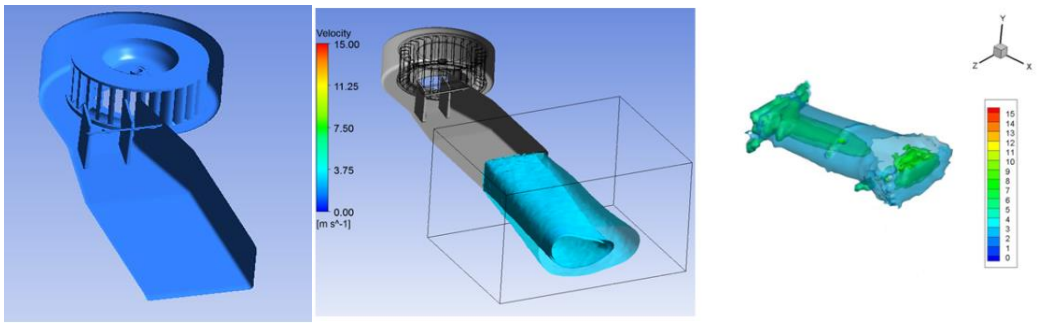


Figure 4.21 Thermocouple measuring points on the heater surface

Instead of using conventional test methods, the Particle Image Velocimetry Method was utilized to confirm the numerical model results. Numerical results of the airflow model are validated against those obtained by SPIV measurements. Heater housing channel design and heaters' arrangement effects were investigated in the verification studies.

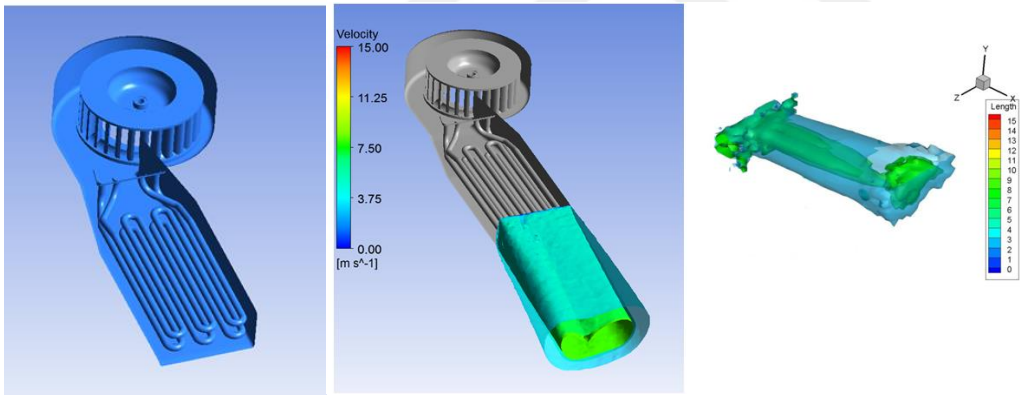
In the first model (Figure 4.22-a), the fan-driven drying system heater channel without resistance geometry was modelled, and the volumetric flow outside the unit is visualized with both CFD (Figure 4.22-b) and SPIV methods (Figure 4.22-c).



a. b. c.

Figure 4.22 Volumetric three-dimensional speed data with a) heater channel without resistance unit, b) CFD and c) SPIV results

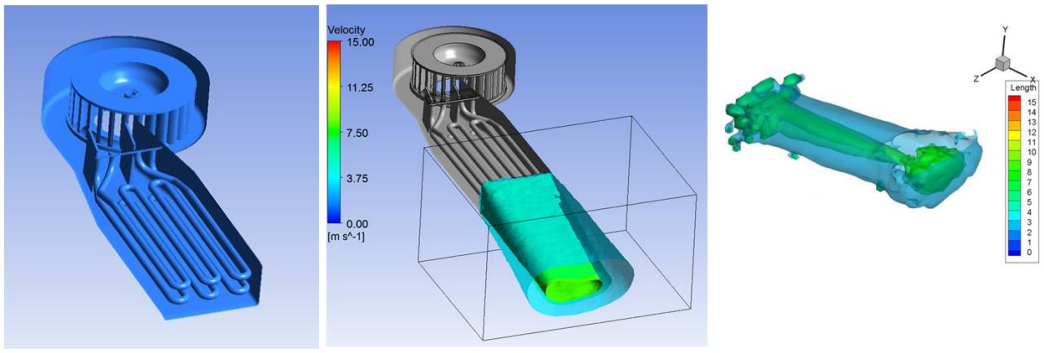
In the second derived model, a fan-driven drying system with a resistance unit in the heater channel was created, as shown in Figure 4.23. Similar the first model, volumetric flow outside the unit is visualized with CFD (Figure 4.23-b) and SPIV methods (Figure 4.23-c) again.



a. b. c.

Figure 4.23 Volumetric three-dimensional speed data with a) heater unit with heaters and without lamellas design, b) CFD and c) SPIV results

As a third combination, air-guiding lamellas geometry was added, and volumetric airflow inside the drying system heater unit with heating resistances was modelled (Figure 4.24).



a. b. c.

Figure 4.24 Volumetric three-dimensional speed data with, a) heater unit with heaters and lamellas design b) CFD and c) SPIV results

In accordance with the reliability of the flow profiles of the CFD modelling with actual working conditions, heat transfer and radiation models were also included in the analysis. The heat transfer analysis was validated by comparing resistance temperature results between CFD (Figure 4.25) and experimental measurement (Figure 4.21), which were given in Table 4.1 for 750-Watt heater power.

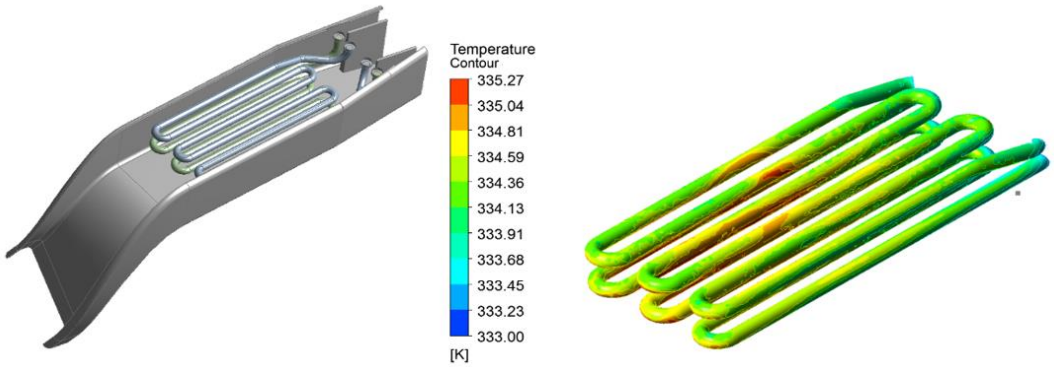


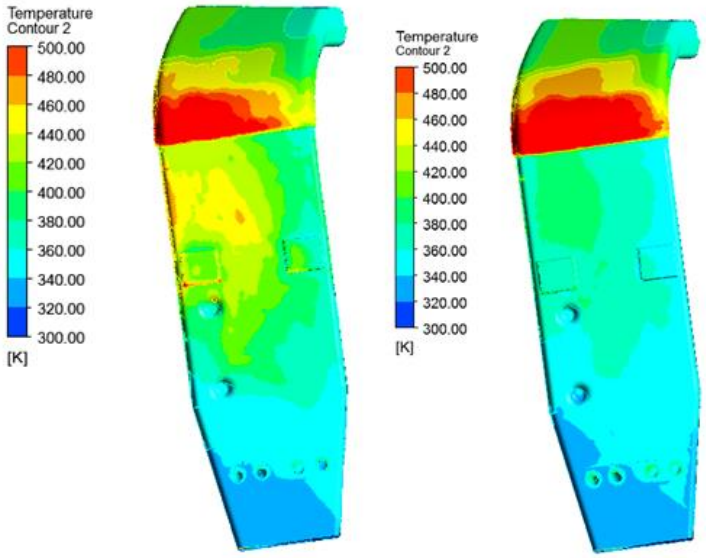
Figure 4.25 750-Watt heater tube's surface temperature distributions according to the CFD result

Table 4.1 Comparison of resistance temperature results between CFD and experimental measurement

Measurements Points	**TC-1**	**TC-2**	**TC-3**	**TC-4**	**TC- 5**	**TC-6**
Experimental Data (°C)	542	605	590	583	504	480
CFD Result Data (°C)	563	603	594	586	503	487
Actual Temp. Difference	-21	2	-4	-3	1	-7

For heat transfer modelling of the heating unit, the heater unit surface material was considered because of its radiation effect on the heat transfer. Analyses are performed

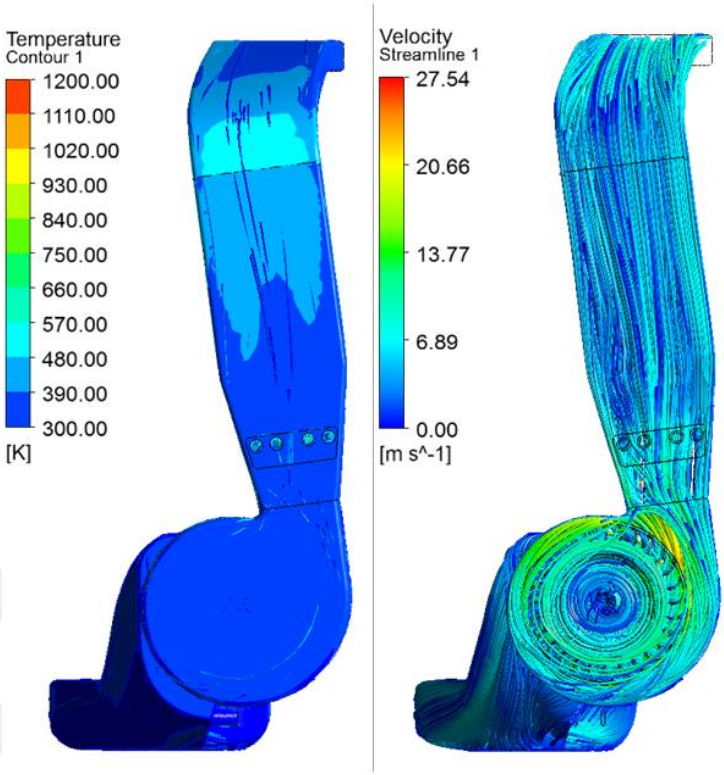
in the case of double resistances work, each equal to 750-Watt power and having 38200 W/m^2 heat flux. The radiation model is selected as Discrete Ordinates, and an anodized aluminium surface (Ɛ = 0.2) is used to analyse the temperature gradients on the external surface of the heater as shown in Figure 4.26.



a. b.

Figure 4.26 The temperature distributions on the outer surface of the heater in the case of two 750-Watt resistances work for a) anodized aluminium surface (Ɛ = 0.2) and b) polished aluminium surface (Ɛ = 0.05)

A rotating frame defines the centrifugal fan flow. The standard k-ε turbulence model simulates turbulent flow, and 2700 rpm fan work is defined. A preliminary result was obtained with the definitions of fan flow and heaters, as shown below. In Figure 4.27, dryer system temperature distributions and streamlines with the effect of fan work are shown.



a. b.

Figure 4.27 a) Temperature and b) velocity distributions across the dryer system

CHAPTER FIVE
DESIGN AND PERFORMANCE DEVELOPMENT STUDIES

5.1 Dryer Unit Design Optimization

In light of the numerical outcomes of established modelling and validation studies, the entire drying system was taken into account, and an optimization study was made to develop a novel design by means of improving drying system efficiency.

Considering the heat transfer mechanism efficiency, obtaining a homogeneous flow structure along the heater channel is critical. Therefore, a heating channel sectional area optimization study was conducted, and a parametric study was made for the channel width in different dimensions, as shown in Figure 5.1.

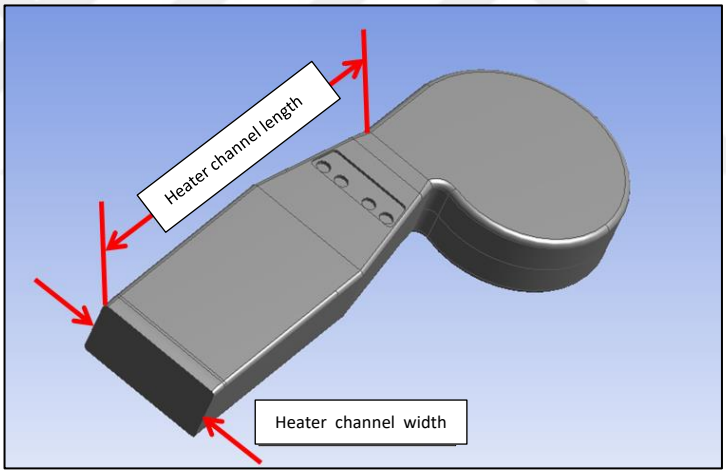
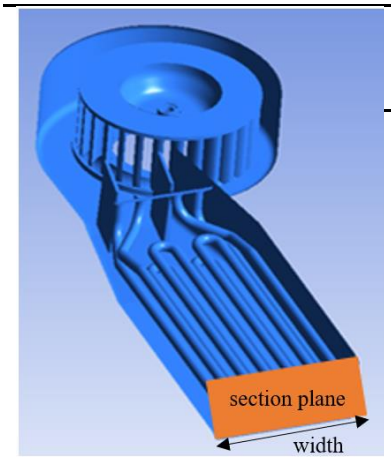


Figure 5.1 Design parameters of the heater unit

The initial width of the heater channel was 88 mm. This value was decreased by 4 mm, 8 mm, 12 mm, and 16 mm, respectively as given Table 5.1, and pressure loss and outlet velocities were examined.

Table 5.1 Heater channel outlet section area

	Parameter	Section Area [mm^2]	Number of Elements	Number of Nodes
	Existing width	3683	5.009.513	924.273
a.	4 mm narrowed width	3520	5.021.536	926.945
b.	8 mm narrowed width	3350	4.985.014	919.775
c.	12 mm narrowed width	3180	4.988.055	920.426
d.	16 mm narrowed width	3014	4.961.806	915.472



As expected, the output velocity of the air from the heater housing increases as the output section is gradually narrowed. As shown in Figure 5.2 and Figure 5.3, as the channel width decreases, the speed increases in the output section up to a certain point and starts to decrease after a certain point. That is, the narrowing of the channel has a negative effect on the speed values in the output section after a specific value.

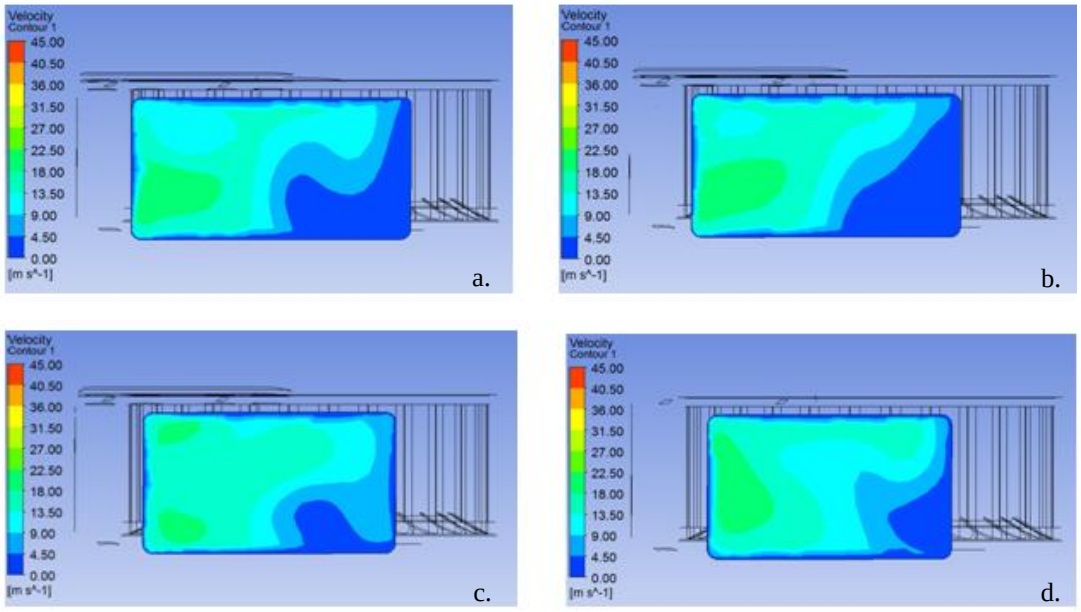


Figure 5.2 Heating channel outlet section velocity distributions at a) 4 mm, b) 8 mm, c) 12 mm, d) 16 mm narrowed width

The speed distributions given in Figure 5.2 show that low velocities occur at the lower right side of the output section. By narrowing the output section, the area of the region where the low velocities occur gradually decreases, and the flow becomes homogeneous. When the velocity distributions of the outlet plane are examined, it is observed that the most suitable design belongs to the design obtained by narrowing the channel by 12 mm.

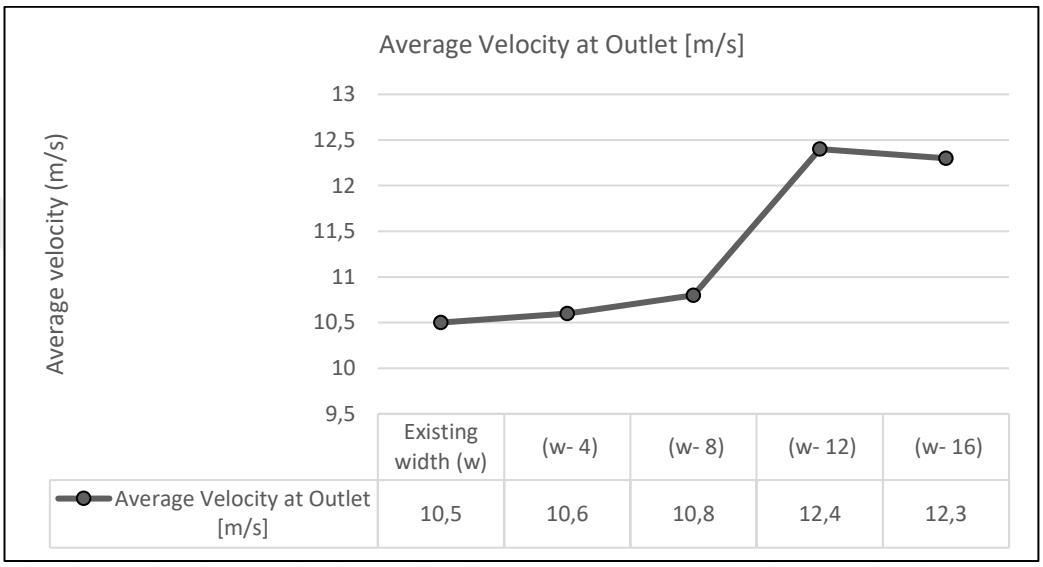
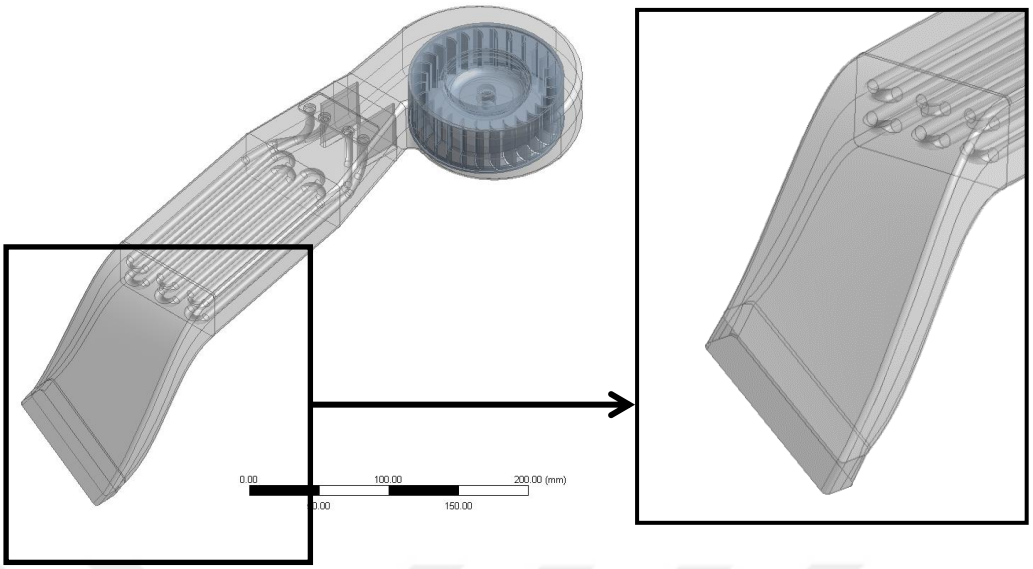


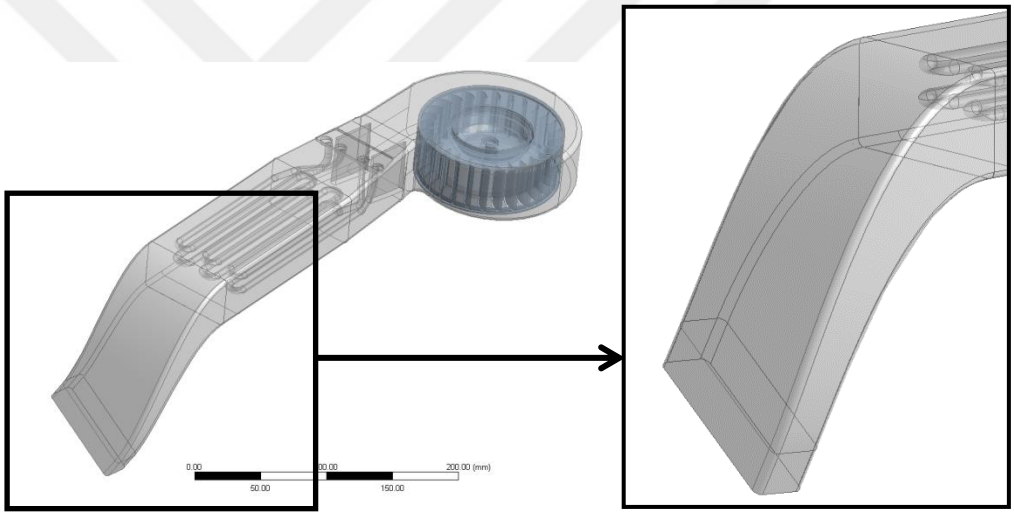
Figure 5.3 Influences of channel width lengths over the average outlet velocity

The optimization study is carried out to obtain a homogeneous flow throughout the outlet within the scope of transforming analysis capabilities into an efficient output. Therefore, different blowing mouth designs are modelled, and flow analysis are run accordingly.

In terms of heat transfer mechanism efficiency, obtaining a homogeneous flow structure along the heater channel is critical. Two different blowing mouth designs were made, and flow analyses were carried out to obtain homogeneous flow throughout the outlet, as given Figure 5.4.



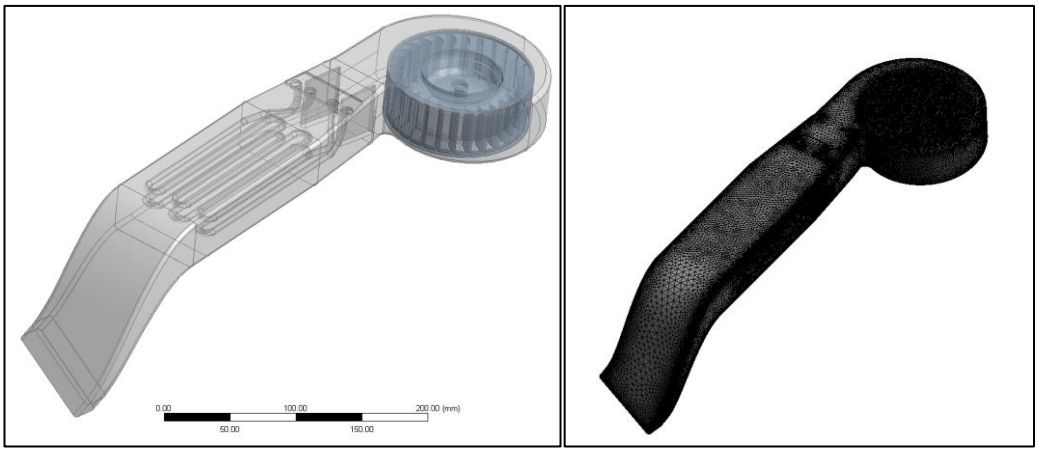
a.



b.

Figure 5.4 Drying system air volume models a) existing design b) proposed design

The numerical model given in Figure 5.5-b considers a tetrahedral grid type with approximately 8.4 million elements and 1.5 million nodes.



a. b.

Figure 5.5 Optimized new heater channel, a) air volume model and b) numerical grid model

A rotating frame is defined for the centrifugal fan region to drive the flow generated by the fan. This rotating frame accurately captures the rotational motion of the fan and its influence on the flow. The k-ε turbulence model is defined to model the turbulent characteristics of the flow. This turbulence model has the ability to capture a wide range of turbulent flow behaviours and is widely used in various CFD simulations.

Numerical study results were obtained after the mathematically converged analysis, shown in Figure 5.6, on the order of 10-4 error values during the 1300 iteration.

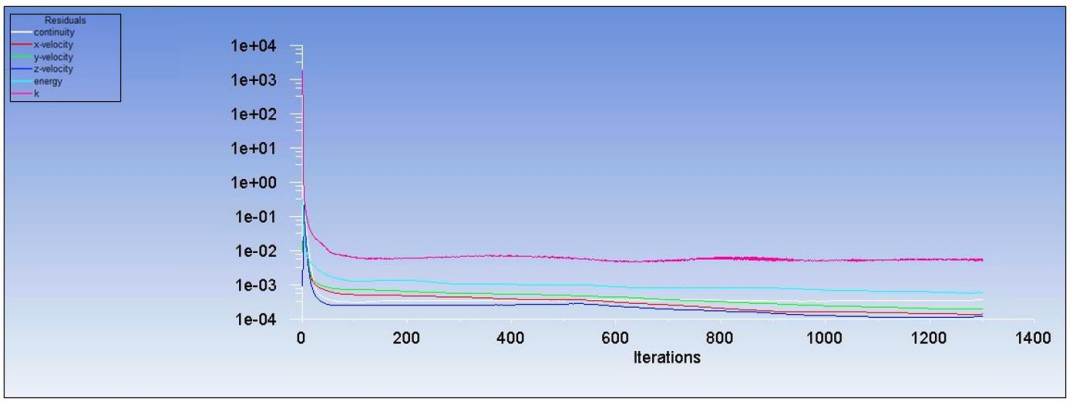


Figure 5.6 Convergency graphic of the numerical analysis.

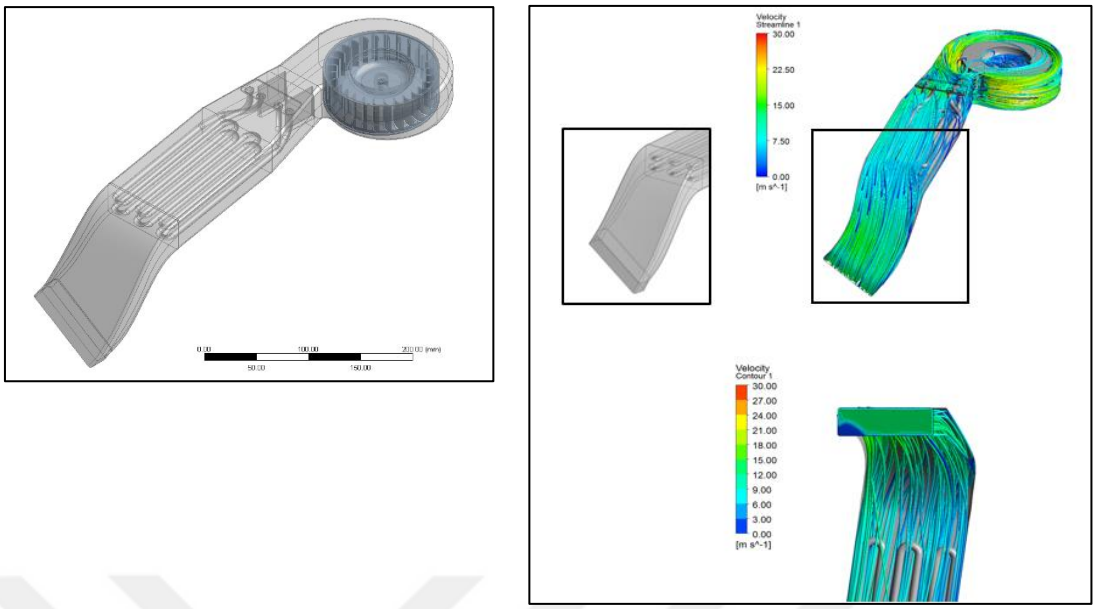


Figure 5.7 Velocity streamlines along the heater channel for existing design

The calculated velocity at the heater channel exit is 8.99 m/s for the current design analysis. As shown in Figure 5.7, the distribution of velocity profiles observed that airflow has irregularities through the channel. As a result of these flow fluctuations, drying airflow at the outlet section did not have a homogenous form.

New blowing mouth geometry designs were prepared to provide a more homogenous flow form at the outlet, and flow analyses were made (Figure 5.8).

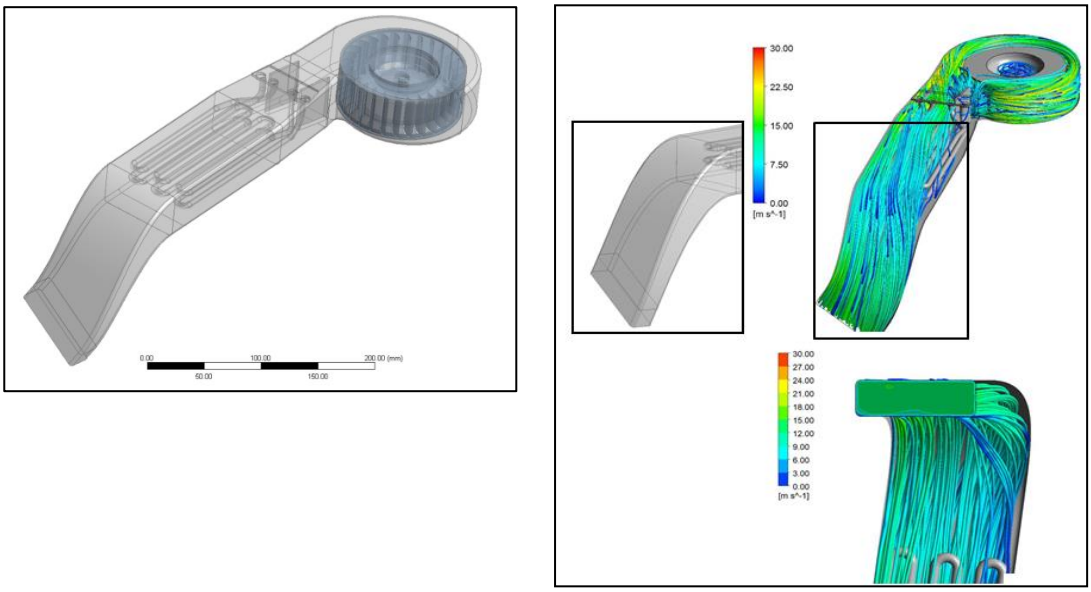


Figure 5.8 Velocity streamlines along the heater channel for the novel design

The average velocity at the outlet was calculated at 13.84 m / s with 0.026 kg /h as the flow rate. When we evaluated the analysis results in this new design, homogeneous flow structure and velocity distribution were obtained.

Airflow through the heater channel became a homogenous flow. The improvement in flow characteristics helps to make a more efficient heat transfer mechanism between air and resistance surfaces and to use energy effectively.

In the comparison between the current design and a proposed new design, Figure 5.9 and Table 5.2 illustrate the placement of the heater resistance and the reduction of its surface area by 10%.

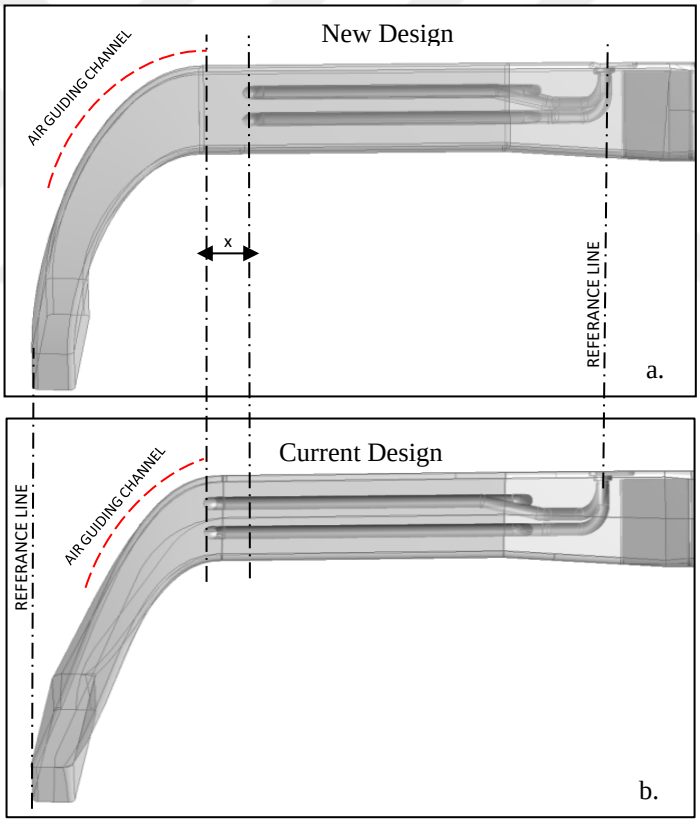
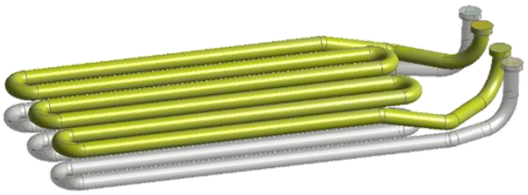


Figure 5.9 Heater placements inside the a) new and b) current design heater channels

By means of novel heating channel design and increased airflow effectiveness for heat transfer, a promising opportunity is gained to make an optimization study for both heaters with 750-watt power.

Table 5.2 Heaters surfaces area



Location of the heaters	Existing Heater Surface Area [m^2]	New Design Heater Surface Area [m^2]
TOP	0.0218	0.0177
BOTTOM	0.0219	0.0178

An energy analysis was conducted on the new heater channel design, and it was found that the outlet air temperature has risen compared to the current design due to an increase in heat flux, as shown in Figure 5.10.

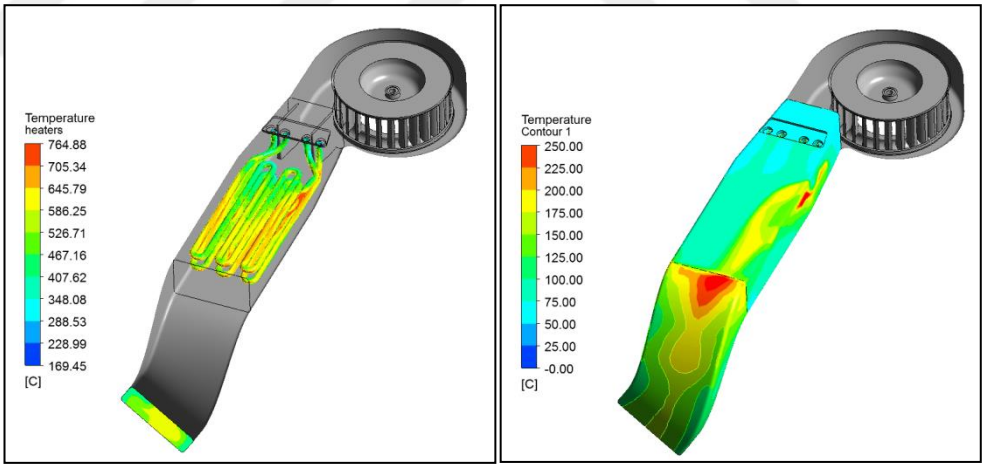


Figure 5.10 Energy analysis results of new heater design

In view of the obtained results, it is interpreted that to retain lower heat flux rates, resistance power can be decreased. The total energy consumption is reduced as a significant gain of the proposed heating channel design.

After the evaluation of the analysis resulting from the novel design, a prototype of the heater channel and suggested resistance geometry (Figure 5.11) was modelled, thus

providing a more realistic verification step for the experimental investigation of the flow characteristic by using the merits of SPIV method (Figure 5.12).

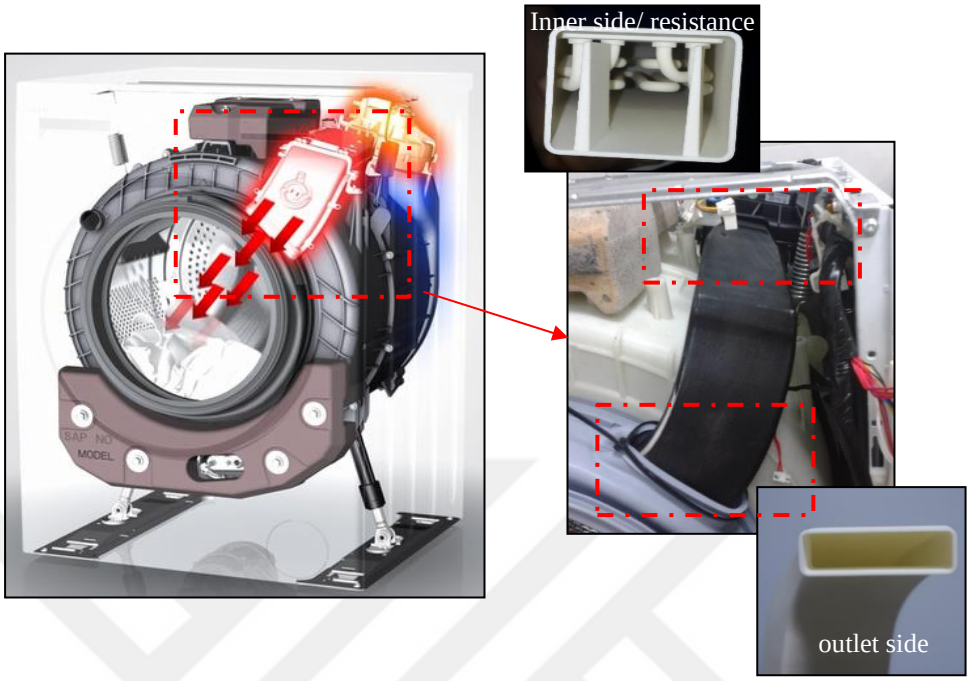


Figure 5.11 Heater channel position and assembly of novel designed heater prototype (Personal archive, 2013)

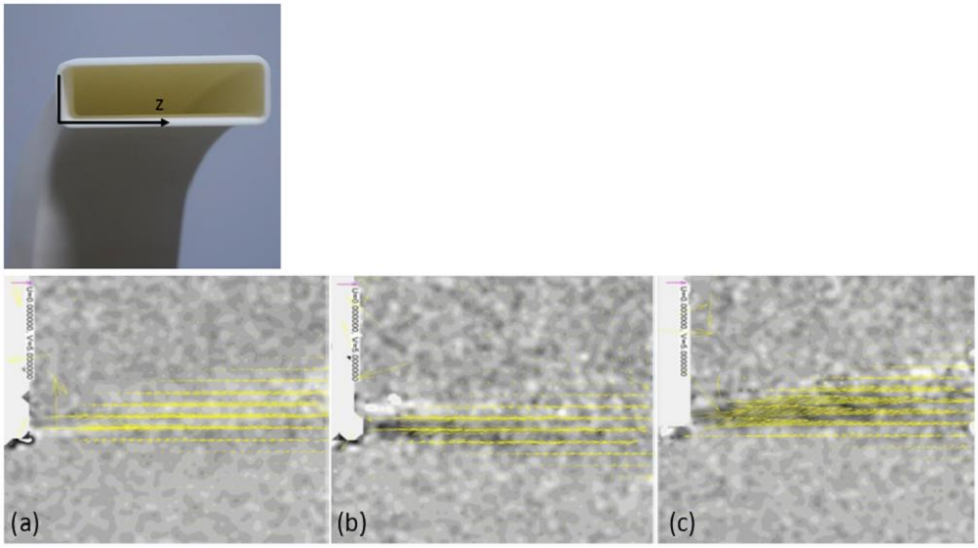


Figure 5.12 Heater channel outlet SPIV measurement plane positions at a) z=0 mm, b) z=40 mm, c) z=80 mm

When these results were examined, it was observed that the flow profile along the guiding plastic was much more homogenous than that occurring in the previous geometry, and the equivalent speed volumes in the jet core were increased. To concurrently evaluate the differences between the current and novel designs, volumetric three-dimensional SPIV velocity vectors were obtained by numerical interpolation from the three-dimensional velocity vector maps as shown in Figure 5.13.

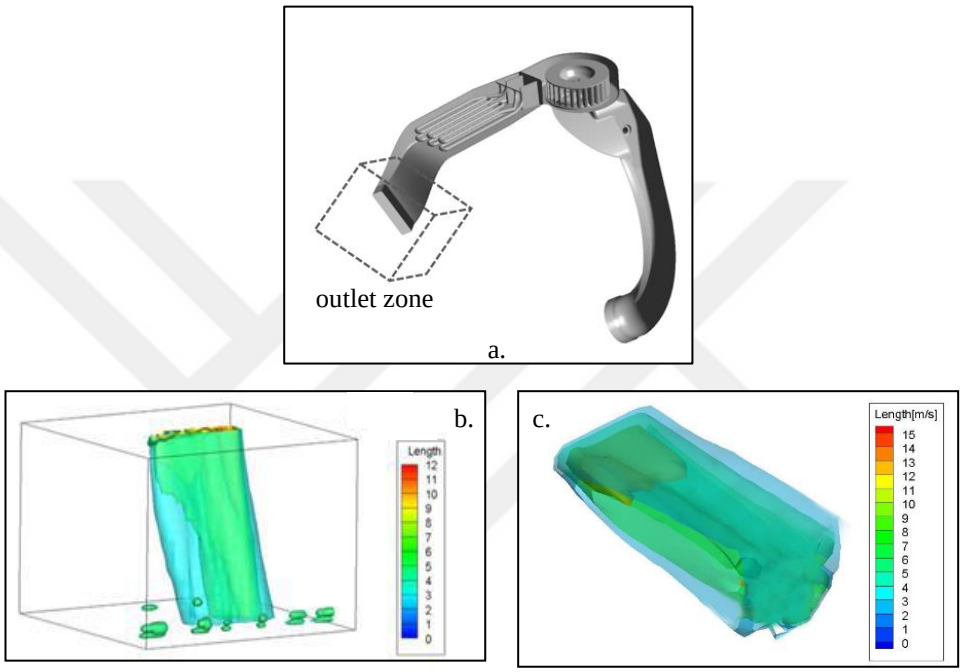


Figure 5.13 a) Heater outlet and equivalent speed volumes for b) current design, c) novel design

According to co-velocity surfaces plotted on volumetric three-dimensional velocity data, the velocity at the core of the new design is 13 m/s, and the current design is 12 m/s. This speed increase was already expected due to the reduction in channel width. However, the fact that the areas of the two cores and flow profiles have also changed substantially indicates that there is also a gain in terms of homogenous flow.

Results of the CFD analysis, shown in Figure 5.13, were compared using experimental SPIV measurements of the velocities along the fan outlet. Airflow at channel output was found to be 13 – 13.8 m/s. Airflow characteristics were also very similar to each other. At this point, the numerical design was validated with SPIV test results by % 94 coherence.

CHAPTER SIX
DROPLET MODEL

6.1 Direct Contact Heat Transfer Model of a Droplet

Regarding modelling the condensation phenomena on liquid droplets, sphere droplets are considered a practical geometry due to their simplicity and real-world applicability (by Boehm, 1987). In this process, the cooler sink fluid is sprayed into the saturated vapor of the fluid under investigation with a velocity v. The vapor condenses onto the droplets and forms a thin film due to the heat transfer among the warmer vapor and cooler fluid. Over time, the condensation process slows down due to the increased thermal resistance caused by the accumulation of the fluid film on the droplets. Additionally, as the fluid's temperature rises, the temperature-driving force reduces, setting a practical limitation on the condensation process.

The heat transfer in the droplet happens mainly through conduction. In spherical coordinates, the temperature equation is the nondimensional conduction equation. The Lock model (by Lock, 1994), as presented in Equation 6.1, describes the heat transfer into the composite film and droplet.

$$\frac{\bar{h}_x x}{k_s} = \frac{2}{\pi^{1/2}} \left(\frac{\vartheta X}{\alpha_s}\right)^{1/2} \tag{6.1}$$

In the given context, X is a variable that represents the distance the droplet travels through the vapor medium. It is defined by X = vt, where v is the droplet's velocity and t is the time. The results mentioned in the statement are applicable in situations where the film thickness is relatively small. In such cases, the term in parentheses, the travel Peclet number, becomes significant. The travel Peclet number relates the convective transport (due to droplet motion) to the conductive transport (within the droplet). It defines the importance of these two heat transfer mechanisms.

For heat transfer, the Péclet number is given in below Equation 6.2:

$$Pe_L = \frac{Lu}{\alpha} = Re_L Pr \tag{6.2}$$

The equation below expresses the rate of droplet growth caused by condensation:

$$\frac{D}{D_i} = 1 + \varphi \left[1 - \exp(-\frac{4\pi^2 \alpha t}{D_i^2})\right]^{1/2} \tag{6.3}$$

$$\varphi = \left[1 + \frac{C_p(T_{sat} - T_i)}{\lambda}\right]^{1/3} - 1 \tag{6.4}$$

In considering the droplet's movement within a vapor-filled setting, its velocity at any given moment is estimated from the below equation:

$$\frac{dV}{dt} = \text{g}\,(\,1 - \frac{\rho_g}{\rho}\,) - \frac{3}{4} C_D \frac{\rho_g}{\rho} \frac{V^2}{D} \tag{6.5}$$

The below equation determines the average droplet temperature :

$$\bar{\theta}(t) = (\,T_M - T_O) \sum_{n=1}^{n=\infty} \frac{6}{\psi_n^3} \frac{(sin\psi_n - \psi_n cos\psi_n)^2}{\psi_n - sin\psi_n cos\psi_n} exp(\,-\psi_n^2 N_{Fo}) \tag{6.6}$$

6.2 JAVA Code Solver

Java Code Inputs:

- Droplet velocity: 0.5 m/s, 1 m/s, 2 m/s, 3 m/s, 4 m/s, 5 m/s where in each case.
- The droplet mass flow rate depends on the velocity at the nozzle exit.
- Initial droplet diameter: 0.62 mm
- Ambient temperature: 69 °C
- Droplet first temperature: 18 ° C
- Channel length: 320 mm
- The Gaussian distribution model is used for droplets with a diameter change between 0.125 mm – 1 mm as a boundary condition to estimate the droplet diameter.

Java Code Outputs:

- Heat transfer coefficient distribution as a function of distance.
- Droplet mass increase as a function of distance.
- Droplet velocity changes as a function of distance.
- Droplet diameter distribution as a function of distance.
- Droplet Temperature difference as a function of distance

As a result of the Java output; heat transfer coefficient rates, droplet mass increases, droplet velocity rates, droplet diameter variation and droplet temperature increase along the channel are plotted in Figure 6.1 to Figure 6.5.

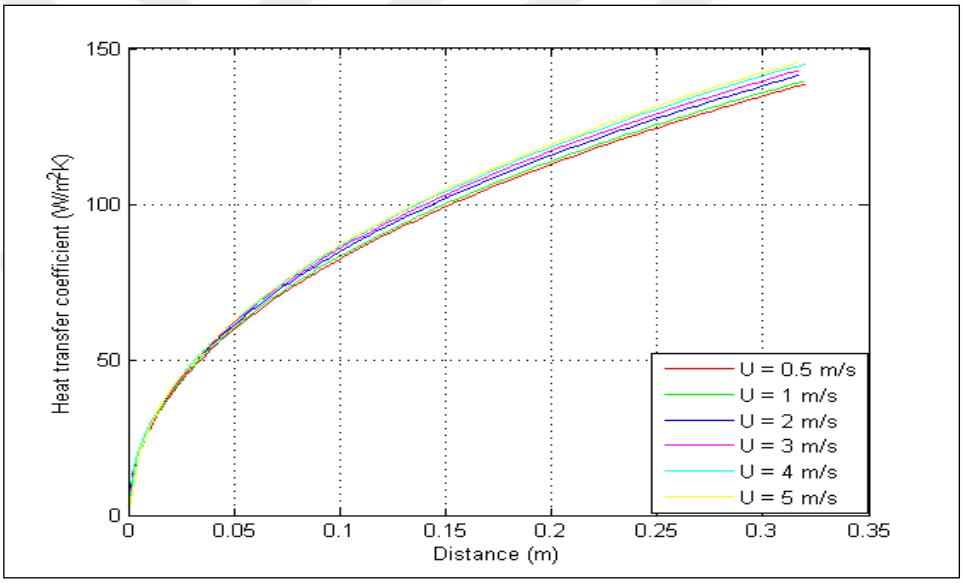


Figure 6.1 Variation of heat transfer coefficient rates along the channel

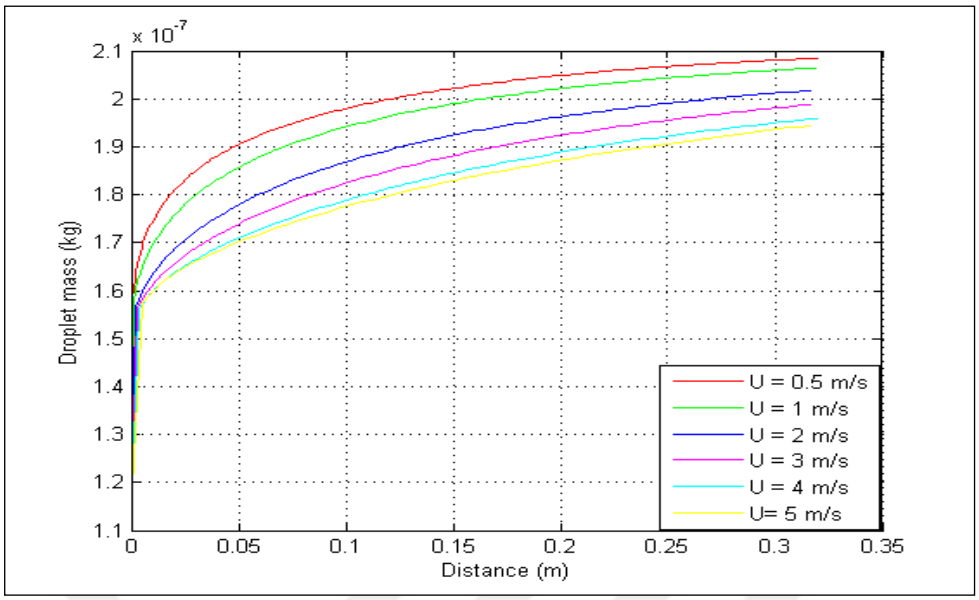


Figure 6.2 Increases in the droplet masses across the channel length

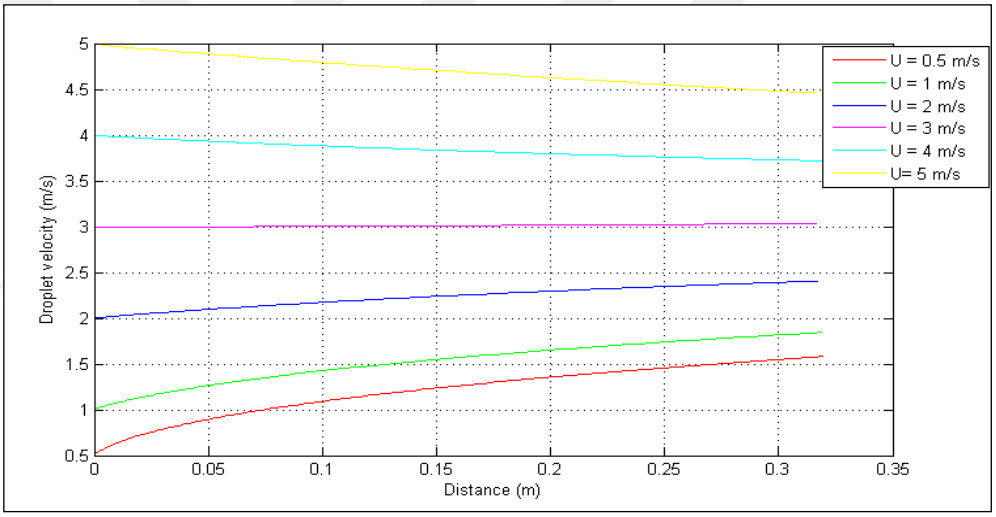


Figure 6.3 Variations in the droplet velocity rates along the channel

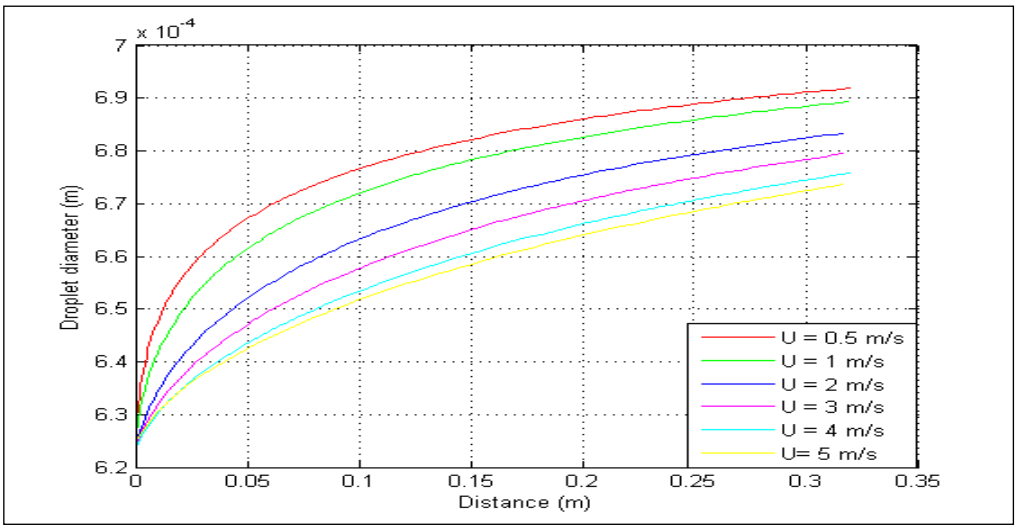


Figure 6.4 Droplet diameter variations in the channel

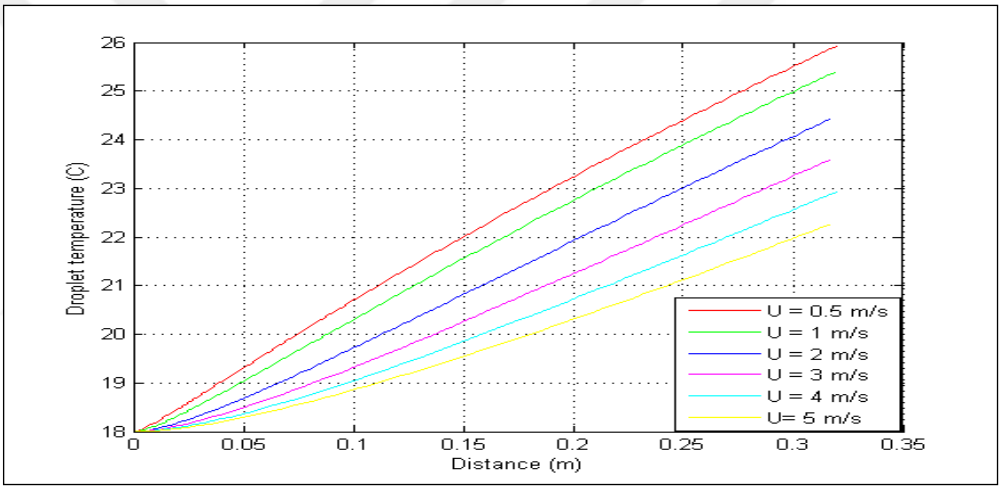


Figure 6.5 Droplet temperature rise along the channel

6.3 Water Droplet Simulation

In Figure 6.6, a lean CFD model of the spray is designed to simulate the water droplet temperature response for the defined boundary conditions reported in Table 6.1.

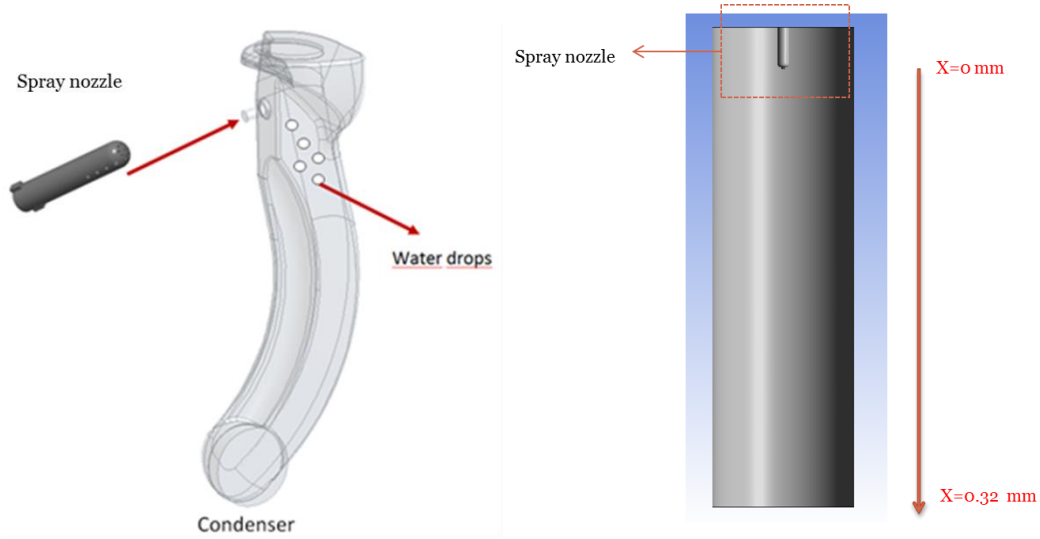


Figure 6.6 Actual condenser model and JAVA -based simulation model

Table 6.1 CFD model inputs

CFD Model Inputs	**Value**
Channel Length	0.32 m
Droplet Diameter	0.6 mm
Droplet Velocity	5 m/s
Droplet First Temp.	18 °C
Ambient Temp. (Moist Air)	69 °C

Spray channel and spray nozzle simulation model and temperature distribution of the droplet along the channel were visualised by CFD method as given in Figure 6.7 and Figure 6.8.

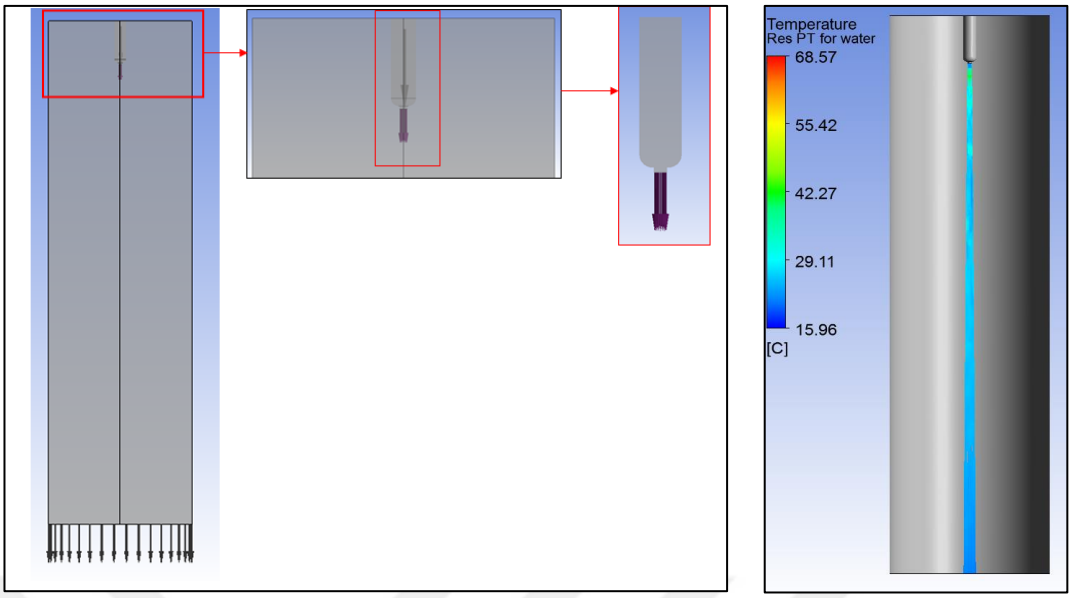


Figure 6.7 Spray channel and spray nozzle model for CFD simulation and temperature distribution of the droplet along the channel

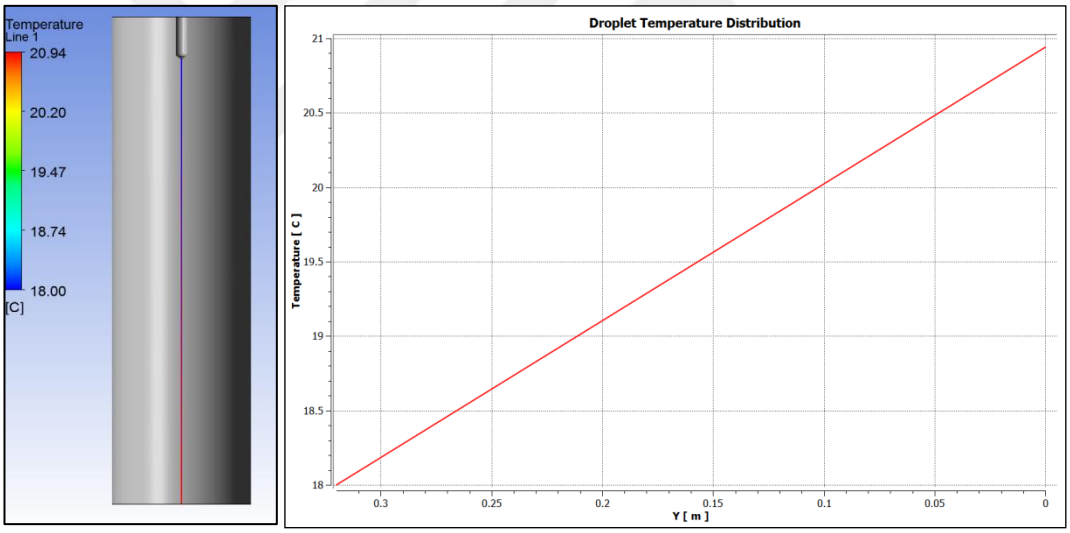


Figure 6.8 Temperature distribution of the droplet along the line

This preliminary study allows us to make a more complex analysis and visualising the droplet modelling.

6.4 Discrete Phase Modeling

Commercial simulation tools include an evaporation model for Discrete Phase Modelling (DPM). This model is based on gradient diffusion. In DPM, the trajectories of particles or droplets are calculated in a Lagrangian frame while coupled to the gas phase in the Eulerian frame through the merits of CFD. This model enables the exchange of mass, momentum, and energy between the two phases.

Turbulence effects on particle trajectories are considered in the DPM model. It finds application in scenarios where particle separation is essential, such as coal classifiers or cyclones. DPM is also utilized in spray drying processes and problems involving liquid fuel or coal combustion.

The force balance equation is used to provide the discrete-phase particle trajectories. This equation considers the effects of gravity and the drag force on the particles. Within the control volumes that cross the particle trajectory, the particles can exchange mass, momentum, and heat with the gas phase.

When using DPM, there are three particle types: inert particles, droplets, and combusting particles. Selecting the droplet particle type enables the modelling of heating, evaporation, and boiling, including energy and mass transfer among the phases.

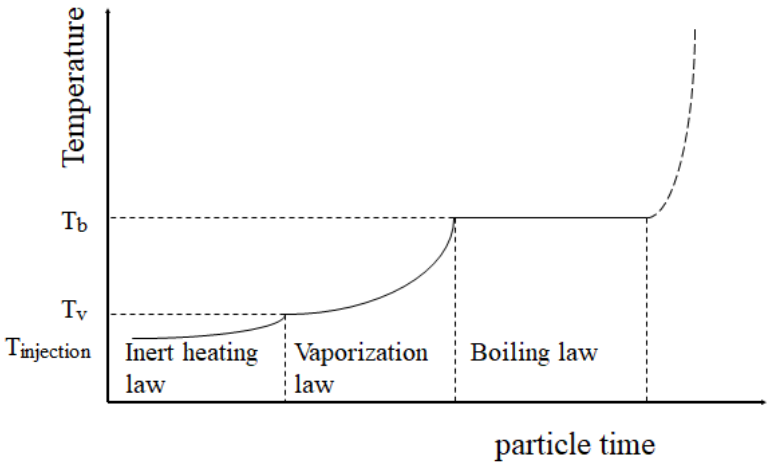


Figure 6.9 The evaporation of a liquid droplet as a function of time

The diagram in Figure 6.9 illustrates the heat and mass transfer process with inert heating law, vaporisation law, and boiling law steps that describe how a liquid droplet evaporates over time after being injected.

The injected particle is heated in the first stage to vaporisation temperature, and vaporization starts as soon as the droplet reaches that temperature. The boiling law defines the mass transfer once the droplet reaches its boiling point.

In the simulation model, the condenser channel receives hot air through the inlet. Liquid drops are injected in a conical pattern given in Figure 6.10 by a nozzle, corresponding to one of the injection types available in the Discrete Phase Model.

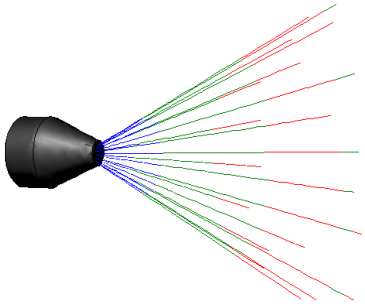


Figure 6.10 A cone injection for 3-D models only where particle streams are injected in a conical pattern

When water droplets are sprayed into the channel, they meet with hot air, causing them to change from liquid to vapor due to heat transfer. The air and vapor mixture then moves downstream within the channel. This simulation allows for studying the behaviour of the water droplets and their interaction with the hot air, enabling analysis of the phase change process and the subsequent flow patterns within the condenser channel.

The solution occurs in two stages:

1. Achieve flow convergence without using DPM and without any evaporation.
2. Initiate DPM injection to resolve the current phase change issue.

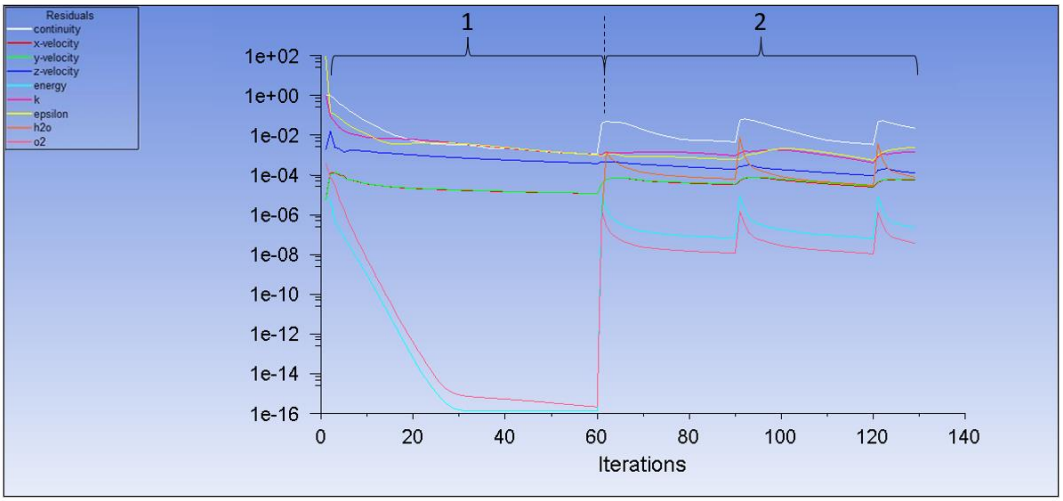


Figure 6.11 Solution residuals

6.4.1 Simplified Model for DPM

In order to avoid the complexity of the analysis, a geometrically simplified channel model with the same dimensions as the exact condenser part was prepared first. As like in the previous thesis studies, below boundary conditions were used for the CFD model as given in Table 6.2.

Table 6.2 Specification for channel model

CHANNEL	DROPLET	AIR
Channel Length: 0.32 m	Droplet Diameter: 0.4 mm	Moist Air Temperature: 400 K
Channel Diameter: 0.07 m	Droplet Velocity: 45 m/s	Air Velocity Inlet: 0.1 m/s
Spray Injection Point: 0.3 m	Droplet Temperature: 291 K	
	Injection Angle: 20 °	

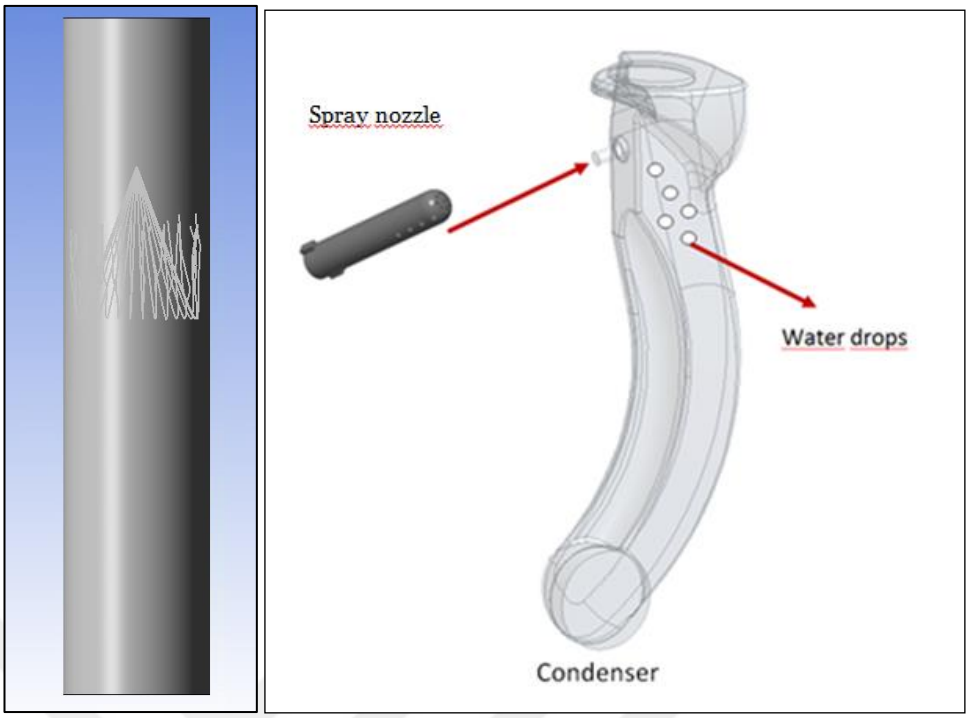


Figure 6.12 Spray channel model and actual condenser model for CFD simulation

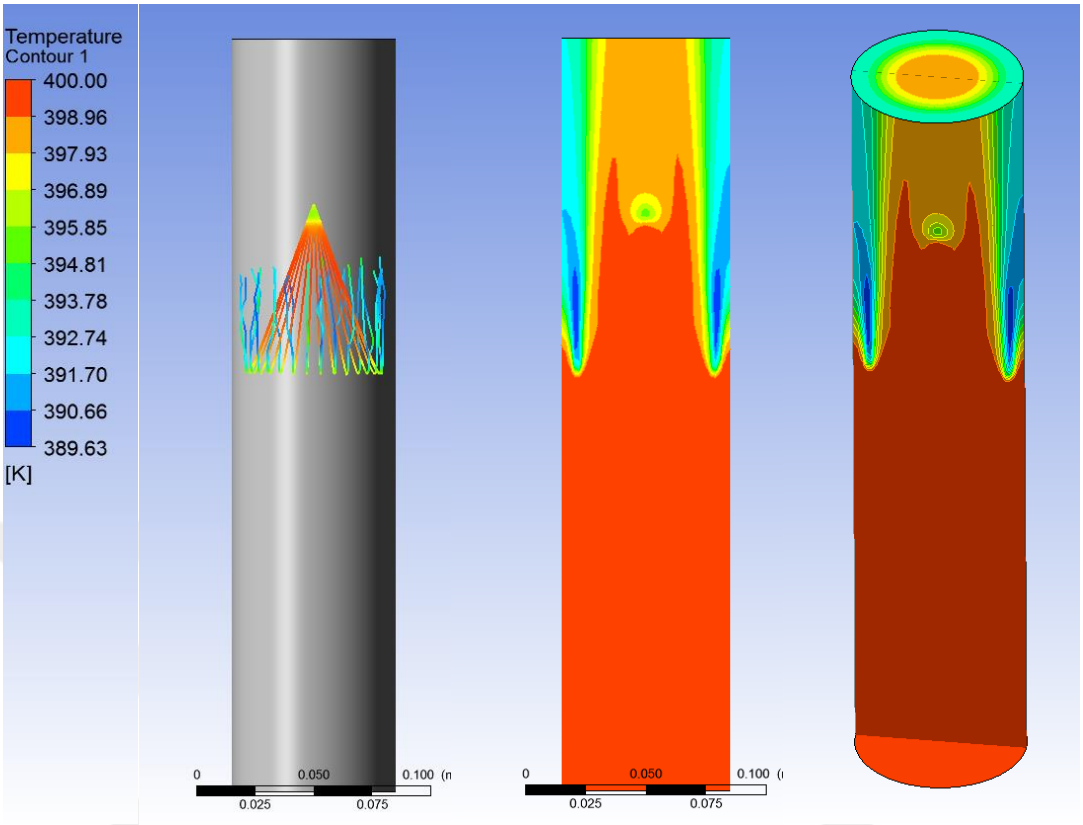


Figure 6.13 Droplet and air temperature distributions after spray injection for the simplified model

```
/report> dpm-summary

 Fate                  Number          Elapsed Time (s)                      Injection, Index
                                     Min        Max        Avg    Std Dev                  Min                  Max
 ----                  ------  ---------- ---------- ---------- ---------- -------------------- --------------------
 Evaporated              1190   1.125e-01  1.267e-01  1.201e-01  2.203e-03     injection-0   61     injection-0  528
 Trapped - Zone 7          10   9.260e-02  1.160e-01  1.078e-01  6.407e-03     injection-0  718     injection-0  492

                   (*)- Mass Transfer Summary -(*)

 Fate                       Mass Flow (kg/s)
                          Initial      Final     Change
 ----                  ---------- ---------- ----------
 Evaporated             9.917e-06  0.000e+00 -9.917e-06
 Trapped - Zone 7       8.333e-08  0.000e+00 -8.333e-08
 ----                  ---------- ---------- ----------
 Net                    1.000e-05  0.000e+00 -1.000e-05

                   (*)- Energy Transfer Summary -(*)

 Fate                        Heat Rate (W)          Change of Heat (W)
                          Initial      Final     Sensible     Latent      Total
 ----                  ---------- ----------   ---------- ---------- ----------
 Evaporated            -2.445e+01  0.000e+00    2.965e-01  2.415e+01  2.445e+01
 Trapped - Zone 7      -2.055e-01  0.000e+00    2.492e-03  2.030e-01  2.055e-01
 ----                  ---------- ----------   ---------- ---------- ----------
 Net                   -2.465e+01  0.000e+00    2.990e-01  2.436e+01  2.465e+01
```

Figure 6.14 DPM summary report

6.4.2 Actual Model for DPM

The CFD analysis has identified the appropriate interface models for both the rotational and stationary domains and the fluid and solid domains. The two-phase air & water flow mixture CFD model is developed to simulate the condenser's heat and mass transfer mechanism. Initial conditions of the mass flow inlet of the water, the volume fraction of the air & water, and adiabatic walls are defined. Mass flow inlet is defined by 2700 rpm fan work as initial boundary conditions, while adiabatic conditions are considered for condenser walls.

To understand how phase change modelling works, it is necessary to investigate the cooling and phase change effects of the condenser water spray nozzle's working principle. To verify the CFD results with experimental data, pressures, temperature, and humidity measurements inside the condenser during the drying cycle are measured.

An explicit CFD model of the spraying particles is developed under the operating conditions defined in Table 6.1 to numerically investigate the sprinkling water droplets' interactive heat and mass transfer mechanism.

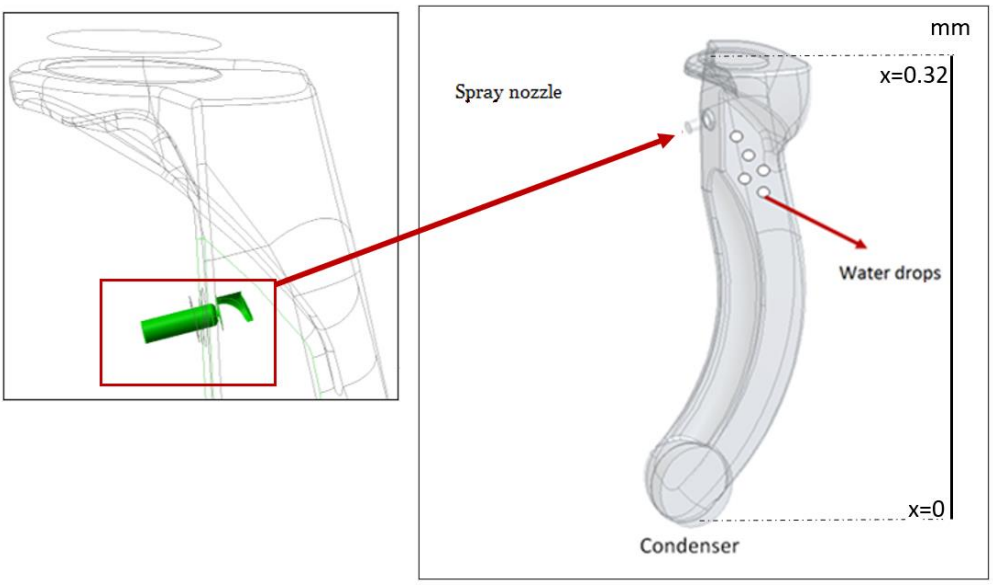


Figure 6.15 Spray nozzle and condenser channel model for CFD simulation

The two-phase finite volume evaporation model was derived from the DPM solver module for the condenser spray model. Definitive droplet parameters are reported in Table 6.3.

Table 6.3. Experimental conditions of droplet.

Model parameter	**Respective values**
Initial droplet diameter (mm)	0.6
Water mass flow rate (kg/s)	0.02
Velocity at nozzle outlet (m/s)	4
Inlet temperature of droplet (°C)	18
Droplet mass (mg)	0.11
Number of droplets per second (1/s)	176.92
Nozzle diameter -D (mm)	2.5
Nozzle outlet area (mm^2)	4.9

The inlet temperature of the water droplet is equal to the mains water's temperature, and it was measured as 18 °C. The initial droplet diameter is visualized by the camera, and it is seen that this diameter varies between 0.3 mm to 0.9 mm, so the initial diameter is accepted as 0.6 mm.

In Figure 6.16, the discrete phase model injection technique is used to inject water droplets into predetermined radial positions. When the water is sprayed and comes into contact with the heated air, it changes phases. The resulting air and vapour mixture then travels downstream. The comprehensive numerical solution representing the phase change process is performed within two distinctive stages. The flow without evaporation is converged in the first stage. Then DPM injection is commenced, as shown in Figure 6.17 by a successful simulation of the complex phase change phenomenon.

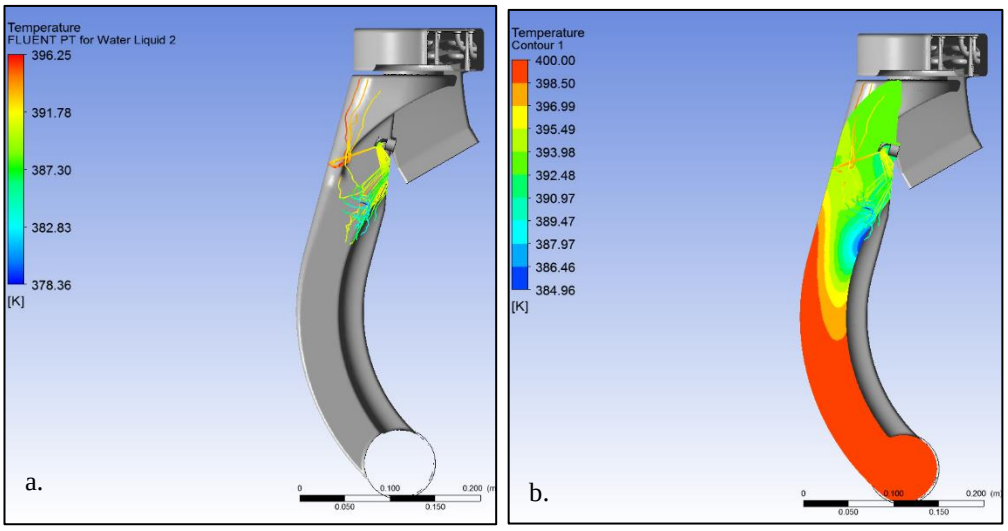


Figure 6.16 a) Droplet temperature and b) air temperature distributions after spray injection for real model

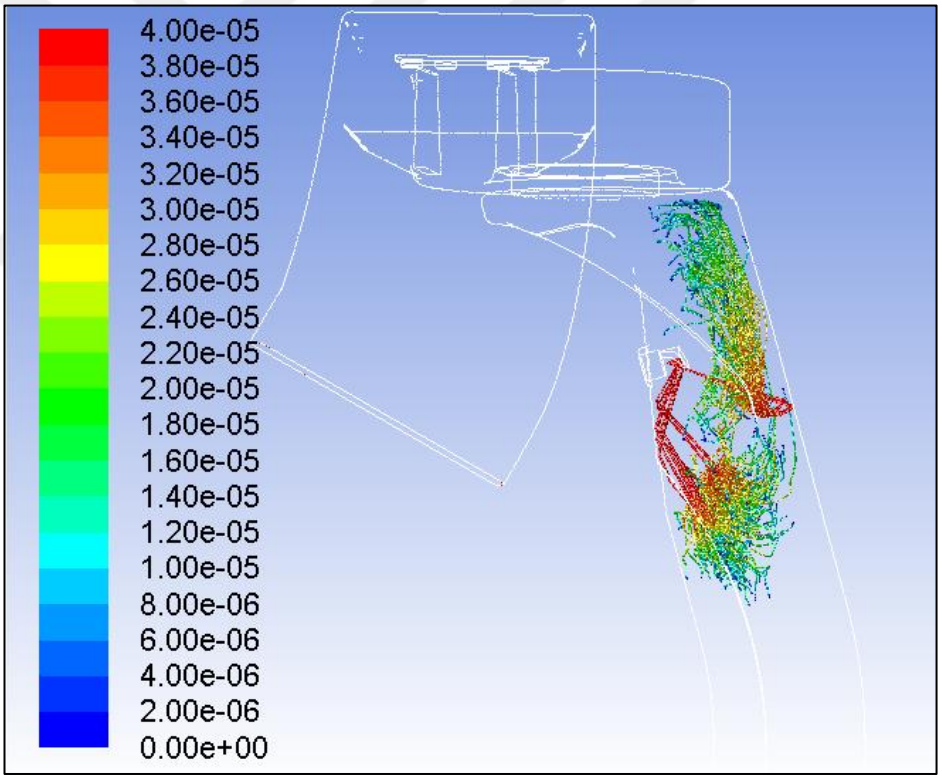


Figure 6.17 Particle track with the change of particle diameter

The total number of the injected spray droplet particles with the specified physical droplet parameters defined in Table 6.2 is calculated as 1200, and evaporation is completed within 0.13 seconds, generating a heat transfer rate of 24 W, as reported in Table 6.4.

Table 6.4 DPM summary report for the actual working condition

Phase	**Number of particles**	**Elapsed time (s)**			
		Min	Max	Avg.	Std. dev.
Evaporated	1200	9.999E-02	1.352E-01	1.157E-01	6.810E-03

Phase	**Mass flow rate (kg/s)**		
	Initial	Final	Change
Evaporated	1.000E-05	0.000E+00	-1.000E-05

Phase	**Heat Transfer Rate (W)**		**Heat Transfer Dynamics (W)**		
	Initial	Final	Sensible	Latent	Total
Evaporated	-2.465E+01	0.000E+00	2.99E-01	2.436E+01	2.465E+01

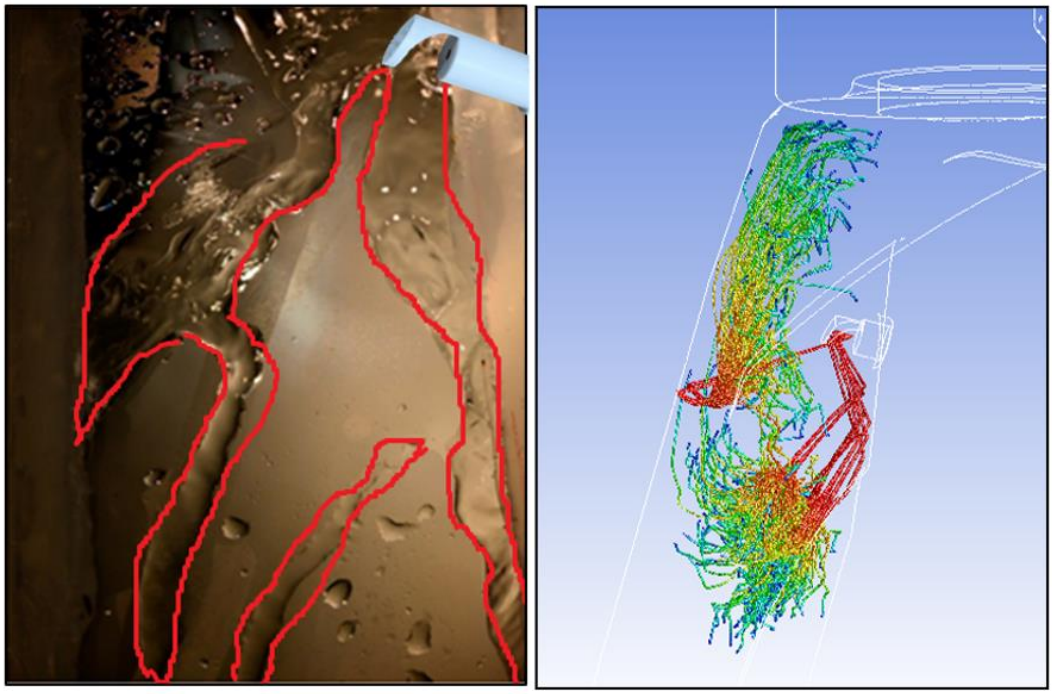
With the help of a sight window on the condenser channel, which we prepared with a transparent PVC part, experimental views of the water spray with and without fan work are visualized in Figure 6.18.



a. b. c.

Figure 6.18 a) Experimental set-up for the sight window of condenser spray channel, b) water spray with fan work and c) water spray without fan work (Personal archive, 2014)

The water flow model of the spray nozzle is illustrated through CFD analysis and compared with the visuals captured by the camera, as depicted in Figure 6.19.



a. b.

Figure 6.19 Particle tracking with a) visualized sprayed model and b) CFD method.

Numerical results reveal that DPM outcomes are in coherence with those found by the CFD method, as mentioned in the previous studies. This thesis report chapter studied the effects of different water droplet sizes and mass flow rates on evaporating performance.

The study aimed to achieve effective evaporation with minimum water consumption. In terms of study, the following conditions are analysed as given in Table 6.5 and comparisons are made according to the actual conditions' particle tracking result as given in Figure 6.20 and Figure 6.21.

Table 6.5 Droplet parameters for 3 different conditions

Parameter	Unit	Actual Condition	1 st Condition	2 nd Condition	3 rd Condition
Droplet Diameter	m	0.0006	0.00004	0.0001	0.0001
Water Mass Flow Rate	kg/sn	0.02	0.00001	0.00001	0.00001
Velocity at Nozzle Outlet	m/sn	4	45	45	5
Droplet Mass	kg	1.1 E-07	3.3 E-11	5.2 E-10	5.2 E-10
Number of Droplets Per Second	1/sn	176,929	298,567	19,108	19,108
Nozzle Diameter (D)	mm	2.5			
Nozzle Outlet Area	m^2	4.9 E-06			

```
Fate                    Number          Elapsed Time (s)                      Injection, Index
                                       Min        Max        Avg    Std Dev                  Min                  Max
----                    ------  ---------- ---------- ---------- ---------- -------------------- --------------------
Evaporated                 400   6.264e-01  2.149e+00  8.916e-01  2.251e-01     injection-1  252     injection-1 1105

                  (*)- Mass Transfer Summary -(*)

Fate                          Mass Flow (kg/s)
                         Initial      Final     Change
----                     ---------- ---------- ----------
Evaporated                3.333e-06  0.000e+00 -3.333e-06

                  (*)- Energy Transfer Summary -(*)

Fate                          Heat Rate (W)          Change of Heat (W)
                         Initial      Final     Sensible     Latent      Total
----                     ---------- ----------   ---------- ---------- ----------
Evaporated               -8.218e+00  0.000e+00    9.967e-02  8.119e+00  8.218e+00
```

Figure 6.20 DPM summary report for the actual working condition

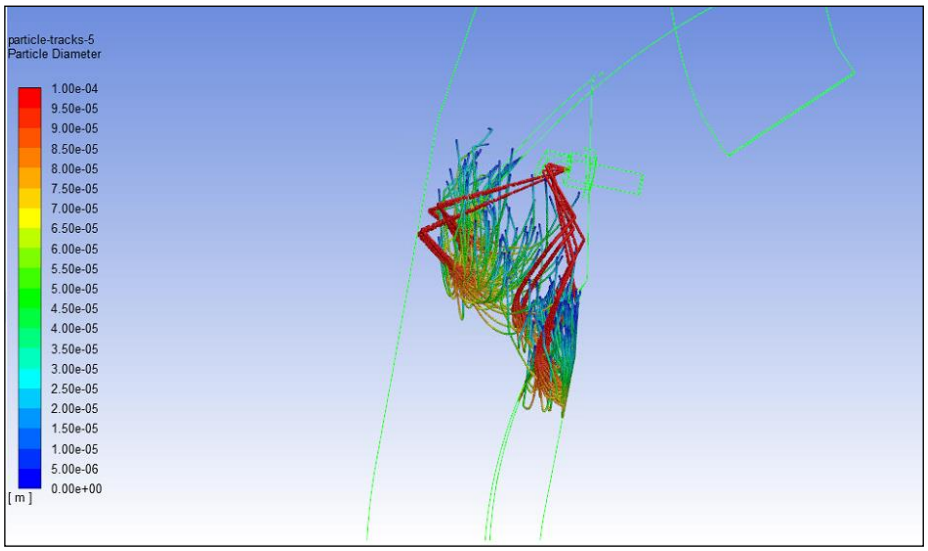
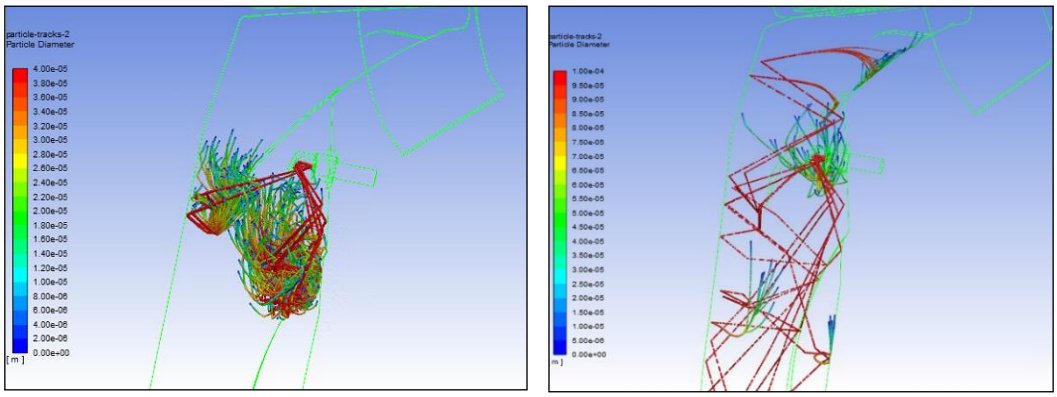


Figure 6.21 Particle track of particle diameter variance for actual condition

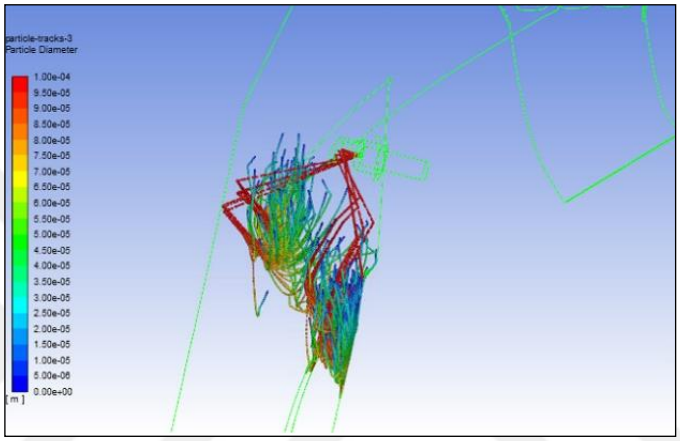
A two-phase and steady-state finite volume evaporation model was derived with a DPM solver module for the condenser spray. Summary of the operational conditions for droplet diameter, water mass flow rate, velocity at nozzle outlet and number of droplets are given in Table 6.6.

Table 6.6 Summary of the operational conditions

Real Condition	**1 st Condition**	**2 nd Condition**	**3 rd Condition**
Droplet Diameter	↓	↓	↓
Water Mass Flow Rate	↓	↓	↓
Velocity at Nozzle Outlet	↑	↑	↔
Number of Droplets Per Second	↑	↓	↓



a. b.



c.

Figure 6.22 Particle tracks of particle diameter variance for 3 different conditions a) 1st Condition, b) 2nd Condition, c) 3rd Condition which are given in Table 6.4

Efficient evaporating performance was obtained with minimum water consumption by the 3rd condition, remarkable results are achieved as given in Figure 6.23.

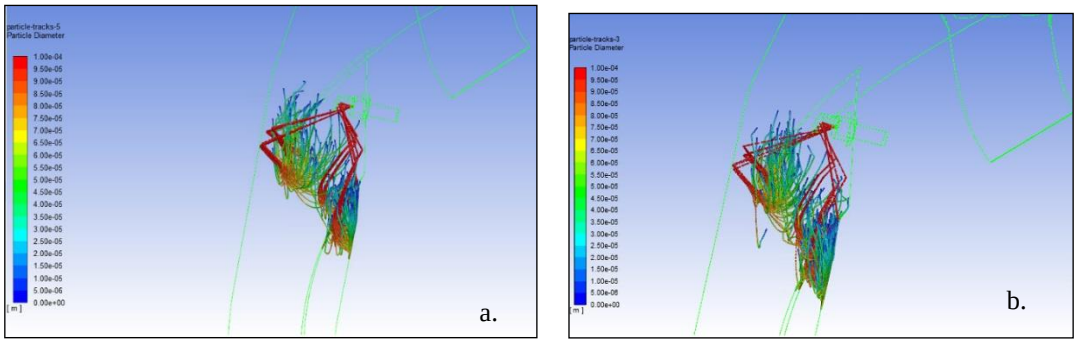


Figure 6.23 Particle track of particle diameter variance for a) actual condition and b) efficient 3rd condition

CHAPTER SEVEN
LAUNDRY DRYING

7.1 Mathematical Model to Simulate the Dehumidification Process

Literature related to this subject is composed of insightful and commanding experimental and CFD simulation-based research studies. Some promising and scientifically satisfactory research studies in the compiled literature deal with the numerical modelling of stratified two-phase flows driven by the coupled heat and mass transfer mechanism. The advantages of direct contact condensation have been thoroughly researched and explored in relation to concurrent heat and mass transfer across an unstable steam-water interface.

Mabrouk et al. (2006) examined the coupled mass and heat transfer that takes place throughout the process of air and porous material. The mechanism, schematically depicted in Figure 7.1, is typically considered the mass transfer of moisture from the porous substance to the air.

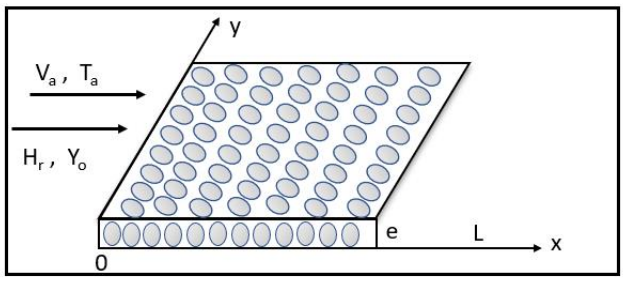


Figure 7.1. Schematic of cotton sample inside dryer tunnel (Mabrouk et al, 2006)

Under the influence of in-equilibrium operating conditions, thermal exchange among two mediums is the primary process maintaining the continued moisture transfer from the textile component to the hot air stream. The linear fall caused by the regulating heat and mass transfer processes is the conventional description of the moisture content fluctuation in the porous fabric substance with regard to total drying time. It is crucial to understand that the energy exchange and the phase shift of the contacting substances, such as air and water, do not simply follow a directly

proportionate relationship that drives the inner framework of porous materials. Ip and Wan (2012) introduced non-stationary mathematical models centred around the thermo-physical characteristics of fabric materials to address the drawbacks of linear models and obtain more accurate simulation results. These non-linear models account for many mechanical and physical characteristics of the drying materials, such as mass density, flow viscosity, thermal conductivity, diffusion characteristics, cohesive characteristics, and flow kinetics. To better depict the drying process's intricacies and increase the simulation results' precision, these qualities are considered while determining the empirical non-linear model parameters.

The available moisture in the fabric is transformed into a vapor phase after the required amount of energy is transferred from the process air to establish the governing mass transfer process. Simultaneously occurring moisture reduction in the process of air and fabric temperature increase is a complex and complicated interlinking mechanism whose underlying driving force should be identified to understand better the essentials of this extensive coupled heat and mass transfer process. The fabric drying process curve for the three different stages of drying is schematically depicted in Figure 7.2.

Different kinds of diffusion theories have been proposed to design the intrinsic characteristics of the dying process due to the incapabilities of the linear heat transfer models in modelling convection and convection mechanisms.

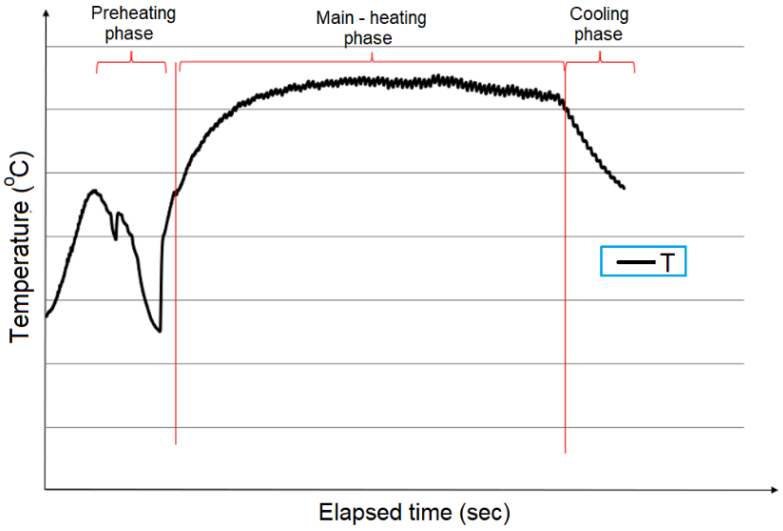


Figure 7.2. The fabric drying process curve illustrates the three different stages of drying.

The amount of water vapor evaporated inside the fabric material is much less than that of its boundary surface in the continuous drying period.

In a drying process, there are mass balance equations for each component, including water, vapor, and air, are given as:

- Phase transition of water inside the fabric.

$$\rho^s \dot{X}^l = -divW^l + \Psi^l \tag{7.1}$$

- Phase transition of vapor respectively inside the fabric.

$$\rho^s \dot{X}^v = \Psi^v \ll \rho^s \dot{X}^l \tag{7.2}$$

- Phase transition of air respectively inside the fabric.

$$\rho^s \dot{X}^\alpha = 0 \tag{7.3}$$

The mass flux of water:

$$W^l = -\Lambda^l \left[\left(\frac{\partial \mu^l}{\partial T^l} \right) T^l + \left(\frac{\partial \mu^l}{\partial \theta^l} \right) \theta^l + \left(\frac{\partial \mu^l}{\partial X^l} \right) X^l - \mathrm{g} \right] \tag{7.4}$$

$$C^l = \left(\frac{\partial \mu^l}{\partial \theta^l} \right) \tag{7.5}$$

The mass flux of vapor:

$$W^v = -\Lambda^v \left[\left(\frac{\partial \mu^v}{\partial T^v} \right) T^v + \sum \left(\frac{\partial \mu^v}{\partial \theta^v} \right) \theta^v \right] \tag{7.6}$$

$$C^v = \left(\frac{\partial \mu^v}{\partial \theta^v} \right) \tag{7.7}$$

One of the most popular methods for drying clothes is using hot air in a clothes dryer. To ensure effective drying, it is crucial to carefully monitor the moisture levels of the fabric throughout the process until it reaches the minimum moisture ratio (MR). The MR measures the moisture content difference at any time relative to the initial state during the drying.

Fick's second law equation associated with the mass transfer between two adjacent mediums is used to model the tendencies of the drying process prevalent in the falling rate period of moisture-removing material. Then, effective diffusion coefficient (D_{eff}) can be obtained by employing the known Moisture Ratio (MR).

Yılmaz et al. (2017) summarized Fick's diffusion equation for flat geometries:

$$MR = \frac{(X - X_e)}{(X_0 - X_e)} = \frac{8}{\pi^2} \exp\left(-\frac{\pi^2 D_{eff} t}{L^2} \right) \tag{7.8}$$

where $\boldsymbol{X}$ is the moisture content at any time (kg H_2O/kg dry solid), $\boldsymbol{X_0}$ is the initial moisture content (kg H_2O/kg dry solid), $\boldsymbol{X_e}$ is the equilibrium moisture content (kg H_2O/kg dry solid), $\boldsymbol{D}_{\text{eff}}$ is the effective moisture diffusivity ($m^2\ s^{-1}$), $\boldsymbol{L}$ is the flat thickness (m) and $\boldsymbol{t}$ is elapsed time (min).

Natural logarithm of MR (ln(MR)) against the elapsed drying time allows for the calculation of the effective moisture diffusivity and a straight line representing the slope of K can be expressed by the below equation:

$$K = \frac{\pi^2 D_{eff}}{L^2} \tag{7.9}$$

Diffusion activation energy can be determined by the Arrhenius-type equation:

$$D_{eff} = D_0 \, exp\left(-\frac{E_a}{RT}\right) \tag{7.10}$$

where $\boldsymbol{D}_0$ is the pre-exponential factor of the Arrhenius equation ($m^2\ s^{-1}$), $\boldsymbol{E_a}$ is the activation energy (kJ mol^{-1}), $\boldsymbol{R}$ is the universal gas constant (kJ $mol^{-1}\ K^{-1}$), and $\boldsymbol{T}$ is the absolute temperature (K).

The diagram given in Figure 7.3 below illustrates how heat and moisture transfer simultaneously between fabric and hot air in a drum during a process. This information is based on literature studies and is intended to provide a basic understanding of the mechanisms involved.

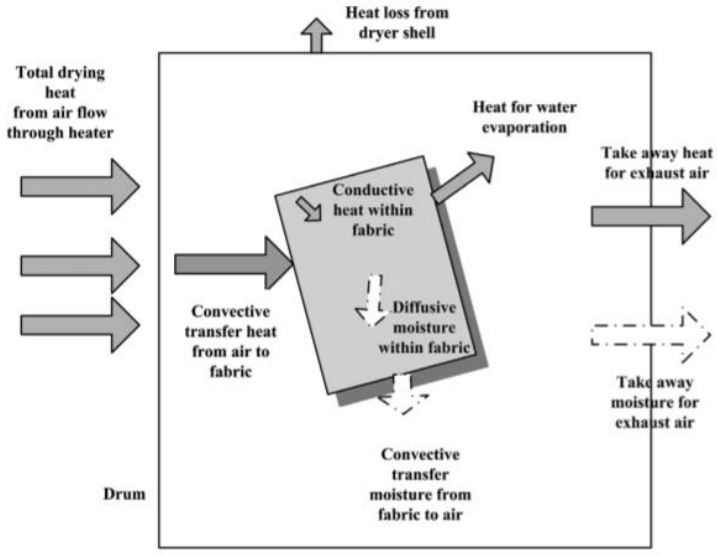


Figure 7.3 Convective textile drying process boundary volume illustration (Yuhui, Jiale & Xuemei, (2016)

In order to confirm the accuracy of the collected data from experiments, a generic finite volume model has been created. This model is used to simulate moisture absorption from cotton laundry and to model the drum and laundry sub-volumes using CFD code, as seen in Figure 7.4.

A mesh grid depicted in Figure 7.5 comprising nearly one million finite elements is generated to simulate the moisture absorption from the sample cotton laundry and to model intrinsically shaped heat and mass transfer mechanisms inside the drum and laundry volumes.

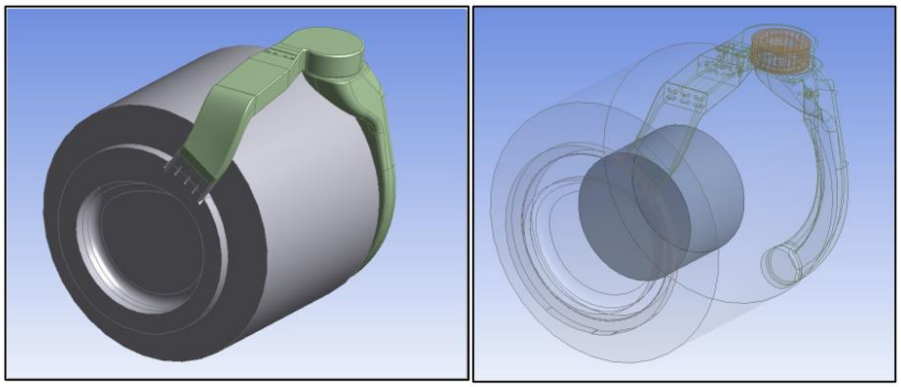


Figure 7.4 Drum and laundry volume model for CFD simulation

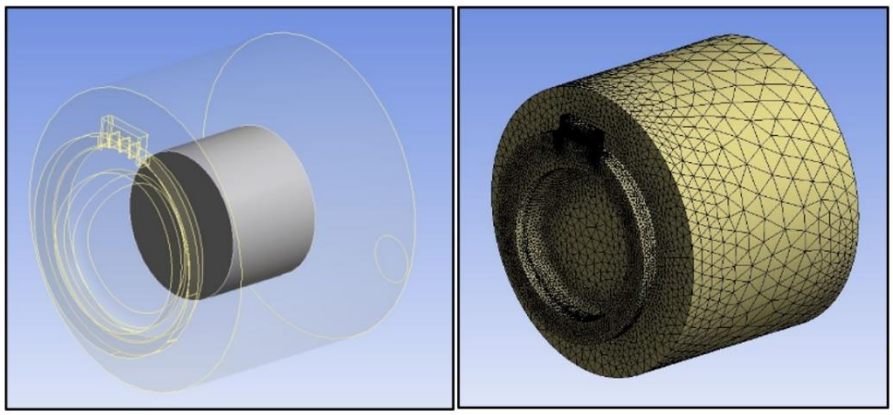


Figure 7.5 Numerical grid model of drum and laundry volume

The cotton-type fabric material is considered for the laundry, and its corresponding material properties are defined according to Table 7.1 to the porous model with a 0.8 porosity ratio.

Table 7.1. Material definition for cotton

Density (kg/m^3)	1350
Specific Heat (J/kgK)	1210
Thermal Conductivity (W/mK)	0.071

A sequential approach is used because of the intrinsic difficulty of the mass transfer from the laundry sample and the majority of direct contact condensation in the water spray. The 2D and 3D temperature distribution of the specimen fabric in a steady state is shown in Figure 7.6. During the linked heat and mass transfer process, a visible temperature gradient occurred within the fabric specimen.

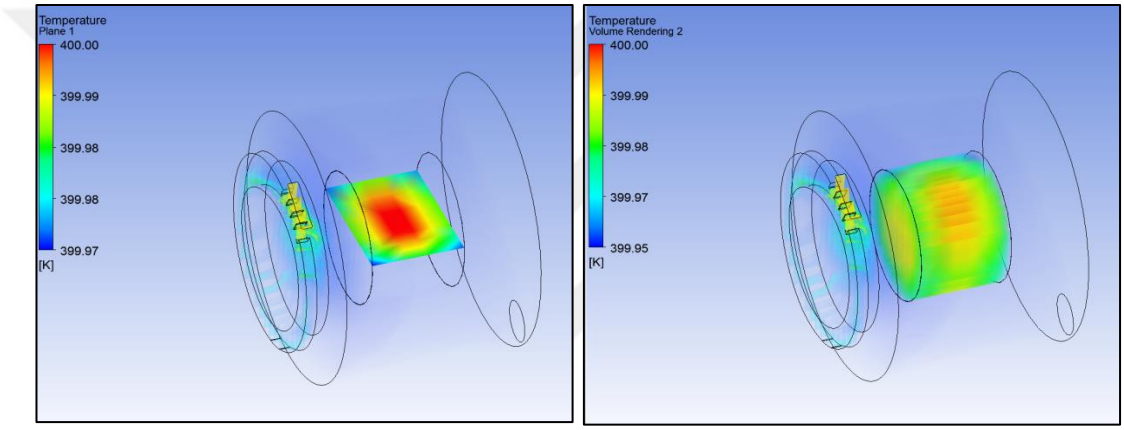


Figure 7.6 Temperature distribution for the laundry

Figure 7.7 shows the inclinations of the velocity streamlines inside the washer-dryer system. Tendencies of velocity streams are affected by the rotating direction of the tumble and circulation of the process of hot air.

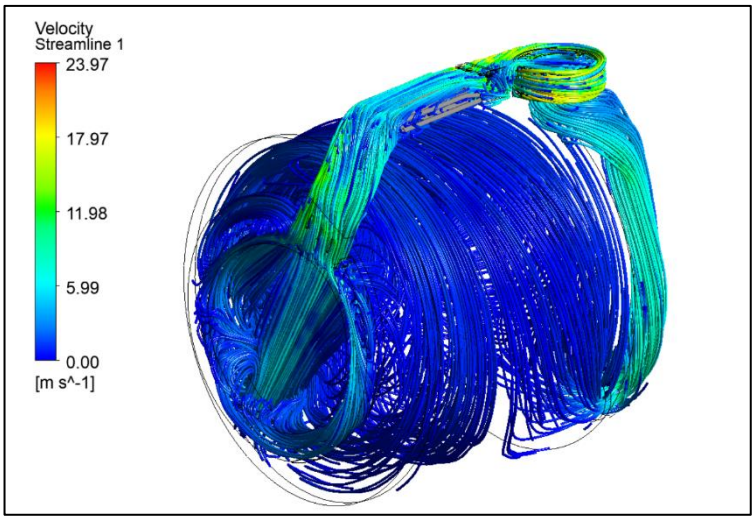


Figure 7.7 Velocity streamlines for the inside volume of the washer-dryer system

Besides, it is worth mentioning that steady state analysis covers the utilization of the Discrete Phase Method, which simulates the air-water mixture in the wet cotton laundry as a surface droplet.

Figure 7.8 visualizes the physical description of the laundry in the tumble generated by the CAD interface. Considering a stationary cylindrical-shaped laundry volume for simplicity, whose diameter is 0.18 m, the initial temperature is 300 K. The flow rate of the process fluid streaming over the laundry is 0.5 kg/s.

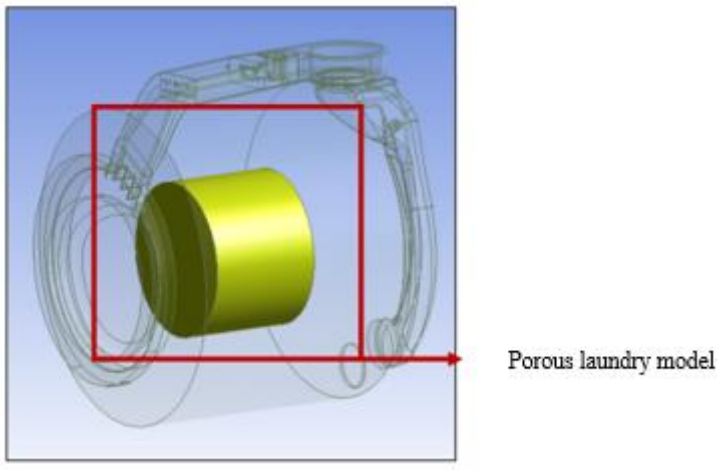
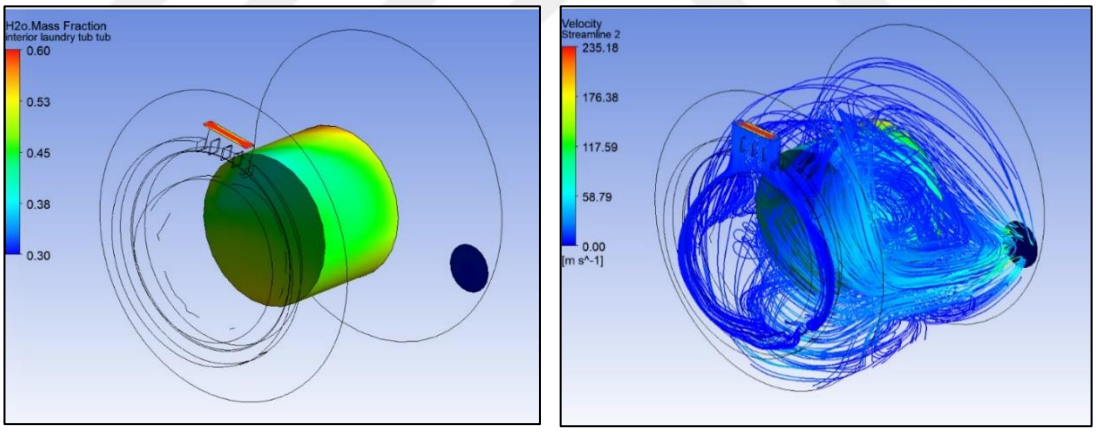


Figure 7.8 Schematic representation of laundry model

Dehumidification of a fabric material through the available thermal energy has been the conventional procedure between industrial applications. It is one of the most accepted moisture removal methods relying on its effectivity in reduced process time as well as its higher capabilities in moisture removal rates efficiency. During the CFD analysis, the mass concentration of moisture in the process air and the evaporation rate in the wet fabric material are tracked. It is crucial to consider the impact of any alterations in the physical characteristics of the two agents as it can significantly impact the results of heat and mass exchange.

Figure 7.9 provides the CFD analysis result of the dehumidification process taking place in the laundry residing in the tumble. It can be clearly observed from the water mass fraction bar in the figure that effective dehumidification is evident for the laundry, such that half of the mass fraction of the water is removed from the laundry during the process. Figure 7.9-b shows the inclinations of the governing streams' velocity streamlines under the rotating drum's influence.



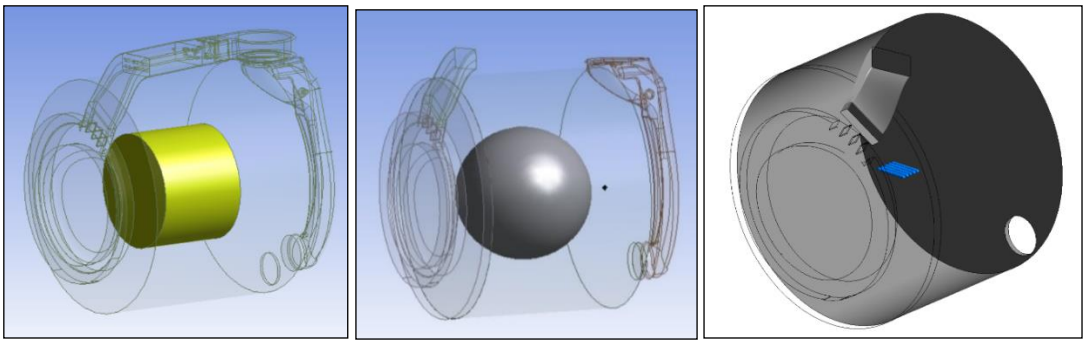
a. b.

Figure 7.9 a) Water mass fraction of the laundry and b) flow distribution inside the drum

Three different source models have been derived to simulate the wet cotton laundry inside the drum. Figure 7.10 shows the source models that simulate the wet laundry in the exhaustive CFD analysis.

Figure 7.10-a schematically explains the first source model, which considers the lateral surface of the cylindrical volume as a wet laundry. In the second approach,

Figure 7.10-b, a bulk spherical volume is put into perspective to model the wet laundry. The final approach, Figure 7.10-c, simplifies the model without imposing restrictions, allowing multiple injection source point definitions.



a. b. c.

Figure 7.10 Moisture source definitions a) surface type, b) spherical one body, c) multiple source points

A detail of the third and selected approach schematic is given in Figure 7.11. Dependent on the application and acceptance criteria, multiple injection source points are defined with 0.1 mm diameter and a total of one hundred sources in five rows.

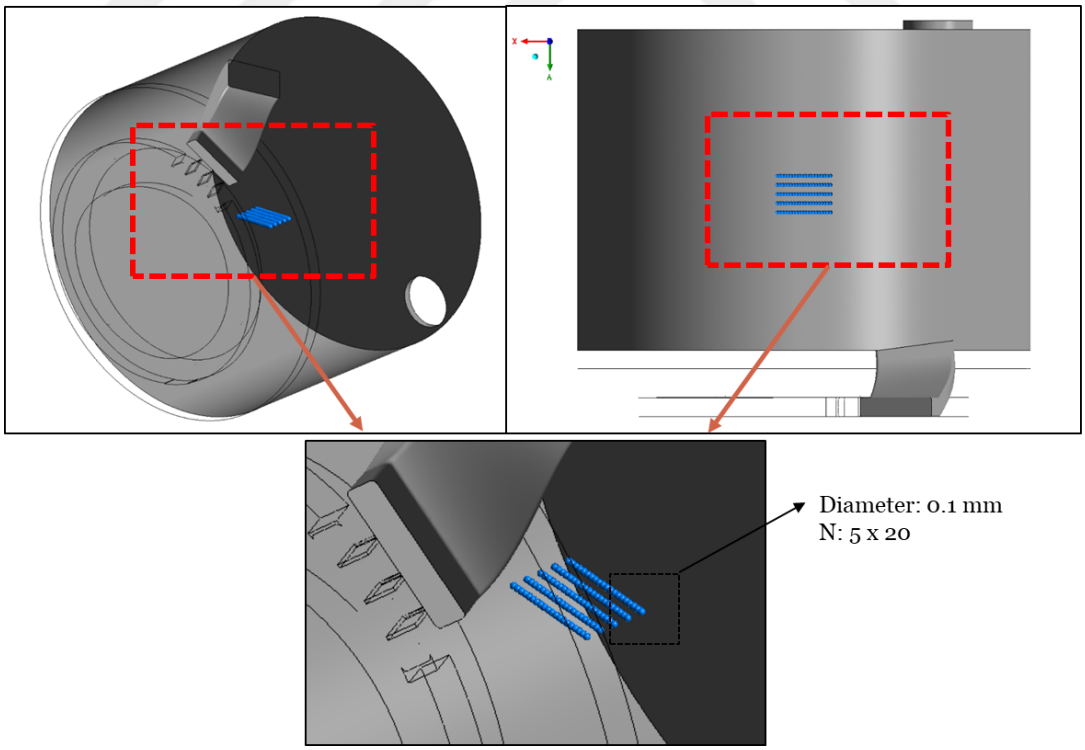
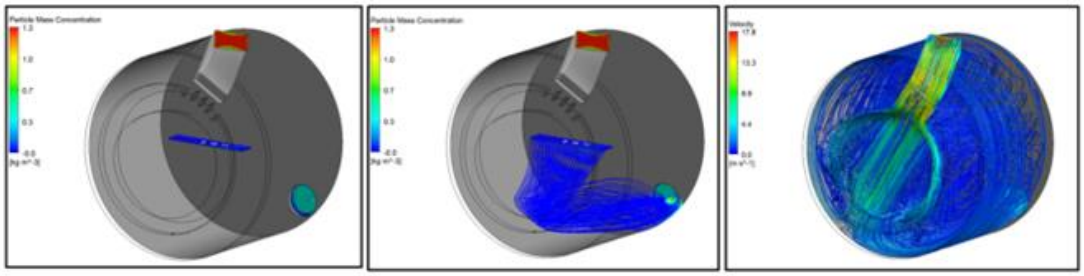


Figure 7.11 Multiple injection source points definition

In order to obtain more realistic conditions and simulate the complicity of the mass transfer phenomena from a laundry, drum rotation has been added to the model. Figure 7.12 shows the particle-track paths, water-mass fraction, and velocity streamlines inside the rotating drum.



a. b. c.

Figure 7.12 a) Multiple injection source b) water mass fraction of the wet laundry source and c) flow distribution inside the rotating drum

The Particle Image Velocimetry flow visualisation experiment's data were used to validate the computational findings of velocity distribution from CFD modelling by specifying it as an inlet boundary condition.

Advanced hardware and sensitive components are needed for the Stereo Particle Image Velocimetry (SPIV) approach and an adequately planned experimental setup for the velocity measurements. A camera, laser, fog generator, computer, software to manage the parts and post-processing, a timer box, and cables comprise the bulk of the SPIV system. In the experiment, a high-energy light source, usually a laser, is combined with appropriate lenses to form a light sheet after seeding the air with particles. The camera captures the light that is scattered by the particle. The camera is synchronized with the laser source to ensure that the pictures are shot at the right time. The displacement of particles during a given time is then calculated using successive image pairs from the camera. Each interrogation region receives a velocity vector as a result of this study. These velocity vectors are combined to create a vector field representing the flow properties under investigation as given Figure 7.13.

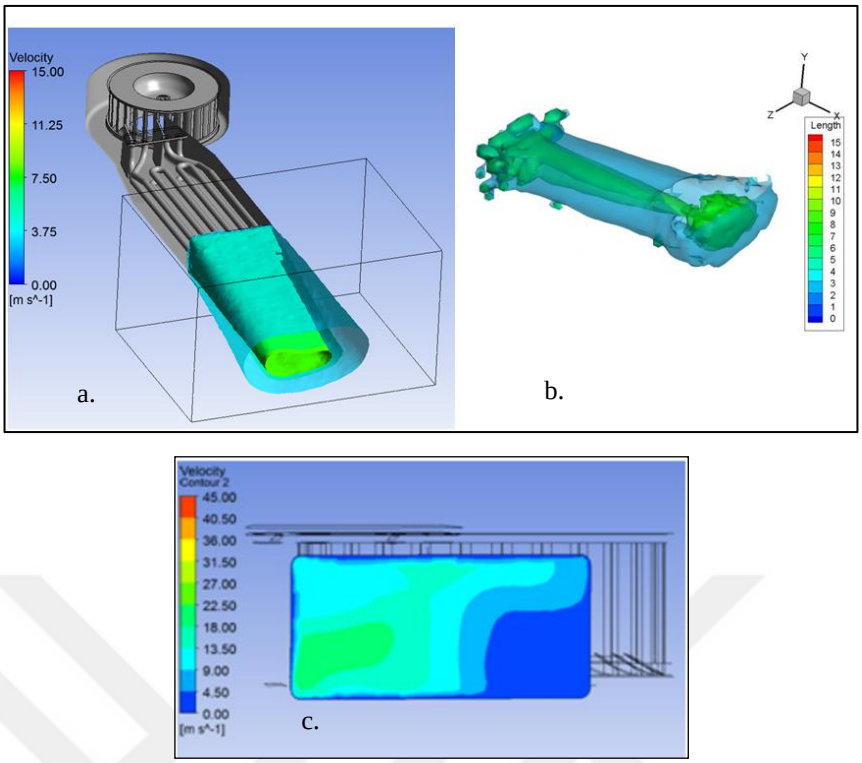


Figure 7.13 a) CFD and b) SPIV results of the velocity distribution and c) velocity map at the heater outlet

SPIV measurements were used to investigate the flow distribution in three dimensions in the out-flow region of the washer and dryer heater unit. In order to visualise the 3D flow structure of the washer-dryer heater unit output, the SPIV data from multiple planes are used to reconstruct the velocity fields. These SPIV results were then used as inputs for CFD analyses. Figure 7.14 shows the velocity fields produced.

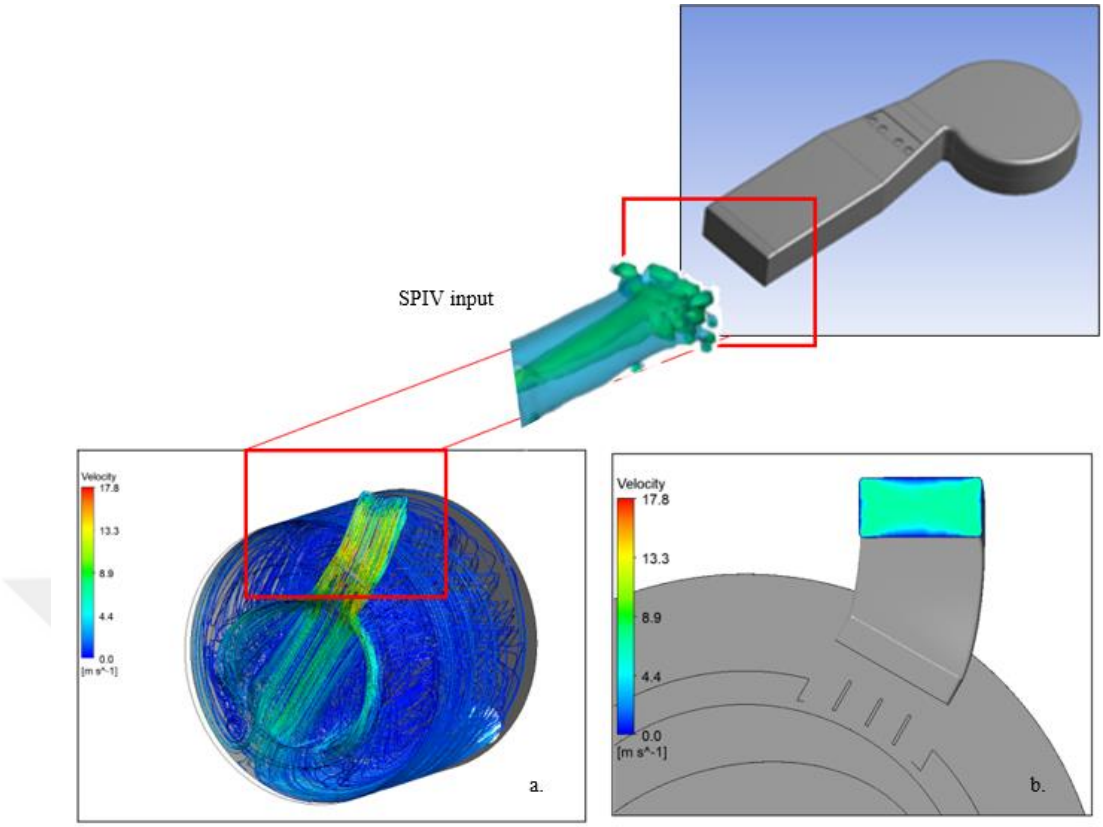
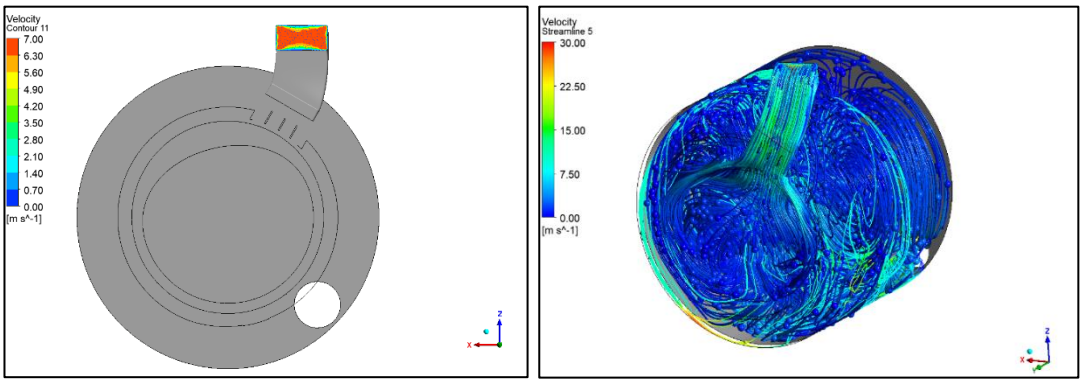


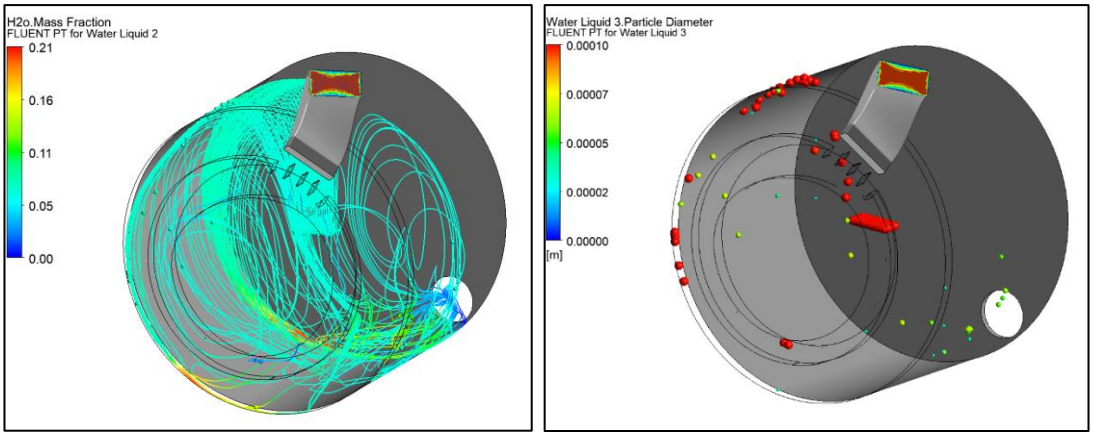
Figure 7.14 Defining the outlet velocity distribution as a boundary condition for the drum inlet

Experimental air flow characteristic (velocity vectors) was defined as inlet according to the SPIV measurements inputs. Results of the CFD analysis, which were made with SPIV data source as a boundary condition, were evaluated. Through the experimental SPIV measurements of the velocities along the heater, the outlet was obtained that air flow at channel output was nearly 8 m/s as depicted in Figure 7.15.



a. b.

Figure 7.15 SPIV data assisted velocity distribution simulation a) at inlet and b) inside the drum



a. b.

Figure 7.16 a) H_2O mass fraction and b) water liquid particle diameter distribution

Fate	Number	Elapsed Time (s)			
		Min	Max	Avg	Std Dev
Incomplete	14	6.723e-01	1.472e+01	9.134e+00	4.139e+00
Evaporated	66	4.435e-01	5.521e+00	7.668e-01	7.461e-01

(*)- Mass Transfer Summary -(*)

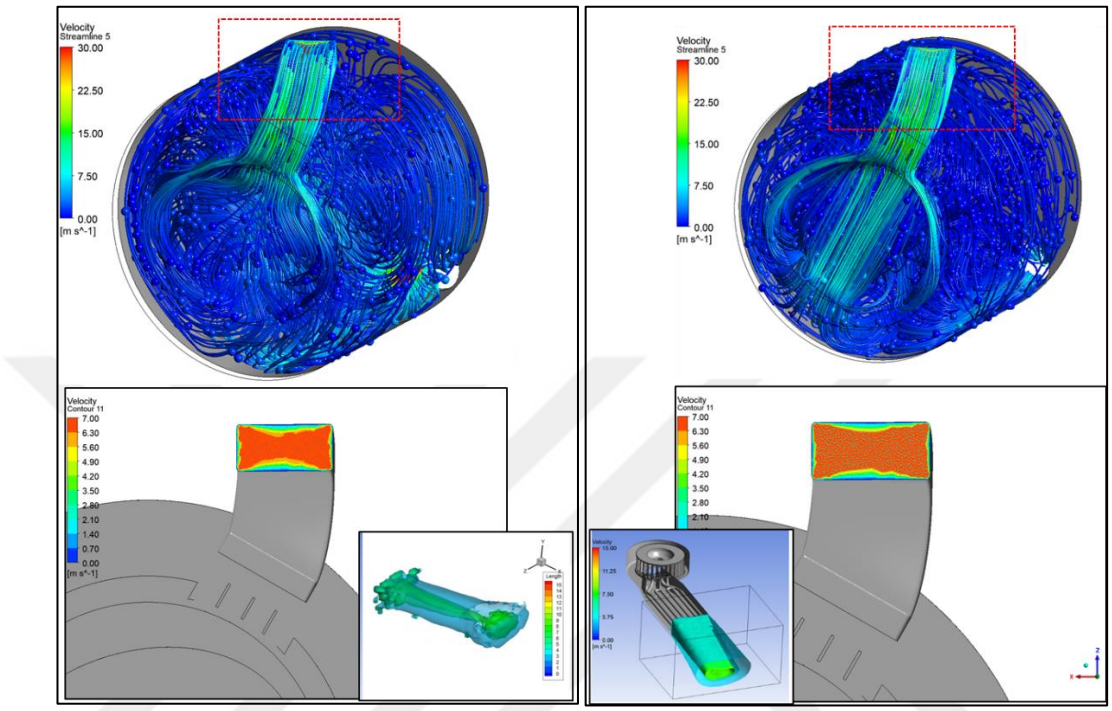
Fate	Mass Flow (kg/s)		
	Initial	Final	Change
Incomplete	1.400e-03	6.312e-04	-7.688e-04
Evaporated	6.600e-03	0.000e+00	-6.600e-03
Net	8.000e-03	6.312e-04	-7.369e-03

(*)- Energy Transfer Summary -(*)

Fate	Heat Rate (W)		Change of Heat (W)		
	Initial	Final	Sensible	Latent	Total
Incomplete	-3.399e+03	-1.569e+03	-4.269e+01	1.872e+03	1.830e+03
Evaporated	-1.602e+04	0.000e+00	-5.106e+01	1.607e+04	1.602e+04
Net	-1.942e+04	-1.569e+03	-9.375e+01	1.795e+04	1.785e+04

Figure 7.17 DPM summary report

The results of the numerical study, supported by SPIV input, were compared with the constant speed inlet method, as shown in Figure 7.18. It is obtained that constant inlet velocity and experimental boundary condition results were all consistent.



a. b.

Figure 7.18 Comparison of the velocity distributions of a) experimental SPIV input and b) constant velocity input

CHAPTER EIGHT
RESULTS AND DISCUSSIONS

8.1 Results and Discussions

As detailly given in Chapter 3, experimental tests have been performed to fully comprehend the influences of the drying program parameters on the condensation performance. During the one-hour drying cycle, relative and absolute humidity changes are influenced by the temperature and water spray activations, as shown in Figure 8.1.

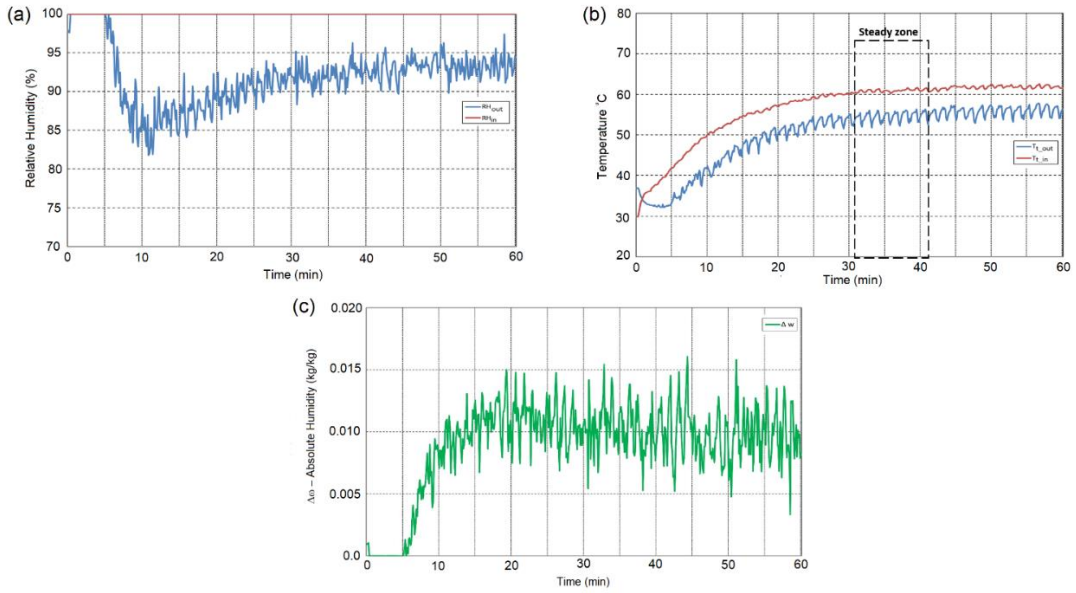


Figure 8.1 a) Relative humidity, b) temperature variation and c) absolute humidity charts

Throughout the experimental tests, relative humidity measurements were taken just above the spray nozzle. These measurements were used to study the heat transfer and mass transfer mechanisms responsible for removing moisture from clothes during drying. Absolute humidity measures the amount of water vapor in a given air sample, typically expressed in grams of water vapor per kilogram of dry air. Relative humidity, on the other hand, refers to the amount of moisture in the air at a specific temperature compared to the amount of moisture that the air could hold at that temperature if it were completely saturated.

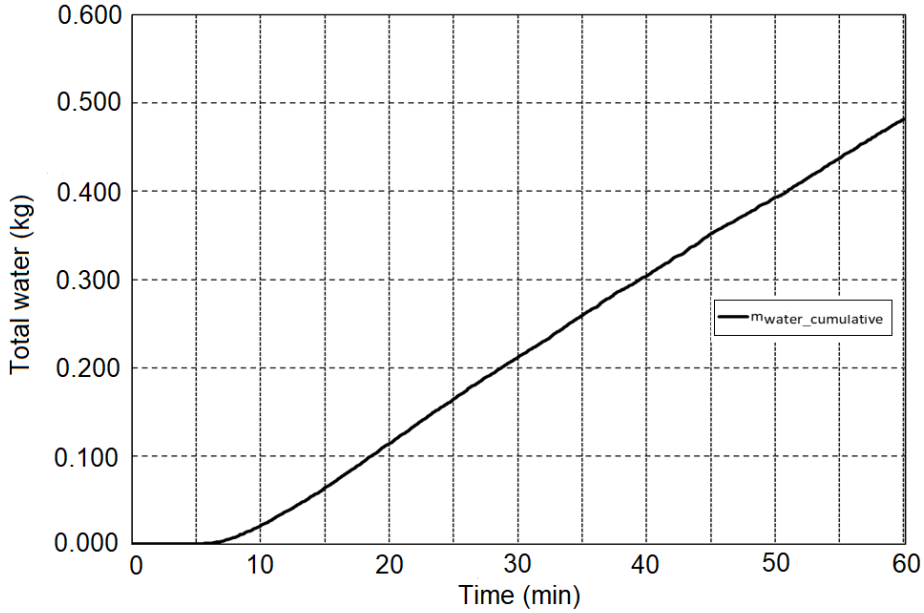
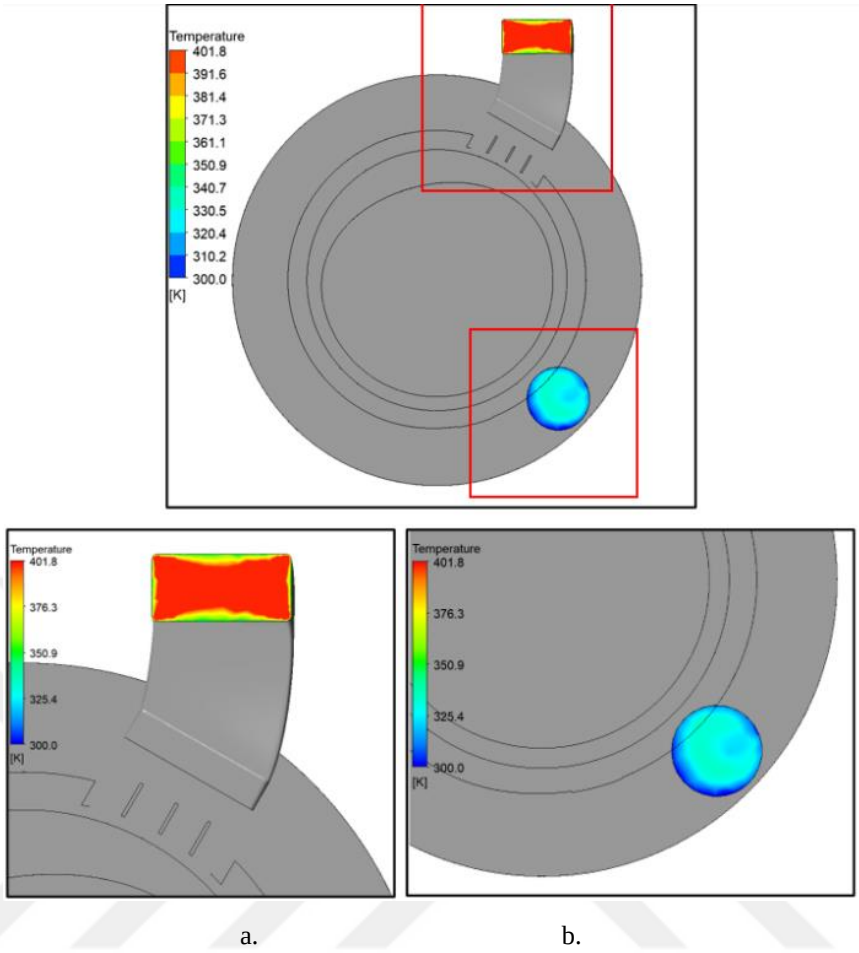


Figure 8.2 Cumulative water measurements

For evaluation, absolute humidity is calculated from the relative humidity data taken from the condenser inlet and outlet during dehumidification and in a steady state time zone where the temperature change is stable. The amount of dehumidification per unit of time is calculated. According to the calculations, during the 1-hour test, 479 gr water (as shown in Figure 8.2) is removed from a 4 kg standard test load from the 35th minute to 45th minute time zone. The average mass flow is calculated as 0.143 g/s. These test outputs are noted for the following evaluations to compare the reliability of the DPM analysis.

The numerical outcomes of the simulations made for discrete phase modelling of the droplet evaporation, verified by SPIV input values, are compared to those measured in actual test conditions, as previously mentioned in Chapter 3.



a. b.

Figure 8.3 Temperature distributions for a) drum inlet and b) drum outlet

Temperature distribution at the drum inlet is shown in Figure 8.20-a has occurred from the resulting effects of the heater output temperature, which is around 127 ℃. In Figure 8.20-b, the temperature of the drum outlet is shown to be 62 ℃. This value matches well with the condenser inlet temperature profile in the steady zone depicted in Figure 8.1-b.

Variations in water particle diameters and their respective tracking lines during the analysis time are simulated in Figure 8.4 and Figure 8.5. The 100 units of particles with 0.1 mm particle diameter have a mass flow rate of 0.00014 kg/s.

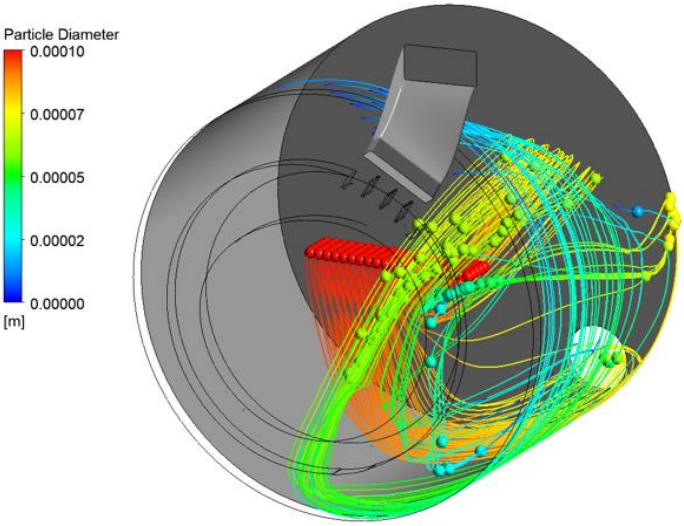


Figure 8.4. Water liquid particle diameter tracking lines by time

A general assumption is made that when average water droplet diameters are reduced from 0.1 mm to 0, supposing that the interactive mass transfer between two mediums is fully completed and the total evaporation process is accomplished.

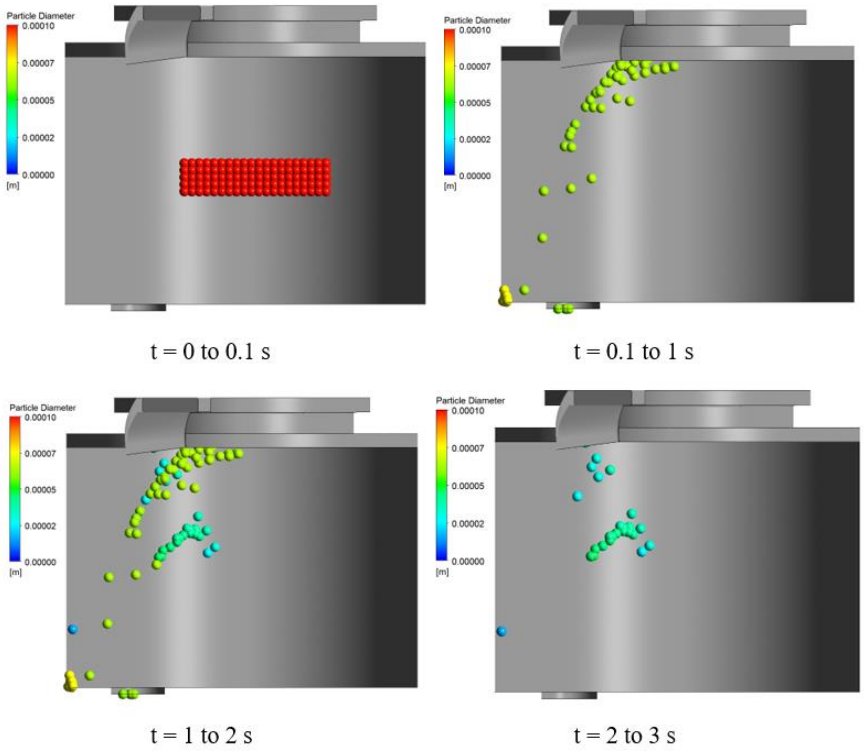


Figure 8.5 Particle diameter changes from t:0 to t:3 seconds

During the evaporation process simulation, it is calculated that 88 units of water droplets with 0.126 g/s mass flow are fully evaporated, and 12 units of water droplets are partially evaporated. During the evaporation process simulation, it is calculated that 88 units of water droplets with 0.126 g/s mass flow are fully evaporated, and 12 units of water droplets are partially evaporated. Hence, the total change in mass flow is determined to be 0.138 grams per second. The reduction in particle diameter over time is illustrated in Figure 8.6.

When comparing these simulation results to the expected mass flow rate of 0.143 grams per second, a minor deviation of approximately 3% is observed. This slight difference indicates that the outcomes from the computer simulations align well with the experimental data gathered under actual operating conditions.

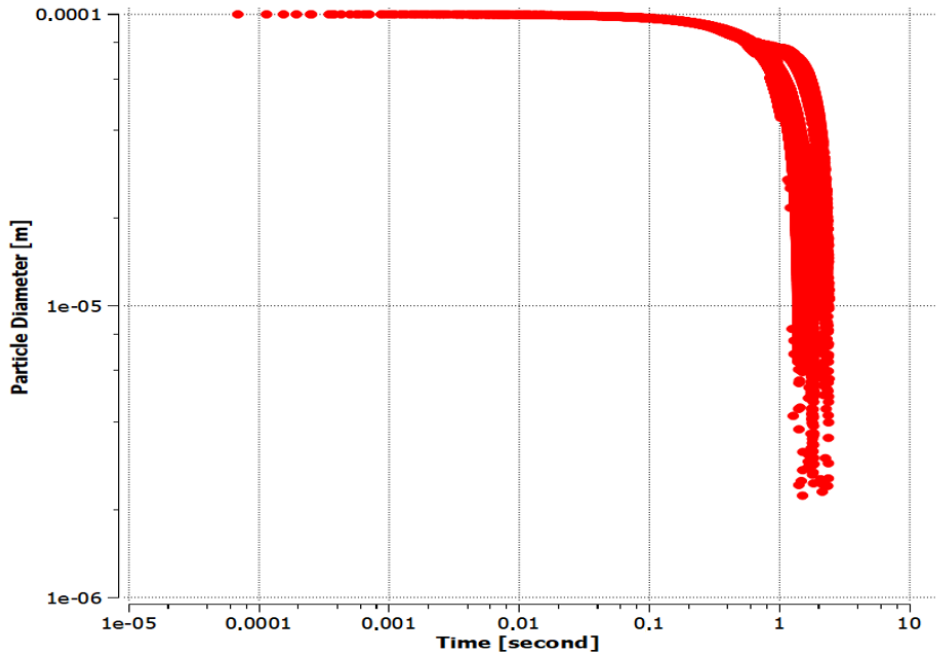


Figure 8.6 Reduction in the particle diameter with respect to elapsed time

All DPM summaries for incomplete and evaporated particle changes, mass transfer, and energy transfer results are respectively shown in Table 8.1, Table 8.2, and Table 8.3.

Table 8.1 DPM summary

	Elapsed time (sec)				
Phase	Number of particles	Min	Max	Avg.	Std. dev.
Incomplete	12	6.822 E-01	1.506 E+00	1.025 E+00	3.122 E-01
Evaporated	88	1.259 E+01	2.441 E+00	1.902E+00	3.343 E-01

Table 8.2 Mass transfer summary

Phase	**Mass flow rate (kg/s)**		
	Initial	**Final**	**Change**
Incomplete	1.716 E-05	4.395 E-06	-1.276 E-05
Evaporated	1.258 E-04	0.000 E+00	-1.258 E-04
Net	1.430 E-04	4.395 E-06	-1.386 E-04

Table 8.3 Energy transfer summary

Phase	**Heat Transfer Rate (W)**		**Heat Transfer Dynamic (W)**		
	Initial	Final	Sensible	Latent	Total
Incomplete	-4.166 E+01	-1.080 E+01	-2.238 E-01	3.109 E+01	3.087 E+01
Evaporated	-3.055 E+02	0.000 E+00	-9.736 E-01	3.065 E+02	3.055 E+02
Net	-3.472 E+02	-1.080 E+01	-1.197 E+00	3.376 E+02	3.364 E+02

The flow characteristics of a washer-dryer system fan and blowing channel were analysed using the CFD method in a study. SPIV (Stereoscopic Particle Image Velocimetry) tests were conducted at the device's outflow region to validate the numerical model. The results obtained from these measurements were compared with the novel experimental measurement methods. The findings of the study indicate a high level of agreement between the numerical simulations and experimental results, with a convergence ratio of approximately 94%. This means that the numerical predictions closely matched the observations from the experiments, providing a reliable and accurate representation of the system's behaviour.

Verification of these analysis by the SPIV test results shows that the numerical model simulates the actual state of the fan. Thus, the CFD method is presented as a reliable solution in the selection of the appropriate fan, to design a washer & dryer or dryer channel geometry and to evaluate the drying performance according to the heat transfer and flow characteristics formed inside the system.

The numerical and experimental methods developed in this study serve as valuable tools for designing a complex dryer unit, both in terms of individual components and the system as a whole. These methods can effectively assist in optimizing the design of the dryer, considering various factors such as the inclusion of fans and heaters. By utilizing these methods, engineers and designers can better understand the intricate interactions and performance of the dryer unit, leading to more efficient and effective designs.

CHAPTER NINE
CONCLUSIONS

The subject of this thesis study is to conduct a numerical investigation into a household appliance's heat transfer and flow characteristics. Household appliances refer to electrical or mechanical machines that perform various functions within a household setting. Major home appliances, often known as white goods, are a broad category of equipment that includes a variety of units, such as air conditioners, dishwashers, laundry dryers, fridges, water heaters, washing machines, stoves, and cookers. The study aims to analyse and understand the heat transfer and fluid dynamics phenomena specific to the chosen household appliance. Domestic technology is the incorporation of applied science into the home. Fluid dynamics and heat transfer play a crucial role in household appliances such as clothes dryers and washing machines. In the scope of this thesis study, a commercial household-type washer & dryer machine is selected due to its complex and not common drying system technology.

In order to stay competitive in the current appliance market, it is essential to improve the system's efficiency while also prioritizing the mechanical aspect. Therefore, obtaining a comprehensive understanding of the underlying phenomena governing the working principles of the dryer system in washer & dryer machines is paramount. This detailed knowledge enables manufacturers to optimize the design, improve energy efficiency, and ensure the reliable mechanical performance of the dryer system. By delving into the intricacies of the dryer system, manufacturers can develop innovative solutions that enhance efficiency and meet the evolving demands and expectations of consumers in the appliances market.

Literature research examine theoretical calculations, numerical solution methodologies for drying technologies, clothes drying phenomena, direct contact condensation, and centrifugal fans. This study reveals the weaknesses of studies that need to consider fluid flow and heat transfer evaluations for washer and dryer units. This thesis study proposes new models and techniques to address this deficiency.

A three-dimensional model of a washer & dryer machine dryer unit is designed, and Computational Fluid Dynamics and Heat Transfer (CFDHT) analyses are conducted. The findings are compared to experimental data taken from the inside of the dryer unit. This study's key finding is that conceptual, mathematical, and experimental results were consistent within an acceptable range of 3% to 6% error percentages. It should be highlighted that numerical investigations have been conducted under ideal circumstances and in a virtual configuration. A few overlooked elements, such as assembly pieces, sealings, drums, tubs, and other structural losses, bring this disparity. Even if experimental and CFD findings are not exactly a match for one another, they are all linearly coherent.

The development of a numerical approach for heat and mass transport calculations in a washer and dryer unit using a commercial computational fluid dynamic program was another goal of this study. It also aimed to make performance and design process improvement studies simple, quick, and affordable. Numerical approaches, for instance, provide the potential to identify design issues, evaluate various solutions, and improve the system promptly without incurring significant testing expenses in engineering research and development projects.

A Finite Volume Numerical model for the transient drying process of a laundry simulation was presented based on heat and mass transfer properties. A mathematically constructed 3D numerical model technique can make accurate predictions about the drying phenomena and the flow, temperature, and moisture distribution in the drying volume inside the washer and dryer.

This study introduces a novel approach for modelling an efficient drying process, which is found to be effective and insightful. The main objectives of washer-dryer machine producers regarding sustainable development are to minimize both water and energy usage. The numerical results obtained from experimental tests and analysis methods provide valuable information on determining the optimal termination point of the drying process. This knowledge contributes to developing an efficient drying

algorithm, enabling more responsible water usage, and significantly impacting household energy consumption rates.

The numerical results reveal the model's reliability in reducing the experimental drying data density for textile drying. Throughout this study, practical and reliable engineering tools and methodologies have been provided to achieve an optimized and efficient washer-dryer machine design. These efforts aim to assist producers in reducing water and energy consumption in the device, thereby contributing to achieving sustainable development goals. By incorporating these tools and approaches, manufacturers can enhance the environmental performance of their washer-dryer machines and work towards a more sustainable future.

This research topic is of great importance and has the potential for further exploration, including applying the approach to more complex and advanced drying systems. It is a promising subject for future studies in this field.

Acknowledgment: This thesis study was initially and partially supported by the Republic of Turkey Ministry of Industry and Trade and partly supported by the Vestel White Goods Company with the 00998.STZ.2011-2 encoded SANTEZ project. This thesis study aims to derive a reliable computational method for washer & dryer machine analyses. The thesis results in discussion for a complete assessment of CFD visualization was made according to Vestel Washer & Dryer machine test laboratories. In this context, this SANTEZ project was objected to providing a wide range of experimental data and optimization studies with numerical methods. This thesis study can be developed by preparing a more complex model providing a wide range of experimental data and making time-dependent analyses.

REFERENCES

Adrian, R. J. (2005). Twenty years of particle image velocimetry. Experiments in Fluids, 39(2). https://doi.org/10.1007/s00348-005-0991-7

AHLBORN Thermo-Anemometer probe, FVAD 35- TH5 type https://www.ahlborn.com/download/pdfs/kap09/eng/dthermoane.pdf

Akal, D., Kahveci, K., Akyol, U., & Cihan, A. (2017). Drying kinetics of cotton based yarn bobbins in a pressurized hot-air convective dryer. Proceedings of the Institution of Mechanical Engineers, Part E: Journal of Process Mechanical Engineering, 231(2), pp. 294–308. https://doi.org/10.1177/0954408915594725

Anderson, J. D. (2001). Fundamentals of aerodynamics (3th ed.). McGraw-Hill.

ANSI/AMCA Standard 210-16, ANSI /ASHRAE Standard 51-16, Laboratory Methods of Testing Fans for Certified Aerodynamic Performance Rating, 2016

ANSYS CFX Theory guide and user manuel.

Apanasevich, P., Lucas, D., Beyer, M., & Szalinski, L. (2015). CFD based approach for modeling direct contact condensation heat transfer in two-phase turbulent stratified flows. International Journal of Thermal Sciences, 95, pp. 123–135. https://doi.org/10.1016/j.ijthermalsci.2014.11.015

Bejan, A., & Kraus, A. D. (2003). Heat Transfer Handbook, Volume 1. https://books.google.com/books?hl=en&lr=&id=d4cgNG_IUq8C&pgis=1

Blazek, J. (2001). Computational fluid dynamics: principles and applications, Elsevier.

Boehm, R. F. (2003). Heat Transfer Handbook - Direct Contact Heat Transfer. Heat Transfer Handbook, pp. 1359–1400.

Caughey, D. A. (2004). Computational fluid dynamics. In *Computer Science Handbook, Second Edition* (Fifth Edition). Elsevier. https://doi.org/10.1017/cbo9780511780066

Celata, G. P., Cumo, M., Farello, G. E., & Focardi, G. (1989). A comprehensive analysis of direct contact condensation of saturated steam on subcooled liquid jets. *International Journal of Heat and Mass Transfer*, *32*(4), 639–654. https://doi.org/10.1016/0017-9310(89)90212-3

Chavez, A., & Mayinger, F. (2019). *Evaluation of pulsed laser holograms of spray droplets by applying digital image processing*. https://doi.org/10.1615/ihtc9.2840

Chavez, A., Mayinger, F., & Gebhard, P. (2020). *Measurement of direct-contact condensation of saturated vapor on subcooled droplets by pulsed laser holography*. https://doi.org/10.1615/ichmt.1992.intsympimgtranspproc.360

Czernek, K., Ochowiak, M., Janecki, D., Zawilski, T., Dudek, L., Witczak, S., Krupińska, A., Matuszak, M., Włodarczak, S., Hyrycz, M., & Pavlenko, I. (2021). Sedimentation tanks for treating rainwater: CFD simulations and PIV experiments. Energies, 14(23), 1–15. https://doi.org/10.3390/en14237852

Çengel, Y. (2008). *Fluid mechanics fundamentals and applications.*

Çengel, Y., Boles, M. A., *Thermodynamics: An Engineering Approach, 5th edition*

Datong, Q., Yijun, M., Xiaoliang, L., & Minjian, Y. (2009). Experimental study on the noise reduction of an industrial forward-curved blades centrifugal fan. *Applied Acoustics*, *70*(8), 1041–1050. https://doi.org/10.1016/j.apacoust.2009.03.002

Fletcher, D. F., Guo, B., Harvie, D. J. E., Langrish, T. A. G., Nijdam, J. J., & Williams, J. (2006). What is important in the simulation of spray dryer performance and how do current CFD models perform? *Applied Mathematical Modelling*, *30*(11), 1281–1292. https://doi.org/10.1016/j.apm.2006.03.006

Gabi, M., Dornstetter, S., & Klemm, T. (2003). Flow field and performance of cross flow fans - Experimental and theoretical investigations. *Journal of Thermal Science*, *12*(3). https://doi.org/10.1007/s11630-003-0074-0

Gulawani, S. S., Joshi, J. B., Shah, M. S., RamaPrasad, C. S., & Shukla, D. S. (2006). CFD analysis of flow pattern and heat transfer in direct contact steam condensation. *Chemical Engineering Science*, *61*(16), pp. 5204–5220. https://doi.org/10.1016/j.ces.2006.03.032

Gumruk, S., & Aktas, M. K. (2015). Experimental study of direct contact condensation of steam on water droplets. *Lecture Notes in Engineering and Computer Science*, *2218*, pp.1071–1075.

Incropera, F.P., DeWitt, D. P. (2000). *Fundamental of heat and mass transfer*.

Ip, R.W. L, & Wan, E. I. C. (2012). The New Use of Diffusion Theories for the Design of Heat Setting Process in Fabric Drying. *Advances in Modeling of Fluid Dynamics*. https://doi.org/10.5772/48484

Jacobs, H. . (2006). Direct Contact Heat Transfer. A-to-Z Guide to Thermodynamics, Heat and Mass Transfer, and Fluids Engineering, d(November). https://doi.org/10.1615/atoz.d.dirconheatra

Johann, G., Silva, E. A., Motta Lima, O. C., & Pereira, N. C. (2014). Mathematical modeling of a convective textile drying process. *Brazilian Journal of Chemical Engineering*, *31*(4), pp. 959–965. https://doi.org/10.1590/0104-6632.20140314s00002685

Karadeniz, Z. H., Kumlutaş, D., & Özer, Ö. (2013). Experimental visualization of the flow characteristics of the outflow of a split air conditioner indoor unit by meshed infrared thermography and stereo particle image velocimetry. *Experimental Thermal and Fluid Science*, *44*. https://doi.org/10.1016/j.expthermflusci.2012.07.005

Kumlutaş, D., Karadeniz, Z. H., & Kuru, F. (2013). Investigation of flow and heat transfer for a split air conditioner indoor unit. *Applied Thermal Engineering*, *51*(1–2). https://doi.org/10.1016/j.applthermaleng.2012.08.051

Lee, S. Y., & Tankin, R. S. (1984). Study of liquid spray (water) in a condensable environment (steam). *International Journal of Heat and Mass Transfer*, *27*(3), pp. 363–374. https://doi.org/10.1016/0017-9310(84)90283-7

Lekic, A., & Ford, J. D. (1980). Direct contact condensation of vapour on a spray of subcooled liquid droplets. *International Journal of Heat and Mass Transfer*, *23*(11). https://doi.org/10.1016/0017-9310(80)90156-8

Li, S. Q., Wang, P., & Lu, T. (2015). Numerical simulation of direct contact condensation of subsonic steam injected in a water pool using VOF method and LES turbulence model. *Progress in Nuclear Energy*, *78*, pp. 201–215. https://doi.org/10.1016/j.pnucene.2014.10.002

Lock, G. S. H. (1994). Latent Heat Transfer: An Introduction to Fundamentals, OxfordUniversity Press, Oxford, Chap. 7.

Mabrouk, S. Ben, Khiari, B., & Sassi, M. (2006). Modelling of heat and mass transfer in a tunnel dryer. *Applied Thermal Engineering*, *26*(17–18), pp. 2110–2118. https://doi.org/10.1016/j.applthermaleng.2006.04.007

Madejski, P., Kuś, T., Michalak, P., Karch, M., & Subramanian, N. (2022). Direct Contact Condensers: A Comprehensive Review of Experimental and Numerical Investigations on Direct-Contact Condensation. Energies, 15(24):9312. doi:10.3390/en15249312

Montazeri, H., Blocken, B., & Hensen, J. L. M. (2015). Evaporative cooling by water spray systems: CFD simulation, experimental validation, and sensitivity analysis. *Building and Environment*, *83*, pp. 129–141. https://doi.org/10.1016/j.buildenv.2014.03.022

Siwek, T., Górski, J., & Fortuna, S. (2014). Numerical and experimental study of centrifugal fan flow structures and their relationship with machine efficiency. *Polish Journal of Environmental Studies*, *23*(6), pp. 2359–2364.

Takahashi, M., Nayak, A. K., Kitagawa, S. I., & Murakoso, H. (2001). Heat transfer in direct contact condensation of steam to subcooled water spray. *Journal of Heat Transfer*, *123*(4), pp. 703–710. https://doi.org/10.1115/1.1370510

United Nations Department of Economic and Social Affairs Sustainable Development Goals

Velarde-Suárez, S., Ballesteros-Tajadura, R., Pablo Hurtado-Cruz, J., & Santolaria-Morros, C. (2006). Experimental determination of the tonal noise sources in a centrifugal fan. *Journal of Sound and Vibration*, *295*(3–5), pp. 781–796. https://doi.org/10.1016/j.jsv.2006.01.049

Versteeg, H.K , Malalasekera,W . An Introduction to Computational Fluid Dynamics, The Finite Volume Method (Second Edition). Pearson Education Limited, 2007

Wei, Y., Hua, J., & Ding, X. (2017). A mathematical model for simulating heat and moisture transfer within porous cotton fabric drying inside the domestic air-vented drum dryer. *Journal of the Textile Institute*, *108*(6), pp. 1074–1084. https://doi.org/10.1080/00405000.2016.1219450

Wernet, M. P. (2000). Application of DPI v to study both steady state and transient turbomachinery flows. *Optics and Laser Technology*, *32*(7–8), pp. 497–525. https://doi.org/10.1016/S0030-3992(00)00090-6

Yadav, V., & Moon, C. G. (2008). Fabric-drying process in domestic dryers. *Applied Energy*, *85*(2–3), pp. 143–158. https://doi.org/10.1016/j.apenergy.2007.06.007

Yılmaz, F. M., Yüksekkaya, S., Vardin, H., & Karaaslan, M. (2017). The effects of drying conditions on moisture transfer and quality of pomegranate fruit leather (pestil). *Journal of the Saudi Society of Agricultural Sciences*, *16*(1), pp. 33–40. https://doi.org/10.1016/j.jssas.2015.01.003

Younsi, M., Bakir, F., Kouidri, S., & Rey, R. (2007). Influence of impeller geometry on the unsteady flow in a centrifugal fan: Numerical and experimental analyses.

International Journal of Rotating Machinery, *2007*. https://doi.org/10.1155/2007/34901

Zbiciński, I. (1995). Development and experimental verification of momentum, heat and mass transfer model in spray drying. *The Chemical Engineering Journal and The Biochemical Engineering Journal*, *58*(2), pp. 123–133. https://doi.org/10.1016/0923-0467(94)02943-1

Zeineldin, T. H. M. (2008). *Stationary Objects inside a Multiphysic*